

# 1. INTRODUCTION

## 1.1. Motivation

Modern exploration seismology has been developing very fast as a result of the growing need to provide new energy resources and to exploit the existing ones more efficiently. Definition of an accurate velocity model is one of the most critical steps for the successful imaging of the subsurface. Three techniques of velocity analysis are widely used nowadays: velocity semblance analysis, prestack depth migration, and seismic tomography.

Velocity semblance analysis is based on flattening of events in common midpoint gathers, and it is used to determine stacking velocities. This technique assumes a locally flat layer-cake model of the subsurface and enables velocity estimations for the areas where the structure is simple (Yilmaz, 1987). Prestack depth migration is an effective method for determining velocities because of the sensitivity of the migrated image to the velocity model (Liu, 1997). When the velocity model is correct, data migrated in different domains (offsets, shots, angles) yield the same subsurface image (Kosloff *et al.*, 1996). If the velocity model is not correct, the differences between images can be used to improve the existing velocity model, usually following a layer-stripping approach. Sometimes migration velocity analysis involves velocity errors in shallow layers that tend to accumulate and influence results in deeper layers. The velocity model may have large variation in the lateral direction that does not correspond to the real situation (Kosloff *et*

*al.*, 1996). Both the semblance and the migration velocity analyses are “local” methods of velocity determination.

Seismic tomography has been developed to avoid the difficulties associated with the semblance or the migration velocity approaches (Bishop *et al.*, 1985; Stork, 1992; Kosloff *et al.*, 1996). It provides a sliced picture of the velocity distribution in the Earth, and combines geologic property estimation and imaging into one concept (Stewart, 1991). While other approaches separate velocity model building from imaging, traveltime tomography determines both interval velocities and reflection interfaces (Zhou, 1997a and 1997b). Seismic tomography suffers from problems characteristic of most geophysical inversion methods, such as non-uniqueness and instability, and it has difficulties associated with picking seismic events and velocity-depth ambiguity. These problems can be ameliorated by incorporating *a priori* geological and geophysical information into inversion, using automatic picking, and longer offsets.

One of the research foci of the Allied Geophysical Laboratories at the University of Houston is the development and calibration of a new 3-D vector VSP imaging technology for the Vinton Dome, oil field in Louisiana. In order to successfully image the complex structure of the area, an efficient and accurate velocity model needs to be built. Hence, the major motivation of this thesis was to develop a tomographic technique that will reduce uncertainties and develop a reliable interface-depth velocity model using vertical seismic profile (VSP) data.

## 1.2. Research objectives

The major objective of this research is to develop a tomographic technique for effective and reliable determination of velocity-interface depth model, that can be applied to the Vinton Dome VSP data. In addition, the objective of this research is to adopt a technique that is applicable to the other types of the seismic data (land surface seismic data, streamer data, ocean-bottom cable data, etc.), and other geological environments.

Tomography traditionally parameterizes the Earth into a regular mesh of cells or grids, and seismic velocities in each cell are calculated in an iterative manner (Mao and Stuart, 1997). Two approaches toward model parameterization have been used in this research: cell-based and deformable layer parameterization. The cell-based parameterization separates a subsurface model into a series of irregular cells, separated by piece-wise planar interfaces. The velocity value in each cell is independent of the neighboring cells. The deformable layer tomography (DLT) is developed by Dr. Hua-wei Zhou as an extension of the cell-based approach. The subsurface is parameterized into a series of layers, and the velocity of each layer is either constant or has vertical gradient, without lateral variation within layers. Portions of a layer can be of zero thickness, or “volume-less”, in order to depict pinch-outs or bed terminations. DLT determines layer geometry and velocity for each layer. There are potentially several advantages of deformable layer tomography compared to the other tomographic approaches: it better simulates the real subsurface geology, it incorporates more *a priori* geologic information, and it enables faster and more stable inversion.

The specific goals of this research are to:

- Evaluate advantages and limitations of the cell-based and the deformable layer tomography using first-arrival and reflection traveltimes, especially addressing its performance on VSP data.
- Enable the use of different seismic events, such as direct waves, turning waves, seismic refractions, P-wave and converted waves reflections, to define the velocity model.
- Define the best tomographic procedure to be applied to the Vinton Dome VSP data.
- Develop the velocity-interface depth model for the Vinton Dome.

The initial research plan for this thesis was to build P- and S-wave velocity models for the Vinton Dome, using P-wave and converted wave reflections. However, the difficulties associated with the recognition of the converted waves in seismic data with relatively poor quality shifted the research interest toward velocity model building using first arrivals, P-wave reflection events, geologic information, and well logs. Once more efficient techniques for separating converted wave modes are developed; I hope to develop a S-wave velocity model using tomographic techniques.

### 1.3. Thesis overview

The thesis is separated into a number of chapters describing different aspects of the research:

- Chapter 1- A brief statement of the research motivation and objectives is followed by an overview of the previous tomographic work, the description of the Vinton Dome geology and the datasets used.
- Chapter 2- This chapter provides details regarding the theory of the seismic tomography, its main application steps, picking, forward modeling and inversion, as well as an overview of some potential pitfalls of the method. Some important considerations for the application of the traveltime tomography for the area of the Vinton Dome follow.
- Chapter 3- Detailed results of the synthetic testing for all applied methods are presented. This chapter is intended to give important implications and conclusions regarding the best practices for building a tomographic velocity model for real data cases.
- Chapter 4- This chapter discusses the most important results of the integrated and interpretive application of first-arrival and reflection traveltime tomography for the area of the Vinton Dome.
- Chapter 5- Conclusions and some recommendations for the future work are suggested.

#### **1.4. Previous work**

The basic idea of tomography to use data outside of an object to infer the values inside of the object was introduced by Radon in 1917 (Stewart, 1991). This idea has been applied in a number of fields, such as medical tomography, electron microscopy, astronomical imaging, and seismic tomography (Stewart, 1991). Seismic traveltime tomography reconstructs a velocity model of the subsurface using traveltime information (Mao and Stuart, 1997). Most of the studies use either first-arrival or reflection tomography.

First-arrival tomography uses the first arrivals which can represent a variety of seismic waves (Zhou, 2002): transmitted waves traveling directly from source to receiver, refracted waves, or turning waves. First-arrival tomography was first applied in earthquake seismology for the study of global Earth structure (e.g. Aki and Lee, 1976; Anderson and Dziewonski, 1984). First-arrival tomography, as well as tomography in general, was later applied in exploration seismology to estimate velocity variation in cross-borehole profiling (e.g. Zhou *et al.*, 1993), to estimate velocity variation between a borehole and the surface sources or receivers in the VSP surveying (e.g. Chiu and Stewart, 1987), or to determine velocity structure from surface seismic surveying (e.g. Kosloff *et al.*, 1996). According to Mao and Stuart (1997), most of first-arrival tomographic methods parameterize the subsurface with cells, and the cell velocities are determined by tomographic inversion. Since only first-arrival traveltimes are used, there

are usually too many unknown parameters to be solved and therefore first-arrival tomography yields only quantitative estimates of the smoothly varying velocity distribution.

Reflection tomography uses the traveltimes of seismic waves that have propagated through the region of interest before and after reflection from an interface (Mao and Stuart, 1997). It is usually used in surface seismic reflection data (e.g. Bishop *et al.*, 1985; Stork, 1992). Reflection tomography provides a higher resolution tomogram than first-arrival tomography, since more raypaths are usually used (Mao and Stuart, 1997). Both velocities and reflection depths are found by reflection tomography. There are three approaches toward reflection seismology (Williamson, 1990): (1) inversion for the velocity only, assuming that the depth and the shape of a reflector are known, (2) parameterization of the model in suitable way that the inversion for both the velocities and the interface position can be performed, and (3) iterating between imaging the reflector using an established migration technique with a current velocity field, and redetermining the velocity field based on the migration results.

Seismic tomography is readily applied for crosshole and surface seismic data. There are fewer published examples of velocity model building using traveltime tomography for vertical seismic profiling data. Early tomographic studies involved integrated velocity model building using VSP and other types of seismic data. Chiu and Stewart (1987) used well logs, VSP data and surface seismic data to construct a 3D tomographic velocity model. The model contains curved interfaces separating regions with constant velocity.

They concluded that surface seismic data provided a broad lateral seismic coverage, while VSP data provided better velocity constraints, which may be needed to resolve ambiguity of the surface seismic data. Chen *et al.* (1990) used reverse VSP, crosshole data, and surface seismic data to construct a tomographic model of the subsurface. Joint use of different data enabled them to overcome the limitations of each of the individual datasets and construct a more reliable tomographic model, providing valuable information about the structure and stratigraphy of the reservoir.

Mao and Stuart (1997) used both transmitted and reflected waves to define velocity values and reflector position using seismic tomography for VSP data alone. Their analyses of the ambiguity in determination of velocity and depth of the reflection interfaces show that depth perturbation is more sensitive to the reflection traveltimes anomalies, while velocity perturbation is more sensitive to the transmission traveltimes anomalies. Joint use of first arrivals and reflections enabled them to define a 2D velocity model using a cell-based parameterization of the subsurface model for the VSP data. Lizzaralde and Swift (1999) performed a weighted, damped least-squares inversion of VSP first-arrival traveltimes to construct a smooth velocity-interface depth model. They constructed a 1D model of the part of the oceanic crust penetrated by the borehole.

Recent studies incorporated a definition of anisotropic velocities using VSP data. Le Begat and Farra (1997) used direct P-wave measurements from VSP data to construct a 1D velocity model. P-wave traveltimes and polarization tomography enabled them to define a transversely isotropic velocity model. Zhang *et al.* (2003) presented a traveltimes



inversion approach that uses the reflection traveltimes from offset VSP data, to construct the horizontal and vertical velocities for stratified anisotropic media. The method is developed for elliptically anisotropic media and provided 1D velocity models for an oilfield in northwestern China.

## 1.5. Geology of the Vinton Dome

Vinton Dome is located in Calcasieu Parish (Thomson and Eichelberger, 1928) in southwest Louisiana (Figure 1.1), in the South Louisiana Basin (Constance *et al.*, 1999). Vinton dome was the first Gulf Coast salt dome where oil was found in flank Tertiary sands (Marr, 1971). The first, shallow, production started in 1901 and this has been a producing area ever since (Marr, 1971). There is favorable geometry of the Tertiary sands with faults, shales and depositional geometry that provides the trapping mechanism for oil and gas reservoirs (Constance *et al.*, 1999). Cumulative production of this piercement salt dome exceeds 140 MMBO (Constance *et al.*, 1999).

The salt dome has pierced the overlying sediments, extending almost to the surface (Constance *et al.*, 1999). The Vinton dome area is characterized by extensive faulting, consisting of regional and local trends. There is an intensive radial faulting related to the local salt structure (Constance *et al.*, 1999). The dome has a cap rock that consists of limestone, gypsum and anhydrite, and probably extends over the top of the entire salt mass (Thomson and Eichelberger, 1928).

The area is covered by recent and Pleistocene sediments, which are underlain by Tertiary clastics with regional southward dip (Wilson and Noel, 1983). Regional dips have been modified by growth of the salt dome and subsequent faulting (Wilson and Noel, 1983). Pleistocene surface sediments are underlain by a Post-Anahuac sequence of Miocene to Pleistocene age (Table 1.1), the Anahuac formation of Oligocene to Miocene age, and the Frio and Vicksburg stage of Oligocene age (Warren, 1957). The Frio and Anahuac are among the major producing formations of the Texas and Louisiana Gulf

Coast (Burke, 1957). The Frio formation consists of blanket sands and accounts for most of the production, while the Anahuac is primarily built of shales and produces from a limited sand strata within the shales (Burke, 1957). Since the majority of sands in the Frio formation are productive, these sediments are the major exploration targets (Wilson and Noel, 1983). The major geologic and stratigraphic units used in my seismic interpretation include: the Vicksburg stage, the Frio formation, the Anahuac sediments, the Post-Anahuac sediments and the Pleistocene strata.

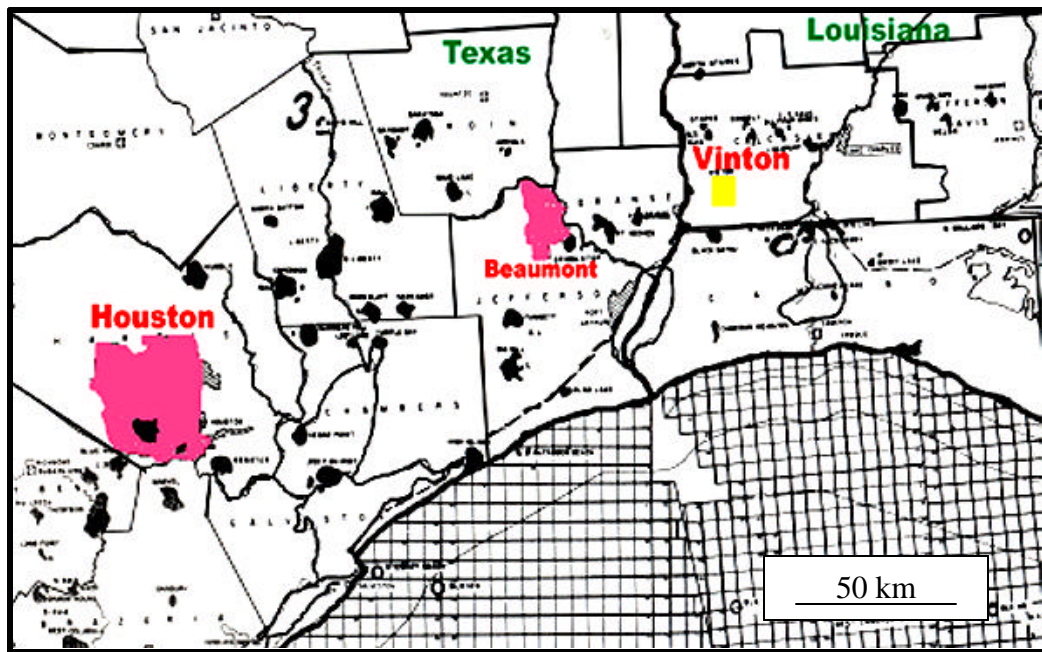


Figure 1.1. Regional position of Vinton Dome

*The Vicksburg stage:* This stage in southwestern Louisiana consists of dark gray to brown calcareous and fossiliferous shales with occasional thin silty sands and sandy silts (Warren, 1957). A list of foraminifera used to mark the top of this stage is given in Table 1.1.

Table 1.1. Correlation chart for Anahuac and Frio sediments, South Louisiana (Adopted from Warren, 1957)

<i>Series</i>	<i>Terminology used</i>	<i>Generalizes zonal terminology</i>	<i>Bethonic index Foraminifera</i>
Pleistocene	Port Hudson (Beaumont clay)		
Miocene-Pleistocene	Post-Anahuac	Zones assume the names of distinctive fossil	Amphistegina spp. Operculinooides sp. Discorbis bolivariensis Marginulina ascensionensis Simphonina davisii
Oligocene- Miocene	Anahuac stage	Discorbis zone	Lenticulina jeffersonensis Discorbis namada Discorbis gravelli
		Heterostegina zone	Heterostegina spp. Bolivina perca
		Margulina zone	Margulina idiomorpha Margulina vaginata Margulina howei
Oligocene	Frio stage	Upper	Miogypsina sp. Cibicides hazzardi
		Middle	Margulina texana Hackberry assemblage
		Lower	Nonion struma Nodosaria blanpiendi Discorbis sp. Textularia seligi
	Vicksburg stage		Cibides mississippiensis Textularia warreni Textularia tumidula Anomalina bilatellaris

*The Frio formation* is the section between the base of the Anahuac sediments and the top of the Vicksburg sediments (Warren, 1957). This formation consists of upper and lower sandy units separated by a middle shaly unit. The separation into three units is based on both lithologic characteristics and fossils (Table 1.1). The sands of the Frio formation represent the major oil bearing formation (Burke, 1957).

*The Anahuac sediments* consist of light to dark gray calcareous shale with thin beds of sand and calcareous sand with occasional thin lentils of limestone (Warren, 1957). The sand units bearing hydrocarbon in this formation have less economic importance than

those in the Frio formation (Warren, 1957). The position of the Oligocene-Miocene boundary is controversial and is considered to be the *Discorbis* zone (Wilson and Noel, 1983).

*The Post-Anahuac sediments* lie immediately above the Anahuac sediments and consist of mostly massive sands and thin silty shales with occasional shell lenses (Warren, 1957).

*The Pleistocene strata* exposed at the surface belong to the Port Hudson series, also known as the Beaumont clay. This series is composed of sand and clays with a thickness of approximately 200 feet (Thomson and Eichelberger, 1928).

## 1.6. Characteristics of the seismic data from Vinton Dome

Three-dimensional surface seismic data and 3D three-component VSP data were collected simultaneously during the survey in 1998 (Constance *et al.*, 1999). Surface seismic data were recorded by a radial receiver grid, and the VSP data were recorded by multilevel downhole three-component arrays cemented in the place. Source lines were concentric (Figure 1.2). The prestack VSP and poststack time migrated data were used in this thesis.

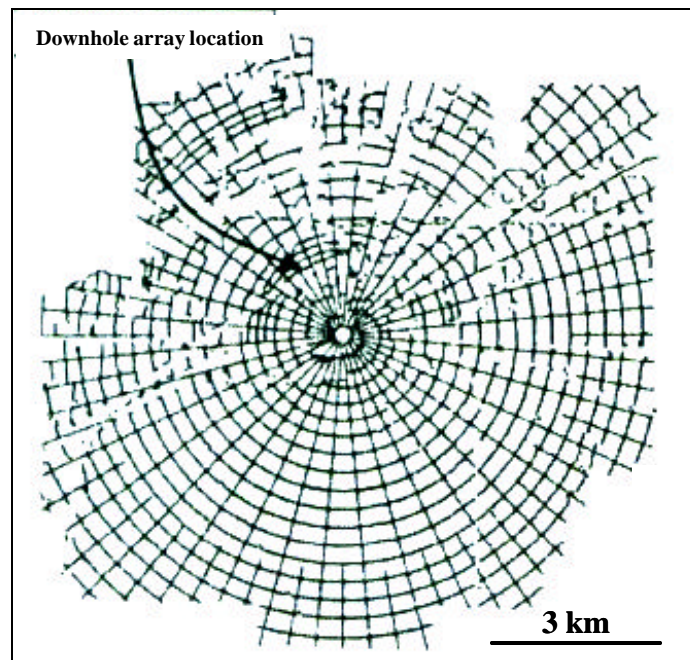


Figure 1.2. Illustration of the surface seismic recording geometry. Receiver lines are radial and source lines are concentric. (Constance *et al.*, 1999)

*Surface seismic-* Receiver lines were radially directed away from the piercement dome, with receiver line spacing from 275 to 365 meters. Long and short lines segments were designed with a angular spacing of  $5^\circ$  (Constance *et al.*, 1999). Receivers spacing was 50 meters along the receiver lines. Source locations were approximately along concentric circles, with shot spacing of 165 meters along the arc (Figure 1.2). This acquisition geometry was designed to produce a wide range of the offset and azimuth coverage. Spatial sampling is denser close to the salt dome, where geologic dips are steeper and faulting is more complex. The high fold enables better illumination of the steep dips near the dome. This acquisition geometry is also designed to avoid raypaths through the salt body (Constance *et al.*, 1999).

*3C VSP-* Two abandoned wells were used to deploy three-component arrays. The VSP dataset was recorded along with the northern half of the surface seismic survey (Constance *et al.*, 1999). Only the western well (G-23) was used in this study. The location of the well and seismic sources is given in Figure 1.3. This well had 80 three-component geophones permanently cemented in the wall of the well at 15.2 meters increments, from 287 to 1491 meters. However, the bottom 18 levels were damaged during deployment and were not operational. The active geophone depth range was 287 to 1217 meters. The objective of this survey was to provide a dataset that will enable better determination of seismic velocities for depth migration, increase resolution, and better image the salt flanks (Constance *et al.*, 1999).

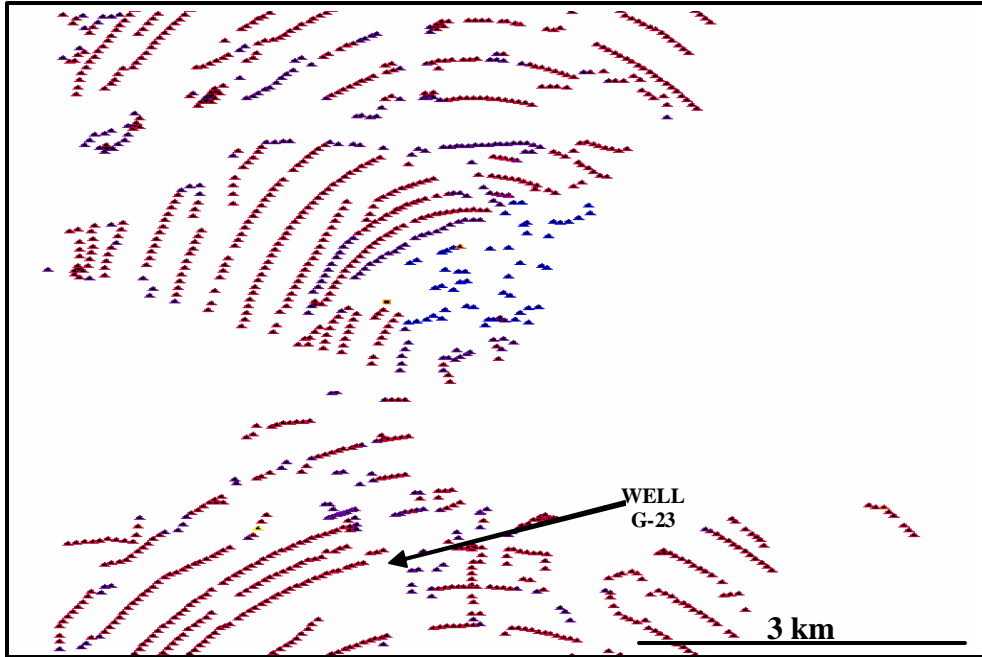


Figure 1.3. Illustration of the three-component VSP acquisition geometry. Seismic sources are shown with triangles, the well G-23 with a square.



## **2. METHODOLOGY: SEISMIC TOMOGRAPHY**

### **2.1. Introduction**

The term tomography is derived from Greek work “tomos”, which means section or slice (Stewart, 1991). Thus, seismic tomography can be defined as a method that provides a sliced picture of the Earth using seismic data. Seismic tomography joins two important aspects of geologic analysis, geologic property estimation and imaging, into one concept. The values of seismic velocities and the position of reflectors are inferred from a seismic record using tomography (Zhou, 1997a; 1997b).

Seismic tomography is an inversion process that constructs a velocity-interface depth model from seismic data. Although seismic tomography can also use waveform data (Aki and Richards, 1980), travelttime tomography is more commonly used to provide a velocity-interface depth model, because it is more robust, easier to implement, and computationally cheaper. Travelttime inversion can be performed using different seismic events: transmitted waves, refractions, turning waves, P-wave reflections, converted waves and other wave-mode reflections.

In this chapter I will give details of the event picking, forward modeling, inversion and model updating, as well as some of the pitfalls of seismic tomography. Since VSP represents a specific exploration method, special considerations regarding advantages and problems for such data will be given at the end of this chapter.

## 2.2. Application procedure

Determining the velocity-interface depth model using seismic tomography is an iterative process that can be separated into several general steps:

- 1) *Picking of different events on common gathers and time sections.* Events need to be recognized on all gathers and picked in a consistent manner, to make sure the same event is picked on all gathers. The result of the picking is determining the traveltimes of first arrivals or reflections.
- 2) *Developing an initial model and forward modeling.* This model represents an initial guess of the subsurface structure, based on the available geologic and geophysical data. Forward modeling is performed to calculate traveltimes in the initial model.
- 3) *Tomographic inversion of velocities and interface perturbations with respect to the initial model.* The traveltimes differences between the picked data and those calculated in the initial depth model are determined. Tomographic inversion calculates model changes to minimize the differences.
- 4) *Quality control of velocity model.* The quality of tomographic model is controlled using statistical and geologic criteria. If traveltimes differences are acceptable in the statistical sense and the modified model correlates with the geologic data, the tomographic process is terminated. If the result is not satisfactory, the modified model is used as a new initial model and steps 1-4 are repeated.

Once a satisfactory velocity-interface depth model is defined, depth migration can be performed. An additional criterion for the quality of a velocity model is the flatness of events on common image gathers after prestack depth migration. If events are not flat, repetition of the steps 2-4 should be performed iteratively.

### **2.3. Event picking**

Picking or data gathering is a time-consuming part of the tomography application. It involves: (1) Survey geometry setting, (2) Processing of seismic records, (3) Identifying and picking seismic events, (4) Quality control, and (5) ASCII format writing (Al-Rufaii, 2002). Since both first arrivals and reflection events have been used during this research, some characteristics of the data picking are described for each of them.

(1) Geometry information of the seismic survey has to be tied to the seismic records. This step needs to be done with care since errors in the geometry information introduce errors and instability in tomographic inversion.

(2) Some processing of the data has to be done to facilitate picking the seismic events. For the first arrivals, processing includes filtering, amplitude balancing, gain recovery, and wavelet shaping (Al-Rufaii, 2003). The initial processing for the reflection data includes static corrections, noise suppression, gain recovery, and prestack time migration (Al-Rufaii, 2002).

(3) The first arrival times are identified and picked carefully in the time-offset domain. The reflection events are identified and usually picked on the prestack data. Identification and picking of the reflection arrivals is challenging, interpretive and a time consuming procedure. Unlike first arrivals, which are relatively easily tracked along a seismic record, reflection arrivals may disappear due to noise, attenuation, dispersion, multiple interferences, and mode conversions. In order to pick reflections in a consistent manner, it is necessary to recognize events from the prominent horizons on each gather,

which is a highly interpretive process. Picking can be performed manually or automatically. Manual picking is time consuming and can be highly influenced by the picking errors and bias of operator, and therefore it is usually applied only to the limited datasets. Automatic picking can be applied using available commercial software packages.

(4) After picking is performed, it is necessary to quality-control the picking. QC involves plotting the picked traveltimes as a function of offset, trying to identify wrong picks.

(5) Finally, the picked traveltimes and the related geometry information are written in a file with specified ASCII format, to be used in the tomographic inversion.

## 2.4. Forward modeling

Forward modeling simulates wave propagation in a subsurface model. The objective of the modeling is to calculate a seismogram that a set of sensors would record for a given model (Carcione *et al.*, 2002). Modeling is based on a ray-theoretical or wave-theoretical approach (Aki and Richards, 1980). The objective is to calculate the traveltimes and the raypaths for a defined model. Traveltime tomography and Kirchhoff migration are based on the ray theory in forward modeling, while wave equation migration methods rely on wave theory.

### 2.4.1. Ray tracing

Ray based forward modeling methods are: one-point, two-point and three-point ray tracing methods (Al-Rufaii, 2002). The shooting method represents a characteristic example of one-point ray tracing (Matsuoka and Ezaka, 1992). In this method, the source location is defined, and rays are propagated in an initially defined direction. If the ray does not reach the receiver, the direction of the ray is modified until the raypath does fall within a user-specified distance from the receiver. The bending method is an example of two-point ray tracing (Van Avendonk *et al.*, 2001), where both endpoints of the raypath are defined. In this approach, the initial raypath connecting two fixed points is systematically perturbed or bent until it converges to the true raypath. The three-point ray tracing involves tracing of rays between a source, a fixed location in the subsurface (that may represent a diffractor or a reflection point), and a receiver (Aki and Richards, 1980).

The **shortest-path method** (Moser, 1991) has been used to develop the ray tracing algorithm implemented in this research. The method uses the solution of the three point ray tracing problem. The ray from the source to the scatter and from the scatter to the receiver follows the shortest-path ray. At the reflectors, the rays satisfy Snell's law. Diffractors correspond to the corners along reflection interfaces (Zhou, 1997a). Determining the reflection positions is made simpler by using a piece-wise planar interface in partitioning the model. The ray tracing is used to determine the traveltimes in the initial depth model.

#### 2.4.2. Model parameterization

The traveltimes picked in real data are compared with the traveltimes in the initial model calculated by the shortest-path method. The goal of the inversion is to minimize the traveltime difference between the real and the model data (Zhou, 1997a). Thus the initial model is modified and the ray tracing is iterated in order to converge to the actual geology. Tomography is applied in an iterative manner and it is assumed that small perturbations in the initial model produce proportionally small changes in the predicted traveltime. Thus, the choice of the initial model and its parameterization plays a major role in accuracy, convergence and resolution of the final solution (Zhou, 1997a; 1997b). There are generally three approaches toward the model parameterization: grid-based, cell-based and deformable layer based parameterization.

#### 2.4.2.1. Grid-based parameterization

Grid-based parameterization is a traditional parameterization approach that separates model space into a grid of cells, each having constant velocity. During tomographic inversion, velocity values are updated in each cell with the ray coverage. Reflector positions may be inferred from velocities, but they are usually smeared in the zones of the velocity changes. Grid based parameterization is traditionally used in the first-arrival tomography (Mao and Stuart, 1997).

#### 2.4.2.2. Cell-based parameterization

A model is partitioned into basic cells, each having constant perturbations in velocity. Interfaces between cells are designed to be piece-wise planar (Zhou, 1997a), describing irregularity and enabling convexity of each basic model cell for the ray tracing (Figures 2.1 and 2.2). A vertical line bounds each of the basic model cells. Each segment of the model interface is a straight line between the two neighboring model vertical lines (Zhou, 1997a). Two adjacent interfaces can be connected at some places, but separated at other locations. An interface may represent a reflector position if the impedance changes across it. The cell-based parameterization enables better simulation of the true subsurface geometry and determination of the velocity value and the position of reflectors than does grid parameterization (Zhou, 1997a). However, cell-based parameterization imposes a relatively high number of unknown parameters to be solved during the inversion process and allows for very strong lateral variations of velocity between two laterally adjacent cells.



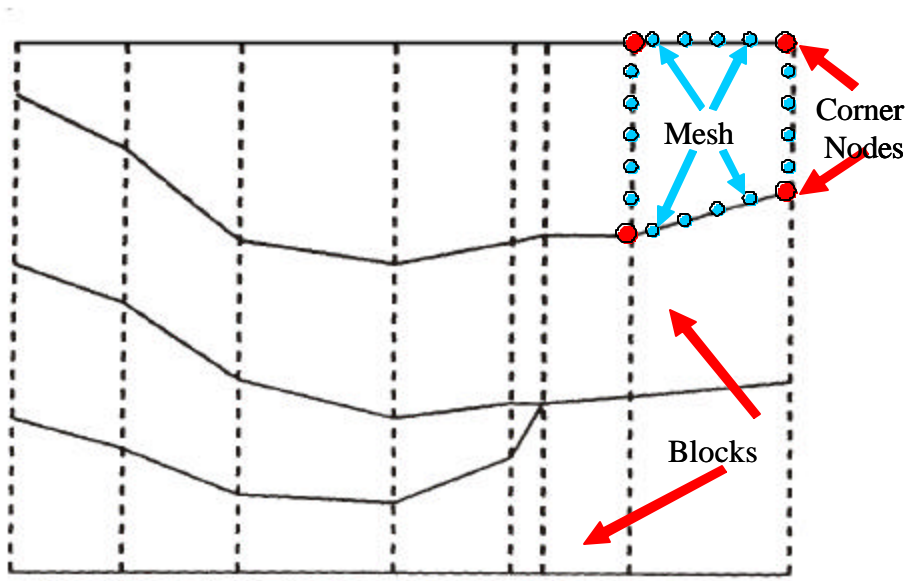


Figure 2.1. Cell-based parameterization in 2D (Zhou, 1997a).

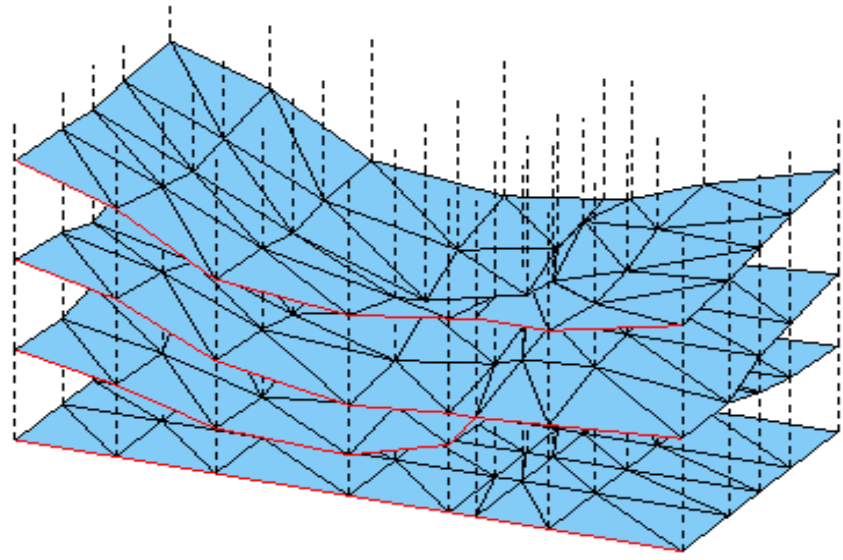


Figure 2.2. Cell-based parameterization in 3D (Zhou, 1997a).

#### 2.4.2.3. Deformable layer tomography parameterization

Deformable layer tomography (DLT) parameterization is an extension of cell-based parameterization developed by Dr. Hua-wei Zhou. The model consists of a series of cells separated by piece-wise planar interfaces. A horizontal set of cells simulates a layer (Figure 2.3) having a unique value of velocity, which can be either constant or vertically varying. Thus, each layer is characterized by a velocity and is separated from neighboring layers by piece-wise planar interfaces. This parameterization permits relatively simple implementation of anisotropy in forward modeling.

There are several potential advantages of DLT parameterization. First, the number of the model parameters is reduced, enabling more stable tomographic inversion and better convergence of the results. Synthetic testing showed that this method provides more stable results than the conventional grid parameterization (Figure 2.4). Second, this parameterization better simulates the real subsurface geology and facilitates incorporating *a priori* geological information. Third, the DLT better defines the “topography” of subsurface reflectors.

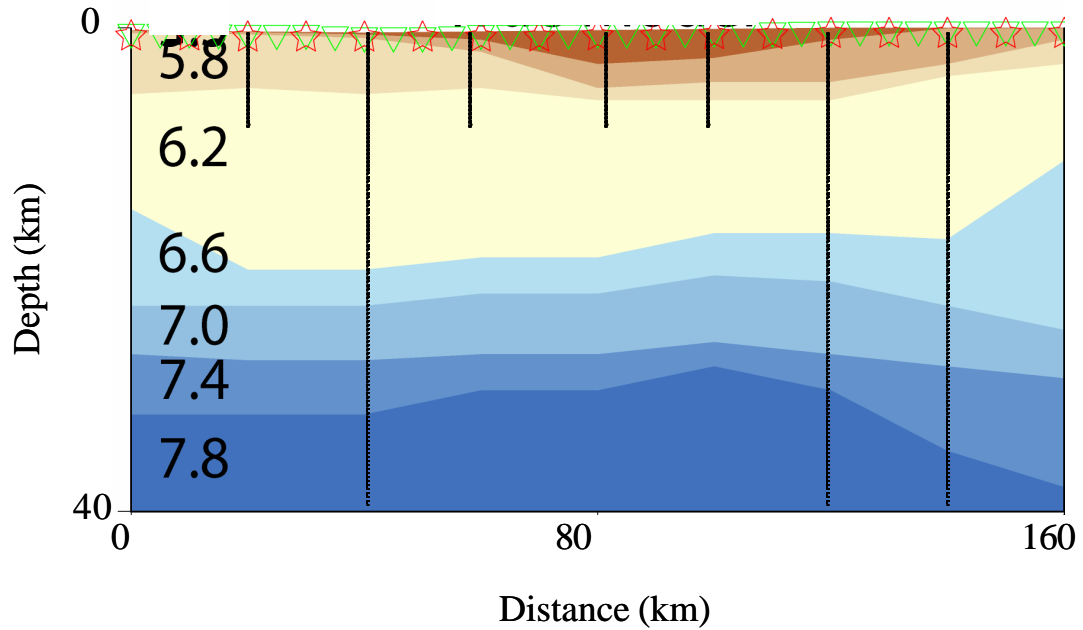


Figure 2.3. Example of the deformable layer parameterization for the LARSE 3 line in Southern California. The model has eight constant velocity layers. Each layer is separated into eight cells. In this problem, DLT constrains velocity values to be equal for each cell corresponding to the same layer. Numbers on the left side of the model indicate values of the velocities in km/s.

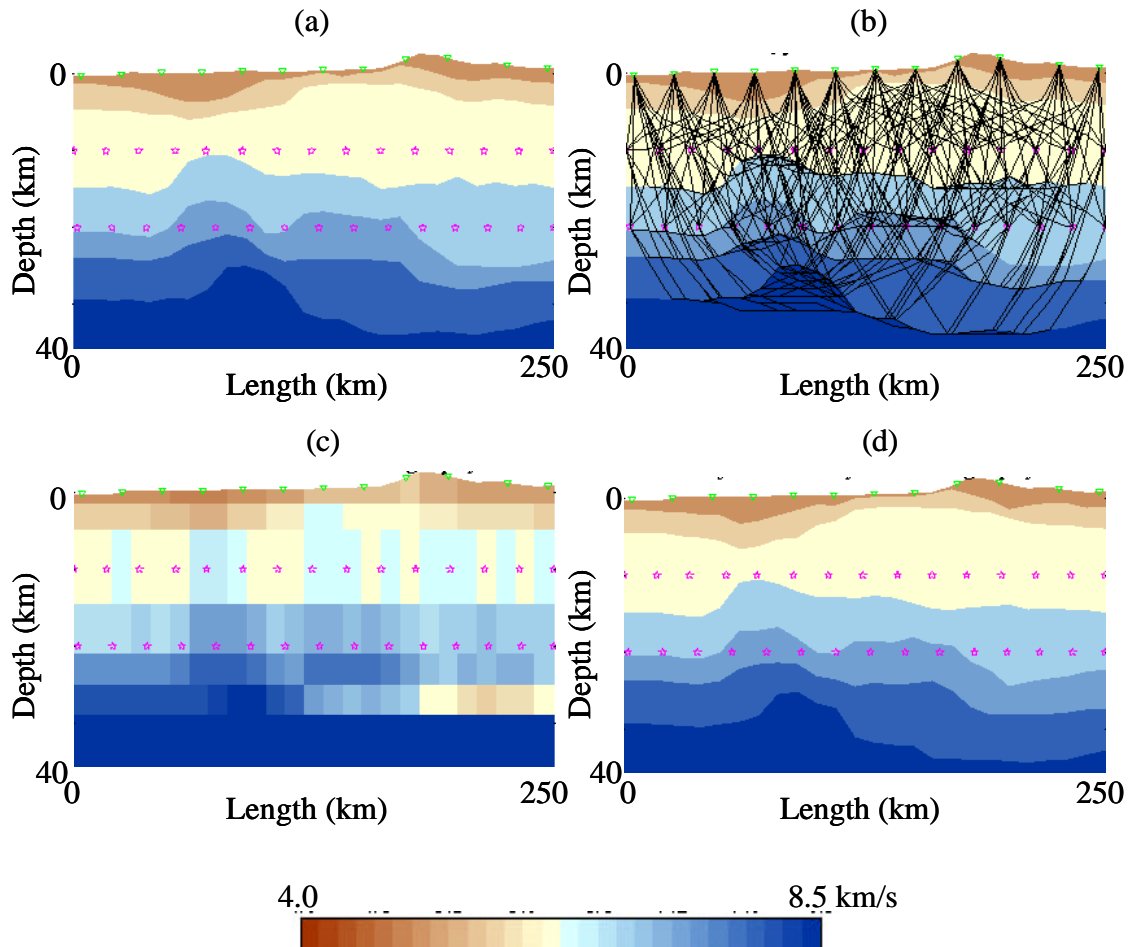


Figure 2.4. Comparison of the results of the synthetic testing between DLT and grid-based tomography. (a) The true model, (b) raypaths in the true model, (c) the conventional grid-based tomography result, and (d) the DLT result. Using the first-arrival turning rays from 30 events (pink stars) to 13 receivers (green triangles), DLT produces a closer match than grid-based tomography (after Zhou, 2002)

## 2.5. Tomographic inversion

An initial model of the subsurface is constructed using *a priori* geological and geophysical data. Once a synthetic seismic response is calculated for the initial model, the true traveltimes are compared to the computed ones. The objective of the inversion is to minimize the traveltime differences between the modeled and the true data in an iterative manner (Zhou, 1997a; Zhou, 2003). The traveltime is given as:

$$t_i = \int_{l_i(z)} s \cdot dl_i(z), \quad (2.1)$$

where  $t_i$  is the traveltime of the  $i^{\text{th}}$  ray,  $s$  represents slowness, and length of the  $i^{\text{th}}$  ray  $l$  is variable with the depth  $z$ .

### 2.5.1. First-arrival tomography

The first arrival is considered to be the first energy that arrives on a receiver. It may represent a variety of seismic events, such as transmitted waves, turning waves, and seismic refractions. The discrete form of equation (2.1) for first-arrival tomography is:

$$t_i = \sum_j^J l_{ij} \cdot s_j, \quad (2.2)$$

where  $l_{ij}$  and  $s_j$  are raypath length and slowness of the  $i^{\text{th}}$  ray segment within the  $j^{\text{th}}$  cell, respectively. Equation (2.2) is used in most practical applications of the first-arrival tomography. Although the traveltime is a linear combination of slownesses, traveltime inversion is a nonlinear problem since the raypath is velocity dependent (Al-Rufaii,

2002). The problem is usually linearized by mathematical expansion as a Taylor series about an initial model. The linearized equation after omitting higher order terms is:

$$dt_i = \sum_j^J k_{-s_{ij}} \cdot ds_j, \quad (2.3)$$

where  $dt_i$  is the travelttime residual,  $ds_j$  is slowness,  $J$  is the total number of slowness cells, and the kernel  $k_{-s_{ij}}$  is the length of the raypath segment that places constraints of the  $i^{\text{th}}$  ray on the  $j^{\text{th}}$  slowness cell. The tomographic solution is obtained by inverting equation (2.4) to determine slowness perturbation of the  $j^{\text{th}}$  cell  $ds_j$ :

$$dt_i = M \cdot ds, \quad (2.4)$$

where  $dt$  is the length of the travel time residual,  $ds$  is a length of the slowness perturbation and  $M$  is the raypath matrix. One of the main problems in seismic tomography is finding the inverse of the raypath matrix  $M$ .

There are three major difficulties associated with finding an exact inverse for matrix  $M$ : (1)  $M$  is not a square matrix; (2)  $M$  is often rank deficient; (3)  $M$  is often poorly conditioned (Al-Rufaii, 2002).  $M$  is not a square matrix because tomography problems are ideally overdetermined (i.e.,  $m > n$ ), but also under-determined (i.e.,  $m < n$ ), or mixed-determined. The rank ( $r$ ) of a matrix  $M$  is the maximum number of linearly independent row (or column) vectors. Therefore, if  $r = \min(m, n)$ , then  $M$  has full rank. If  $r < \min(m, n)$ , which is almost always the situation in seismic tomography, the matrix  $M$  is rank deficient. The raypath matrix  $M$  is poorly conditioned if the ratio of the largest eigenvalue,  $\lambda_l$ , to the smallest eigenvalue,  $\lambda_r$ , is much larger than one. In order to avoid

problems associated with matrix  $M$ , we apply the LSQR algorithm to solve the inverse problem (Paige and Saunders, 1982).

### 2.5.2. Reflection tomography

When partial differentiation with respect to  $s$  and  $z$  is applied to equation (2.2), it is possible to obtain the equation:

$$dt_i = \int_{l_i(z)} ds \cdot dl_i(z) + \int_{l_i(z)} s \cdot \frac{d}{dz} [dl_i(z)] \cdot dz. \quad (2.5)$$

For a defined model partition, the integrals on the right hand side of the equation above can be approximated by a linear combination of Frechet kernels  $k_{-s} = dl(z)$  and

$k_{-z} = s \frac{d}{dz} [dl_i(z)]$  so that

$$dt_i = \sum_j^J k_{-s_{ij}} ds_j + \sum_j^J k_{-z_{il}} dz_l, \quad (2.6)$$

where  $J$  is the total number of slowness cells and  $L$  is the total number of interface nodes that have to be upgraded by inversion. The kernel  $k_{-s_{ij}}$  constrains the  $i^{\text{th}}$  ray and  $j^{\text{th}}$  slowness cell, while the kernel  $k_{-z_{il}}$  constrains the  $i^{\text{th}}$  ray and  $l^{\text{th}}$  interface node. Details of the derivation of two Frechet kernels are given in Appendix A.

The goal of seismic tomography is to invert equation (2.6) to determine the slowness perturbation of the  $j^{\text{th}}$  cell  $\{ds_j\}$  and the depth perturbation at the  $l^{\text{th}}$  grid point  $\{dz_l\}$ . The inversion is performed using the LSQR algorithm (Paige and Saunders, 1982). LSQR solves a system of equations such as  $Ax=d$  by minimizing their norm  $\|Ax-d\|_2$ . LSQR is

analytically equivalent to the standard methods of conjugate gradients, but possesses more favorable numerical properties that handle large and sparse matrices.

The multiscale approach (Zhou, 1997a; 1997b) has been used in all tomographic algorithms. A mathematical definition of multiscale tomography is given in Appendix B.



## 2.6. Limitations of seismic tomography

Seismic tomography shares the limitations common for the other inversion schemes, such as non-uniqueness, instability, ambiguity and resolution. In addition, seismic tomography has problems of the identification and picking of events and the velocity-depth ambiguity. The limitations of the seismic tomography are related to the data itself, the model parameterization, and the nature of the inversion scheme (Al-Rufaii, 2002).

Since seismology deals with finite and discrete datasets, there is always more than one model that fits the data equally well. A tomographic solution is stable if small changes in the measured data, which is contaminated by noise, lead to insignificant changes in the model. The primary causes of non-uniqueness and instability in the tomographic solution (Kosloff *et al.*, 1996) include uncertainty in the seismic data, recording geometry, poor ray coverage, noise, and insufficient and inaccurate model parameterization. In order to reduce non-uniqueness and instability, it is necessary to perform damping by applying local smoothing within each cell or layer and at the same time allowing velocity discontinuity across interfaces (Al-Rufaii, 2002). In addition, *a priori* seismic (well information, VSP) or geological information constrains the solution. However, these constraints are at different scales of the subsurface velocity and this needs to be accounted for.

The tomographic inversion scheme used in this research handles non-uniqueness in a statistical and deterministic manner (Zhou, 1997a). The average and standard deviation of the traveltimes differences between the true and predicted traveltimes are statistically

measured and analyzed. The final solution has the lowest average and variance deviations between the observed and the computed traveltimes. Local smoothing and damping are applied deterministically, allowing for velocity discontinuity along interfaces with no smoothing. *A priori* information is incorporated into the initial model in order to minimize the problem of non-uniqueness (Zhou, 1997a).

The amplitude and the phase of the seismic events are affected by several factors, such as subsurface heterogeneity, dispersion, attenuation, energy partitioning between different modes along interfaces, source strength, and noise, which can cause weak and fuzzy seismic arrivals (Al-Rufaii, 2002). This can influence identification and picking of several seismic events. In order to reduce picking errors, it is necessary to process data and enhance event continuity. Automatic picking is faster and more efficient than manual picking, and it can be performed in areas with very good quality. However, it is always necessary to control the quality of the data and examine the picking confidence. It is necessary to perform manual picking in the areas with poor data quality and for non-continuous seismic events.

The velocity-depth ambiguity of traveltime analysis mainly depends on two factors: the offset-depth ratio and the accuracy of the traveltime picks (Lines, 1993). It is possible to reduce the ambiguity by increasing the offset range of the data and the precision of the traveltime picks. In addition, both first arrival and reflection traveltimes are used in this research, reducing ambiguity in determining both the velocity and the interface positions (Mao and Stuart, 1997).

## 2.7. Vinton Dome VSP tomography

### 2.7.1. Characteristics of the VSP datasets

Vertical seismic profiling (VSP) is a seismic method where seismic signals generated at the surface of the Earth are recorded by the geophones placed at various depths in a well (Hardage, 1985). If the source is located close to the well, a zero-offset VSP is obtained, and if the source is at some distance from the well, an offset VSP is obtained (Yilmaz, 1987). The typical acquisition geometry for the vertical seismic profile data is shown in Figure 2.5.

While geophones on the surface record only upgoing energy (Hardage, 1985), geophones in a well record both the downgoing (raypaths AC, AE and ABF in Figure 2.5a) and the upgoing energy (raypath ABC). The VSP data contain corresponding downgoing and upgoing events on the time-receiver depth plot (Figure 2.5b).

One of the advantages of the vertical seismic profiling is the possibility of the direct detection of the reflector depth (Whitmore and Lines, 1986). Namely, if a geophone is placed at the depth level of a reflector, such as the one noted with E in Figure 2.5a, the upgoing reflection and the downgoing direct arrival will coincide (Figure 2.5b), providing direct information of the depth of the reflector. In addition, the VSP technique provides a method for the accurate measurement of the seismic velocity and lithologic structure near the borehole (Stewart *et al.*, 1984). The resolution of the VSP data is higher than one characteristic for the traditional seismic and lower than the sonic logs, enabling

distinction of subtle features that cannot be defined by surface seismic, and better correlation of the well and traditional seismic data (Balch *et al.*, 1982).

The major factor reducing the image resolution is the limited recording aperture of the VSP data (McMechan and Hu, 1986). Namely, all geophones are placed in essentially the same (x,y) location, greatly reducing subsurface ray coverage. McMechan and Hu (1986) showed on a synthetic example that migration of VSP data recorded in the area of a salt dome can give only a partial subsurface image. In order to recover the complete subsurface image, it is necessary to simultaneously record surface and VSP seismic data.

The major difficulty when applying seismic tomography to VSP data is the lack of crossing rays. In order to constrain velocities and interface positions, it is necessary that rays mutually cross. Since all VSP receivers are placed in essentially the same (x,y) location, there is very little crossing of rays. This factor needs to be carefully examined to determine the confidence of the tomographic result.

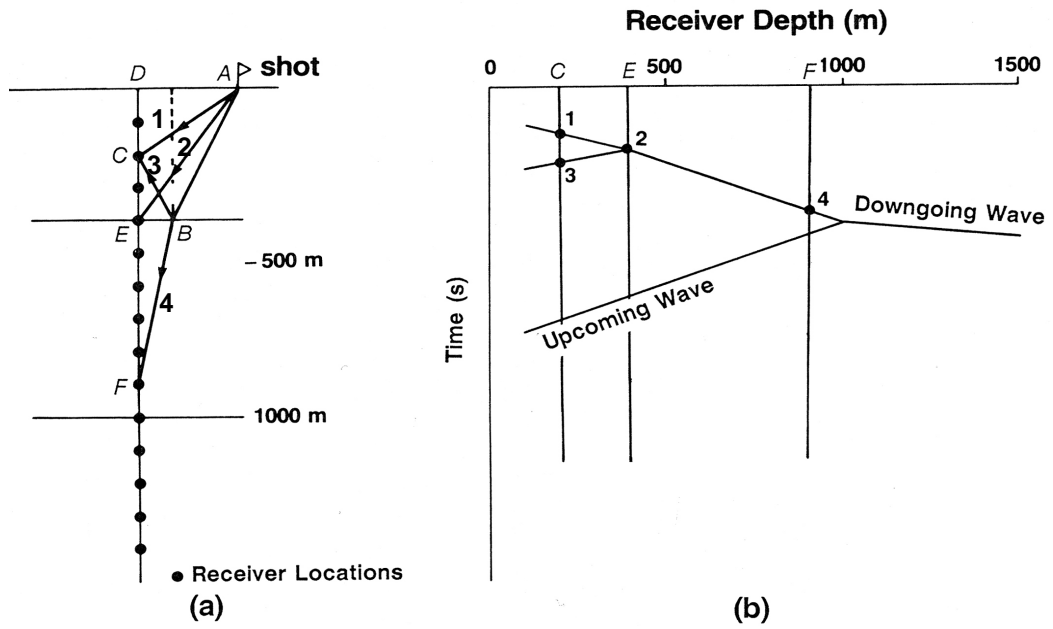


Figure 2.5. VSP acquisition geometry (after Yilmaz, 1987). (a) Raypaths, and (b) corresponding traveltimes.

### 2.7.2. Difficulties in applying tomography for the Vinton Dome

In order to apply seismic traveltimes tomography to the Vinton Dome VSP data, a number of difficulties have to be faced:

- Poor ray coverage and lack of crossing rays,
- Effect of a 3D structure on the 2D data,
- Complexity of the recorded seismic events and the consistency of the seismic events from one gather to another.

The Vinton Dome VSP data were recorded simultaneously with the surface data (Constance *et al.*, 1999). The acquisition was designed to provide an uniform 3D coverage. However, the tomographic algorithms have been applied in 2D. The assumption of any 2D geophysical method is that the structure does not change in the direction perpendicular to the profile (Yilmaz, 1997). In order to satisfy this requirement, radial profile lines have been selected at the Vinton Dome. The maximum number of the seismic sources along a profile was twenty, limiting the ray coverage by the small number of shots. There was also a limited depth range of borehole receivers. Figure 2.6 illustrates the resulting relatively poor ray coverage. Since the well is placed close to the dome's flank, most events reflect from an area corresponding to a small part of the model. More importantly, the amount of ray crossing is relatively small (Figure 2.6), indicating difficulties for application of the tomography in the area.

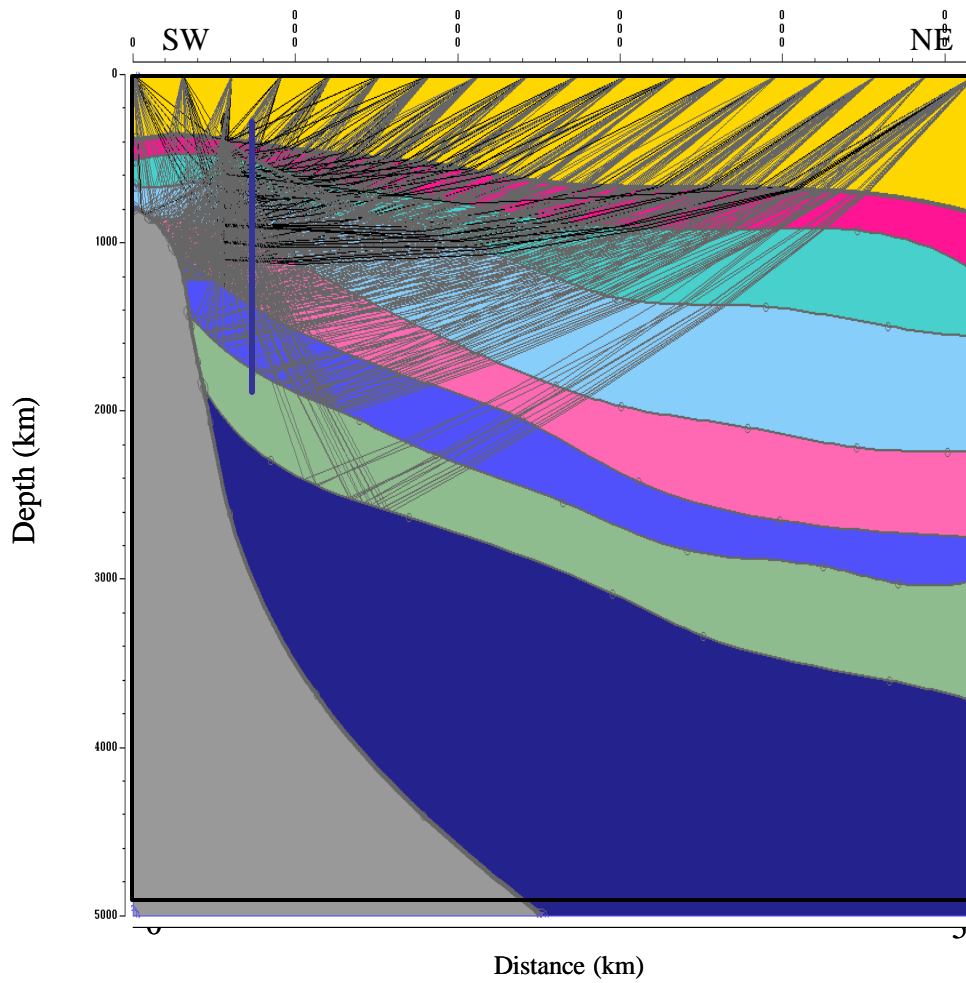


Figure 2.6. A model of the ray coverage of the VSP data for Vinton Dome. Position of the well and sources correspond to the real data acquisition.

Although I selected tomographic profiles to satisfy the 2D requirement, some effects of the 3D structure can be expected. The Vinton Dome is an area with a complex structure and multiple events from the same reflector can be expected as a consequence of 3D structure, especially pronounced in the area around the salt body.

Seismic tomography is a model-based method and the resolution power greatly depends on the definition of the Earth's model. As it was already explained, the data coverage and the ray crossing are limited, and stable tomography inversion is possible for a simplified initial subsurface model. The definition of the initial model is governed by events on the records, and the data recorded around Vinton Dome have a complex character. The complexity is two fold: the number of the events that can be recognized is larger than can be used for modeling, and the character of the events becomes more complicated with increasing offset. Figure 2.7 shows an example of a near-offset common shot gather where a large number of upgoing events can be recognized in the depth range of 1000m. However, due to the poor coverage, all seismic events cannot be used. As a consequence, event recognition becomes an interpretative and complex task, partially facilitated by the fact that seismic events on the VSP records have depth control. In addition, as a consequence of the raypath pattern shown in Figure 2.6, the character of the common shot gathers on larger offsets is complex and event recognition cannot be performed with the required level of confidence. The detailed illustration of these phenomena will be given in the Chapter 4. It will be shown that only a limited number of events present on all gathers can be used for tomographic velocity model building.



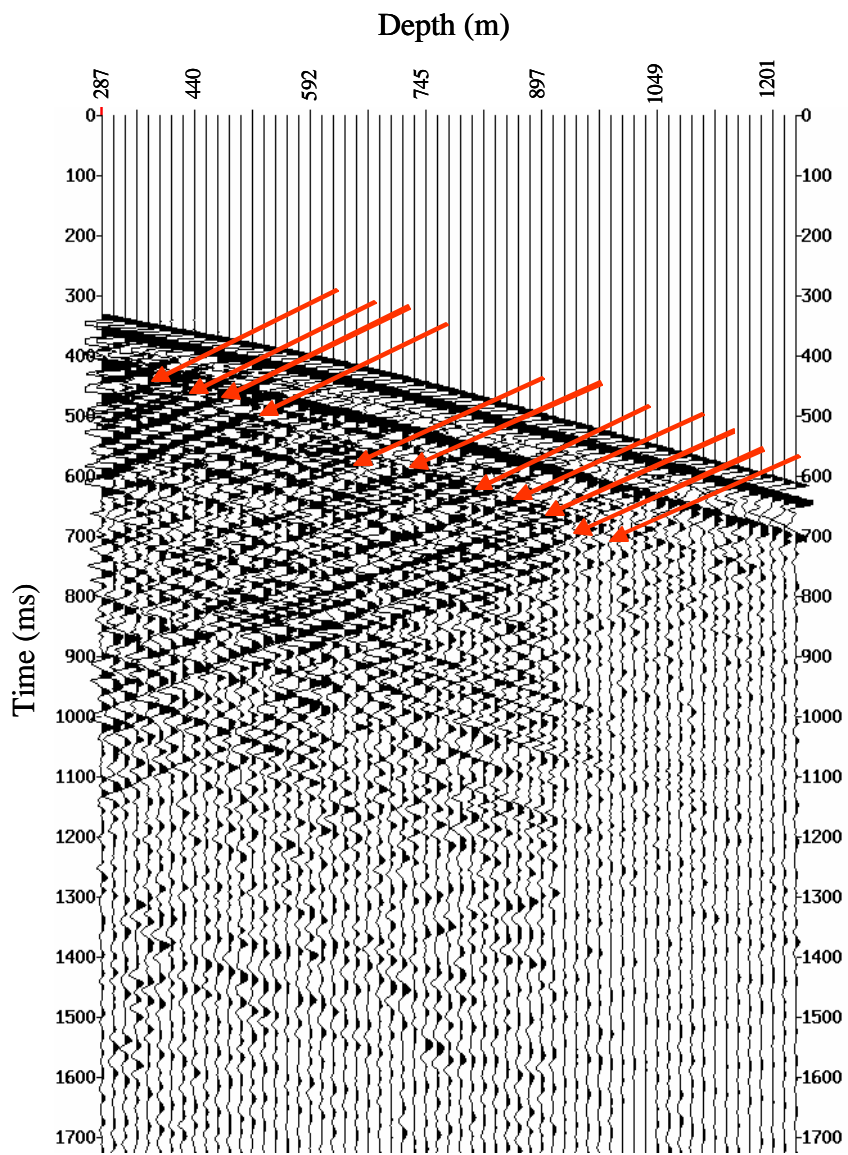


Figure 2.7. Common shot gather for shot 3297 with and offset of 520m. Red arrows indicate some of the upgoing events that can be identified in the upper portion of the section.

### 3. SYNTHETIC TESTING

The primary goal of the research is to adopt a travelttime tomography method that will determine a velocity-interface depth model for the Vinton Dome VSP data. The method has to address several important issues: non-uniqueness, instability, velocity-depth ambiguity, poor ray coverage and lack of ray crossing, complexity and inconsistency of events.

Synthetic testing is used to investigate the performance of an algorithm. Earth models with different levels of complexity can be constructed and used to determine if the model's structure and characteristics can be recovered using tomographic algorithms. Two groups of models have been constructed for the purpose of this research.

The first group of models was designed for an area in Southern California. Models of the Earth's crust, containing both positive and basin features, were constructed based on previously published results (Clayton, 1996; Lutter *et al.*, 1999; Zhou, 2002). I have simulated surface seismic acquisition geometry for these models. The second group of models is based on the Vinton Dome area. Models with dipping sedimentary layers are tested using VSP geometry.

Applied tomographic algorithms have been evolving during this research in order to satisfy the velocity model building requirements. Cell-based parameterization is used first, while the deformable layer tomography approach is developed later as an extension of the cell-based approach. This chapter presents results of the synthetic testing for the following tomographic methods:

- Cell-based first-arrival tomography,
- First-arrival deformable layer tomography,
- Cell-based reflection tomography,
- Reflection deformable layer tomography.

Synthetic examples addressing the performance of the cell-based converted wave tomography and the Kirchhoff migration will be given at the end of this chapter. The synthetic tests were designed to address performance of tomographic algorithms in general, as well as to understand the best practices for the application of tomography for the Vinton Dome.

It is considered that first arrivals are the first events recorded on geophones, and they can be direct waves, refractions, or turning waves. Two models are commonly defined: the true and the initial model. The true model is a representation of the geologic structure of an area. The goal of the seismic tomography is to perturb an initial model and obtain the final tomographic solution that is identical to the true model. The tomographic procedure is performed in several iterations. A smaller number of iterations indicates a faster convergence of the tomographic algorithm. The tomographic application is terminated once a satisfactory solution is obtained. The number of iterations necessary to obtain satisfactory solution will be given for each case examined in this chapter.

### 3.1. First-arrival tomography

Two models have been designed to examine the performance of the first-arrival tomography. The first model is an upper crustal model from Southern California. A group of universities and governmental institutions designed the Los Angeles Region Seismic Experiment (LARSE) and acquired wide-angle deep-crustal multichannel refraction and reflection data, using active and passive seismic sources (Clayton, 1996; Lutter *et al.*, 1999). The goal of the LARSE is to better define lithospheric structure in the area. I used crustal models developed by several authors for this area (Lutter *et al.*, 1999; Zhou, 2002) as the true models. A model of the upper 10 km of the crust from LARSE 1 is shown in Figure 3.1a. Twenty-six surface sources with a separation of 10 km and fifty-one surface receivers with a uniform separation of 5 km were used to perform ray tracing in the model (Figure 3.1b). All raypaths are contained in the upper 5 km of the model. The initial model (Figure 3.1c) was flat. Each of six tomographic iterations improved results, and the subsurface geometry was recovered (Figure 3.1f) using only first arrivals.

The second subsurface model represents the Vinton Dome area. Six layers dipping to the right side of the profile are defined (Figure 3.2a), with the VSP survey geometry corresponding to one used during the real data acquisition. Rays were traced from 8 surface sources to 61 receivers in the well (Figure 3.2b). The initial flat-layer model (Figure 3.2c) was updated after first iteration. The geometry of the model is reconstructed only for the area with ray coverage (Figure 3.2d).

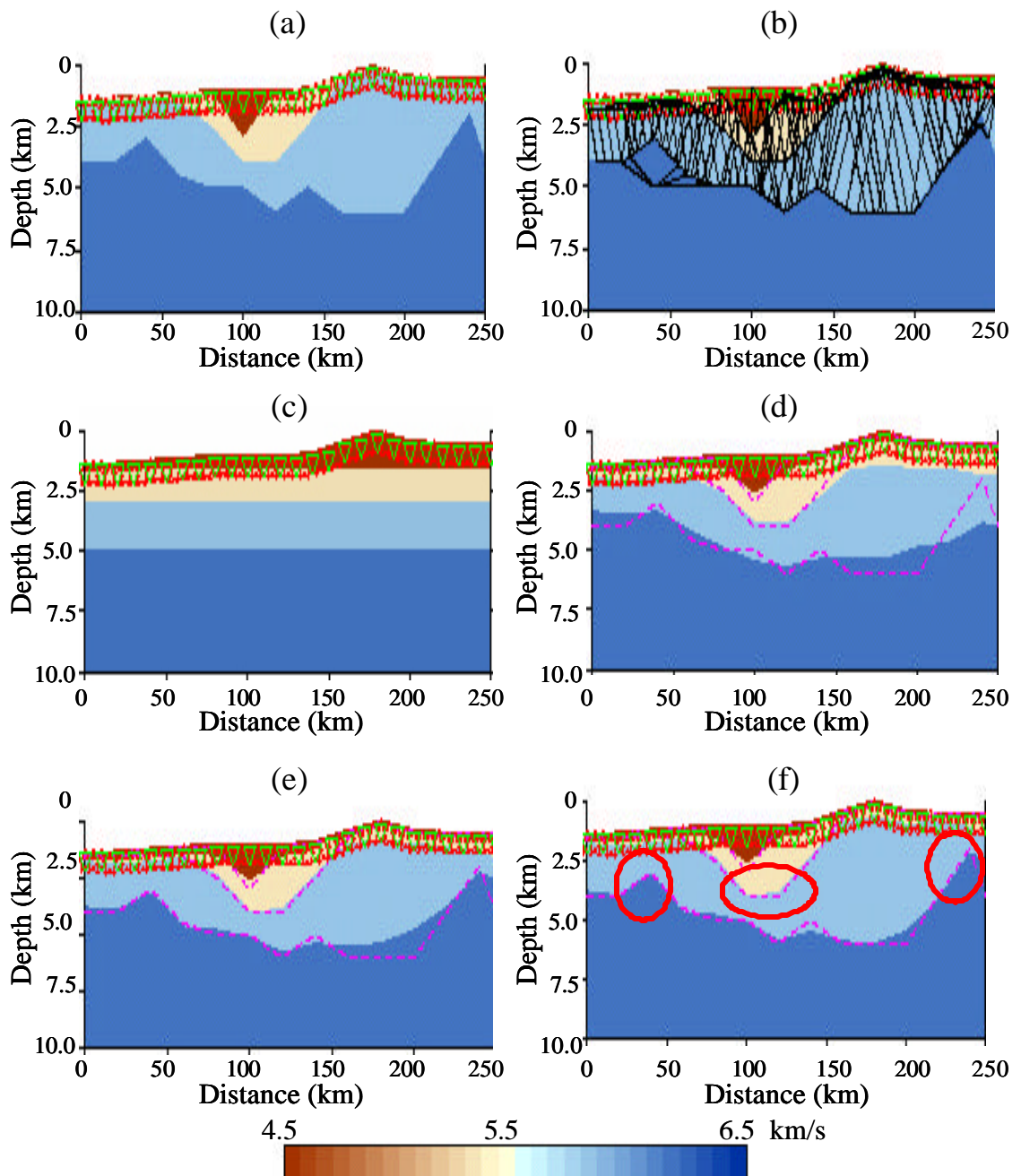


Figure 3.1. Results of the first-arrival tomography applied to the LARSE line in Southern California. (a) True model, (b) raypaths in the true model, (c) initial model, (d) result after two iterations, (e) result after four iterations, and (f) result after six iterations. I used 26 surface sources (red stars) and 51 surface receivers (green triangles) and completely recovered the geometry of the true model (dashed line on d-f). The DLT method proved to be very accurate since pronounced features (indicated with red circles) have been recovered.

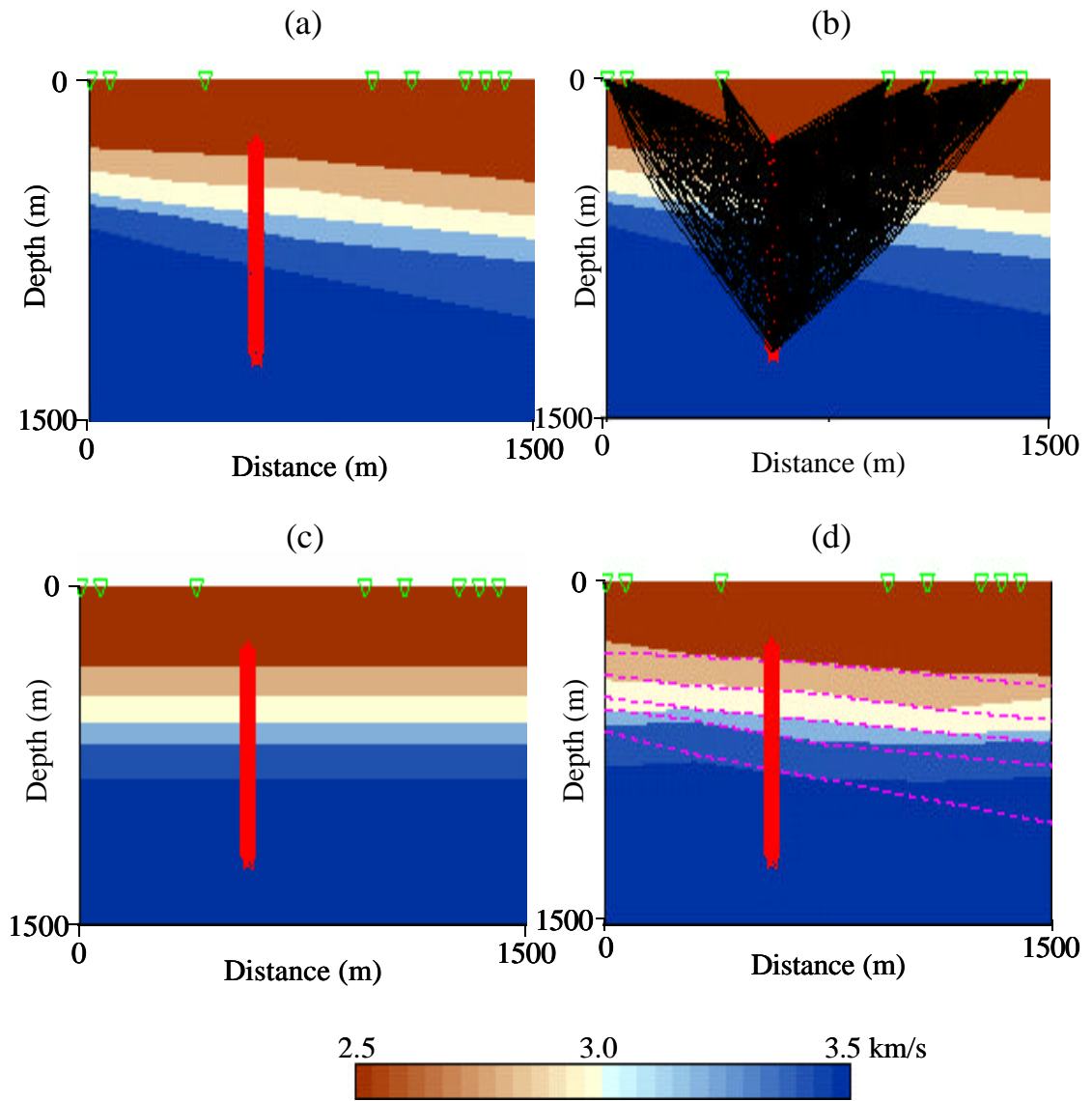


Figure 3.2. Results of first-arrival tomography for the model based on Vinton Dome, using VSP geometry. (a) True model, (b) raypaths in true model, (c) initial model, and (d) result after one iteration. Eight seismic sources (green triangles) generated energy recorded with 61 geophones located in the well (red line). Due to limited aperture and ray coverage, only the geometry of the central part of model is completely recovered.

Both of these experiments assumed that the subsurface velocities are well known, and the inversion is performed only for the geometry information. However, for the Vinton Dome area, the exact velocity values are not known, and therefore it is not possible to directly use the tested method to determine the velocity-interface depth model. Two additional synthetic experiments (Figures 3.3 and 3.4) were designed to understand if it is possible to recover some of the velocity information using first arrivals. For the synthetic example shown in Figure 3.3, inversion for the velocity values has been performed, assuming that geometry of the subsurface reflectors is known. Inversion for both velocities and interfaces has been performed for the synthetic case showed in Figure 3.4. For both experiments, first-arrival tomography recovered the velocity values in the cells covered by the raypaths. Thus, first-arrival tomography can reduce the range of velocities and enable more stable seismic inversion.

These synthetic tests imply that:

- It is essential to determine ray coverage in order to be confident in the inversion results.
- First-arrival tomography recovers the geometry of the subsurface reflectors in all areas with ray coverage, when the correct velocity values are specified in the initial model and kept constant during inversion.
- First-arrival tomography provides a good determination of the velocity values, and should be useful at Vinton Dome.
- First-arrival tomography cannot be used to simultaneously determine reflector geometry and velocity values with a high level of confidence.

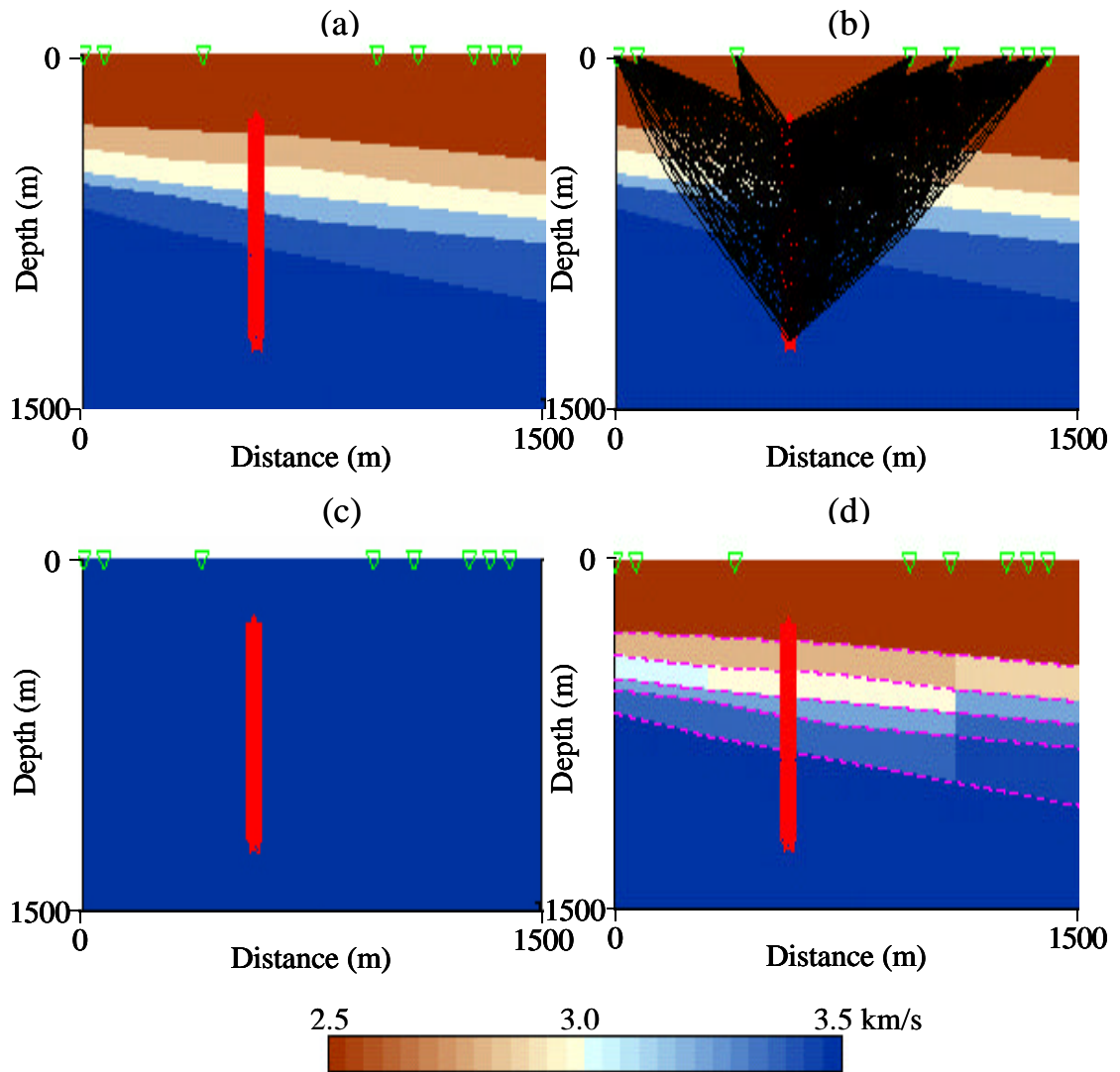


Figure 3.3. Results of the first-arrival tomography for the model based on Vinton Dome, using VSP geometry. (a) True model, (b) raypaths in the true model, (c) initial model, and (d) result after six iterations. Eight seismic sources (green triangles) generated energy recorded with 61 geophones located in the well (red line). I tried to recover only the velocity values, assuming that the reflector geometry is known. Good results are obtained in the area with sufficient ray coverage.



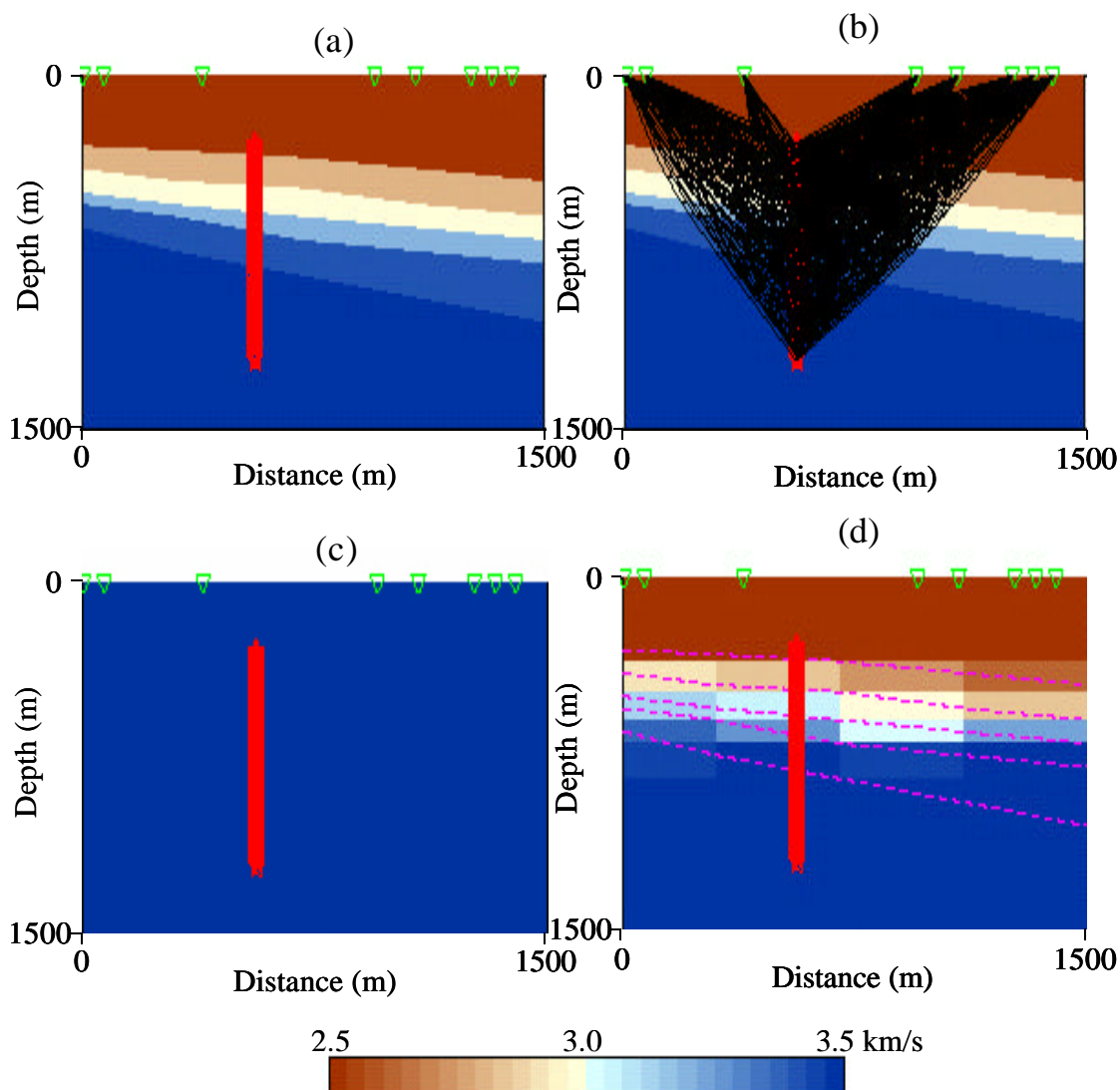


Figure 3.4. Results of the first-arrival tomography for the model corresponding to the Vinton Dome, using VSP geometry. (a) True model, (b) raypaths in the true model, (c) initial model, and (d) result after two iterations. Eight seismic sources (green triangles) generated energy recorded with 61 geophones located in the well (red line). I tried to recover both the reflector geometry and the velocity values for the examined layers, starting with flat layers with uniform velocity. Although I did not manage to invert for the subsurface geometry, the velocity values in the area with ray coverage are well recovered.

### 3.2. Cell-based reflection tomography

In all synthetic tests illustrated in this sections, it is assumed that velocities are known. Therefore, I performed inversion for the interface geometry only. If the inversion for both the interfaces and the velocity values was performed using cell-based reflection tomography, the algorithm became unstable.

In order to test the performance of the cell-based reflection tomography algorithm, two models were designed. A crustal model for the LARSE1 line in the Southern California has depth of 40 km and length of 250 km (Figure 3.5a). Rays are traced from 13 surface sources separated by 20 km to 26 surface receivers (with equal separation of 10 km). The subsurface structure has been completely recovered after three iterations (Figure 3.5c-f), including the “topographic high” in the middle of the profile, corresponding to the structure of the Mohorovicic discontinuity.

In order to illustrate the need to use both first arrivals and reflections for tomographic velocity model building, two tomographic results (using first arrivals vs. using reflection events) are compared for the LARSE 1 model (Figure 3.6). It can be seen that first arrivals (Figure 3.6b and 3.6d) cover only the uppermost portion of the profile and they cannot be used to invert for the geometry of the deeper portion of the section. In order to obtain geometry information on the deeper portions of the section, reflection events should be used (Figures 3.6a and 3.6c). However, reflections cannot completely recover the structure of the shallow part and this implies the necessity of using both the first arrivals and reflections contained within a seismic section.

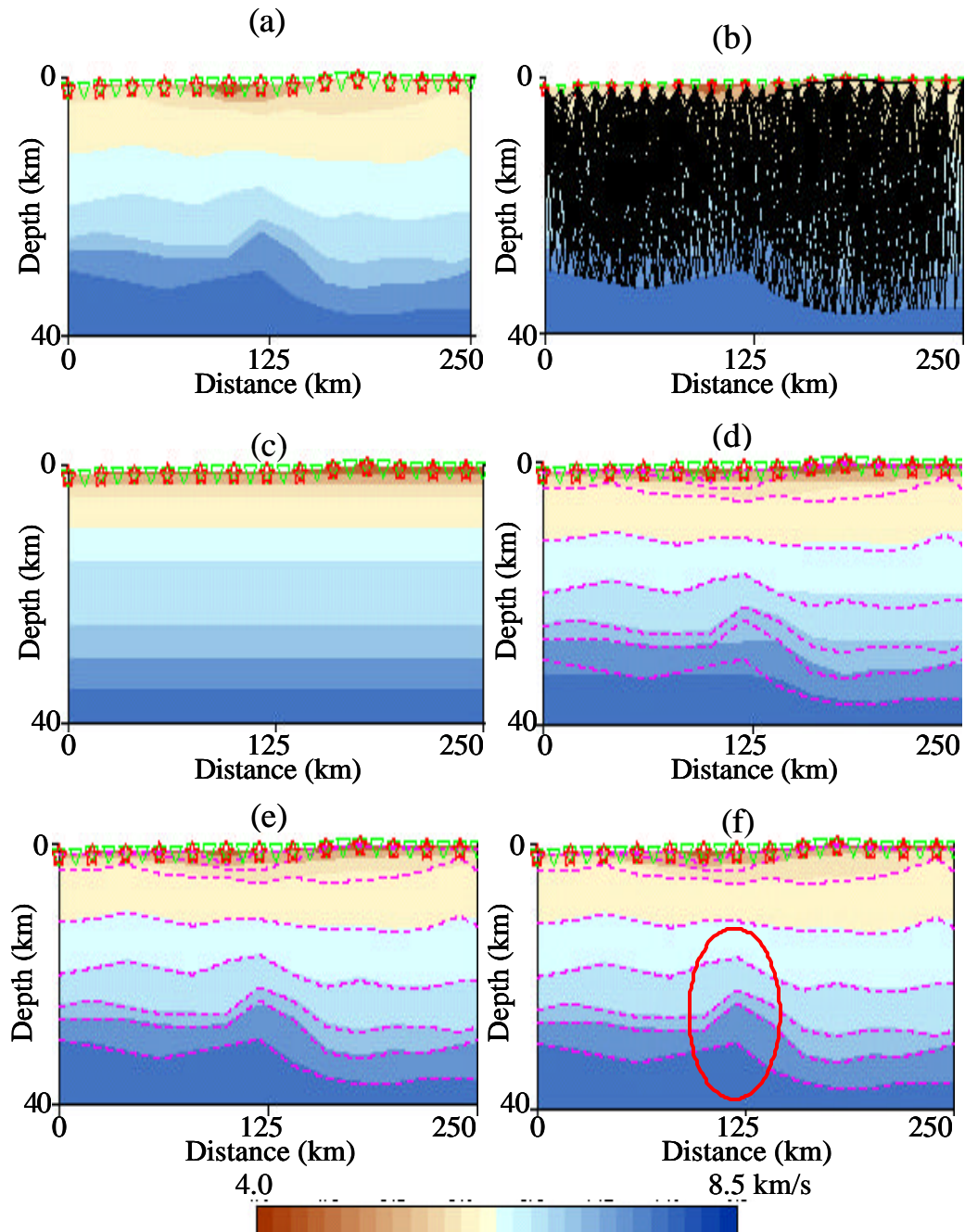


Figure 3.5. Results of cell-based reflection tomography for the model corresponding to the LARSE1 line in Southern California. (a) True model, (b) raypaths in the true model, (c) initial model, (d) result after one iteration, (e) result after two iterations, and (f) result after three iterations. I used 13 surface sources (red stars) and 26 surface receivers (green triangles) and managed to completely recover the interface geometry (shown as dashed line on d-f). The DLT method proved to be accurate, and pronounced features, such as the topographic highs in the middle profile corresponding to the Moho interface were recovered.

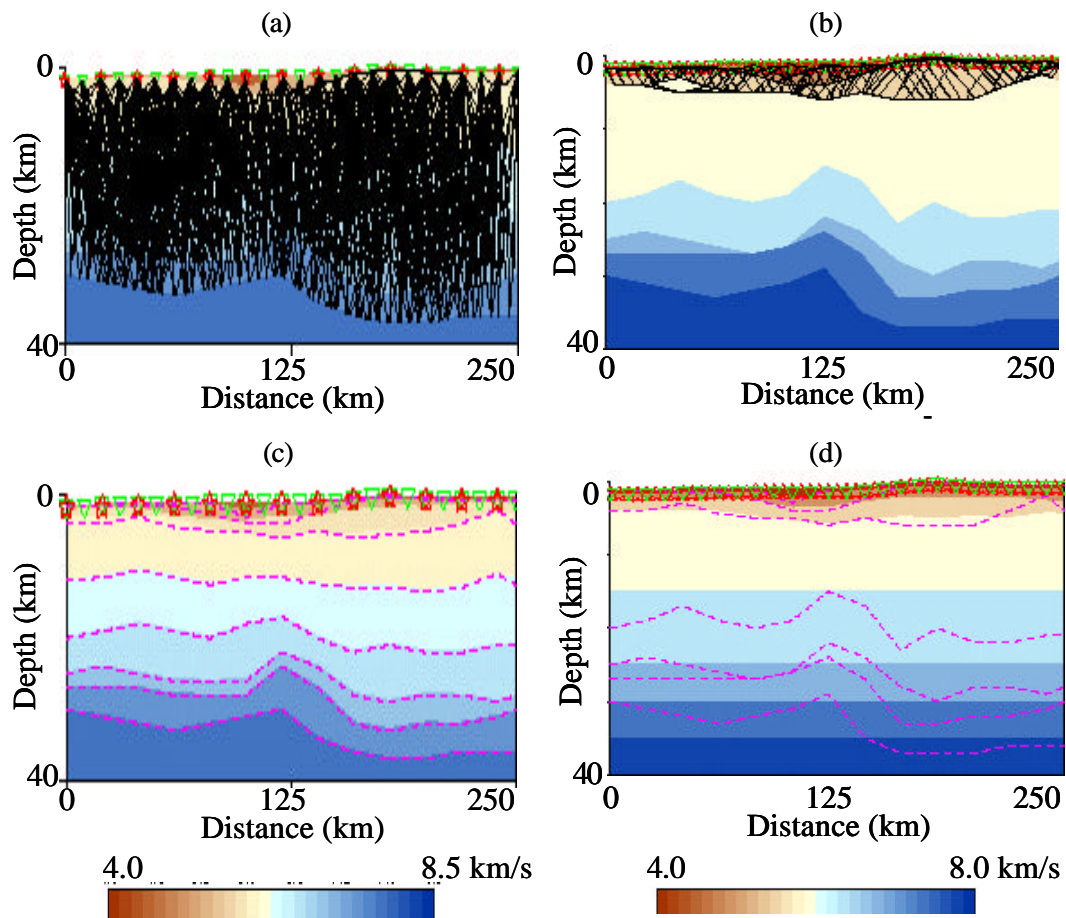


Figure 3.6. Comparison of the results obtained by first-arrival and reflection tomography. (a) Reflection raypaths in the true model, (b) refraction raypaths in the true model, (c) result after three iterations using the reflection DLT, and (d) result after three iterations using the first-arrival DLT. Since refraction events are restricted to the shallower parts of the model, reflections have to be used to construct the velocity model for the deeper section.

In the model corresponding to the sedimentary portion of the Vinton Dome (Figure 3.7a), rays were traced using a realistic VSP survey geometry (Figure 3.7c). For the three-columns model parameterization, subsurface reflector geometry has been completely recovered in the third iteration (Figure 3.7d). Compared to the results of the first-arrival tomography (Figure 3.2), reflection events enable better inversion for the interface geometry. However, small discrepancies between the true model and the inversion results exist at the right side of the model, due to the imperfect ray coverage.

In conclusion, the cell-based reflection tomography is an adequate method for the determination of the subsurface geometry (when true velocity is known). Reflections better recover information in the deeper portions of the section. In order to get information on the shallow portion of the section, it is necessary to implement first arrival traveltimes. Synthetic tests, where both velocity and geometry are unknown, were unstable and did not provide adequate results. Velocity values need to be inferred from other methods, such as the first-arrival tomography.

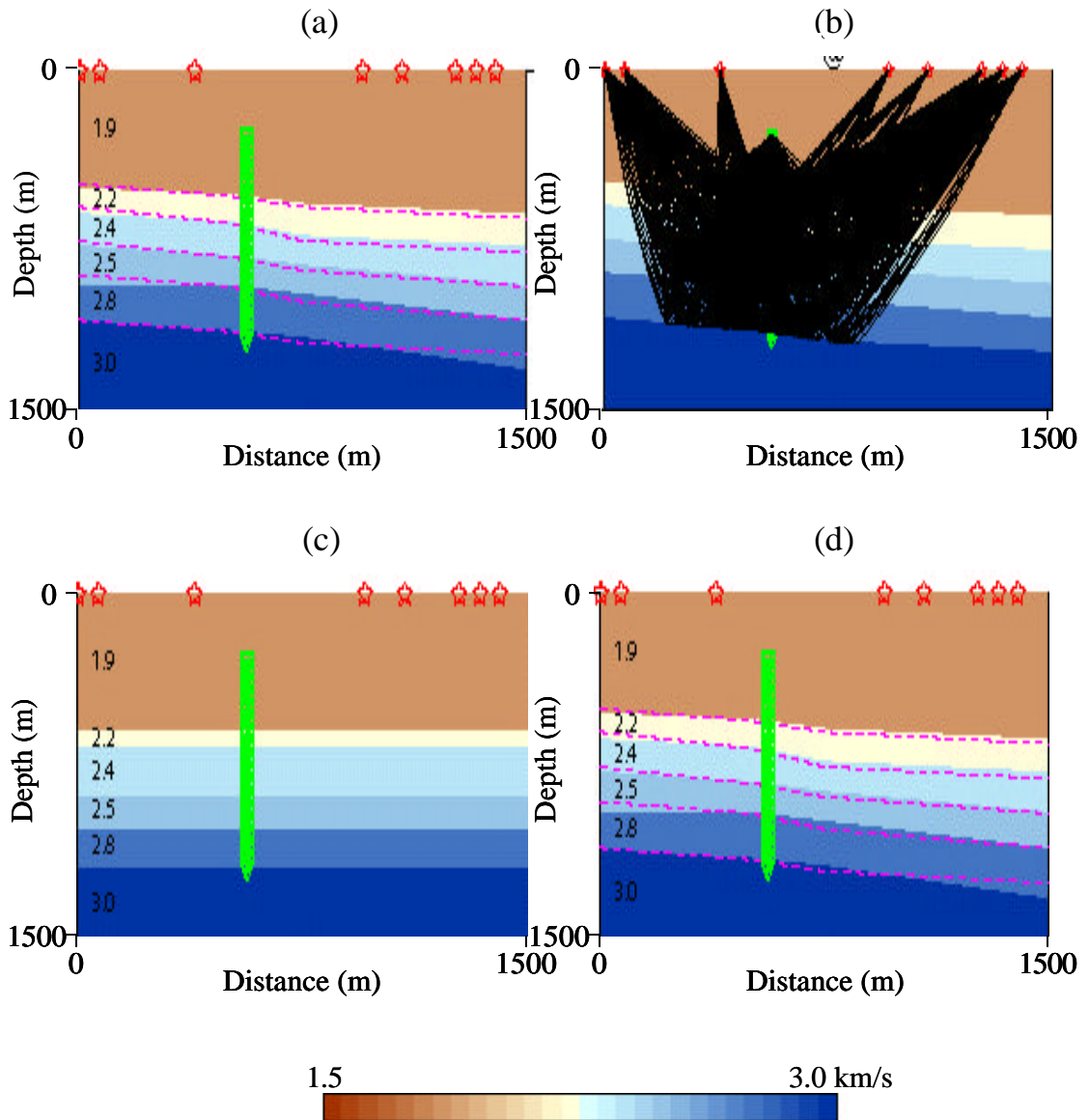


Figure 3.7. Results of the cell-based reflection tomography for the model corresponding to the Vinton dome sediments. (a) True model, (b) raypaths in the true model, (c) initial model, and (d) result after two iterations. VSP geometry corresponds to the real data acquisition. Sources are shown as red stars and receivers as green triangles. Geometry of the subsurface reflectors is recovered after two iterations, except in the areas with poor ray coverage.

### **3.3. Reflection deformable layer tomography**

Since synthetic testing of the cell-based version of reflection tomography showed that the inversion is unstable when both reflection interfaces and velocities are determined, the deformable layer tomography method was developed. DLT allows for both geometry and velocity variation during inversion, with the velocity having the same value for all cells within a layer. This approach toward the model parameterization enables more stability due to the relatively smaller number of unknowns to be determined.

Synthetic testing performed for the LARSE 1 line in Southern California (Figure 3.8) indicates that geometry of the subsurface reflectors can be inverted successfully. Although I allowed varying velocity values during the inversion process, the velocity values obtained during tomographic inversion corresponded to those in the true model. However, when a similar test was performed for a model where the initial velocity values were different from the true, the DLT algorithm did not converge toward the real model. This method is stable if a rather limited range of velocities, close to the real one, is included into the initial model. Therefore, it is necessary to perform cell-based tomography to reduce the range of velocities and improve the knowledge of the subsurface geometry and then use this information in the DLT inversion to improve the result.

Similarly, testing for the VSP Vinton Dome model (Figure 3.9), indicated that satisfactory inversion results could be obtained in the area with adequate ray coverage.

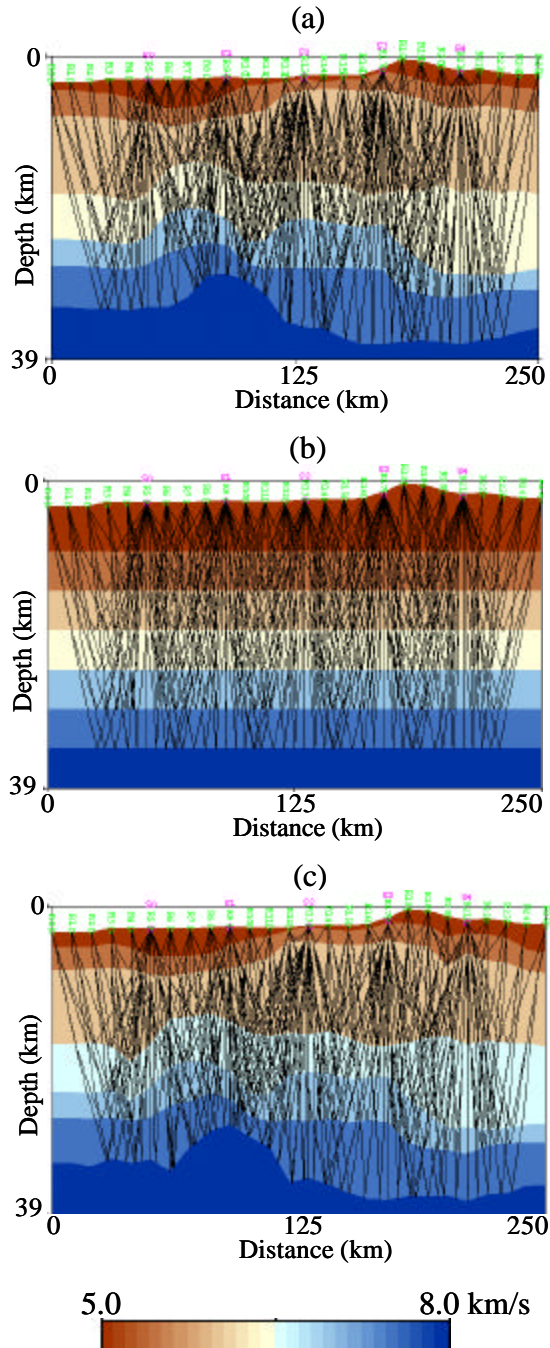


Figure 3.8. Results of the reflection DLT for the model corresponding to the LARSE line in Southern California. (a) Raypaths in the true model, (b) raypaths in the initial model, and (c) result after five iterations. Five surface sources (red) and 26 receivers (green) are used. The subsurface structure is recovered, even in areas with pronounced structure.



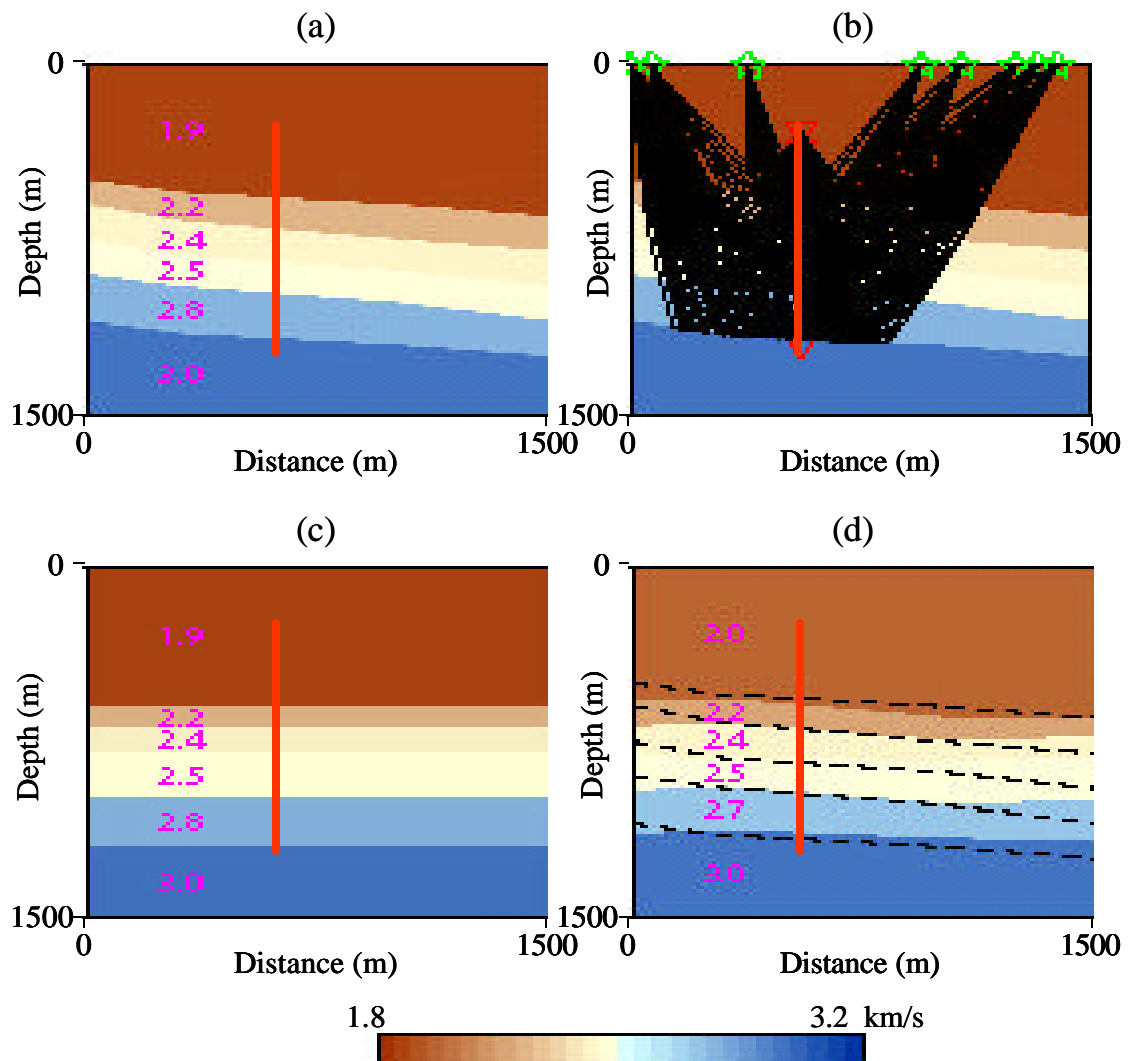


Figure 3.9. Results of reflection DLT for the model corresponding to the Vinton Dome sedimentary layers. (a) True model, (b) raypaths in the true model, (c) initial model, and (d) result after one iteration. I used 8 surface sources and 61 receivers placed in the well (shown with thick red line). Geometry of the subsurface reflectors is recovered in the area with ray coverage.

In conclusion, the deformable layer reflection tomography performs successful inversion for both the velocity values and the reflector geometry in all areas with sufficient ray coverage, for an initial model where the velocity values are close to the true ones. Before performing DLT, it is necessary to reduce the initial range of velocities using the other, previously described tomographic algorithms.

### **3.4. Converted wave tomography**

All synthetic tests described so far were designed for P-waves. As explained earlier, as an extension of this research, I plan to perform S-wave velocity model building using P-S converted waves. An example for the performance of converted wave tomography is given in Figure 3.10. The true P- and S-wave velocity models (Figures 3.10a and 3.10c) consist of 3 dipping layers, with the values of P-wave velocities being two times bigger than the ones for S-waves. Initial models were designed to be flat with the velocity values of each layer being different from the true one. The velocity-interface depth model has been recovered after three iterations for both P-P and P-S reflections.

Since primary emphasis has been given to building a P-wave velocity model using the VSP data, a converted wave deformable layer tomography algorithm is not developed. It is necessary in the next stage of the research to develop a reflection DLT algorithm for converted waves and test it with synthetic and real data.

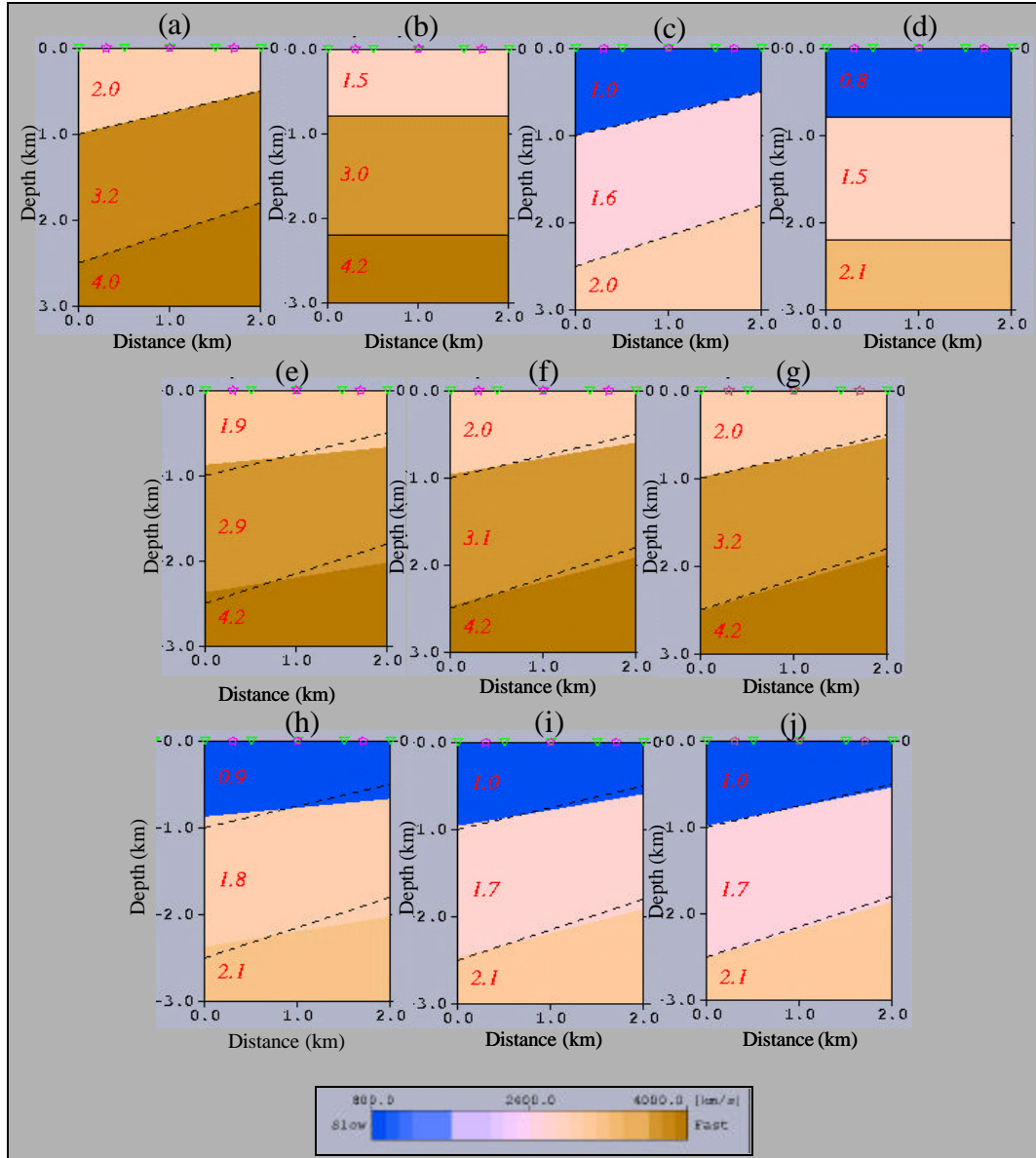


Figure 3.10. Synthetic testing of the cell-based converted wave reflection tomography. (a) True  $v_p$ /interface model, (b) reference  $v_p$ /interface model, (c) true  $v_s$ /interface model, (d) reference  $v_s$ /interface model, (e) 1<sup>st</sup> iteration for  $v_p$ /interfaces, (f) 2<sup>nd</sup> iteration for  $v_p$ /interfaces, (g) 3<sup>rd</sup> iteration for  $v_p$ /interfaces, (h) 1<sup>st</sup> iteration for  $v_s$ /interfaces, (i) 2<sup>nd</sup> iteration for  $v_s$ /interfaces, and (j) 3<sup>rd</sup> iteration for  $v_s$ /interfaces. Stars show position of sources, triangles position of receivers, and dashed line indicates the true interface position.

### **3.5. Kirchhoff migration**

Quality control of a velocity model represents an important part of the traveltime tomography. The first criterion for the quality control is statistical. An additional quality control criterion is the flatness of the events on common image gathers after migration. Dr. Hua-wei Zhou has developed a Kirchhoff migration code. It is designed for a fast evaluation of a velocity model; it needs to be refined further in order to be used for migration purposes. A synthetic example for the performance of this migration algorithm is given in Figure 3.11. The true model (Figure 3.11a) corresponds to the flanks of a salt body, with the VSP receivers in the well. The position of the reflectors after migration is indicated with red circles in Figure 3.11b. It can be seen that Kirchhoff migration gives the reflector position corresponding to the true one, but only in the areas with sufficient ray coverage. This migration algorithm can be also used to examine the ray coverage and the confidence level of the seismic image.

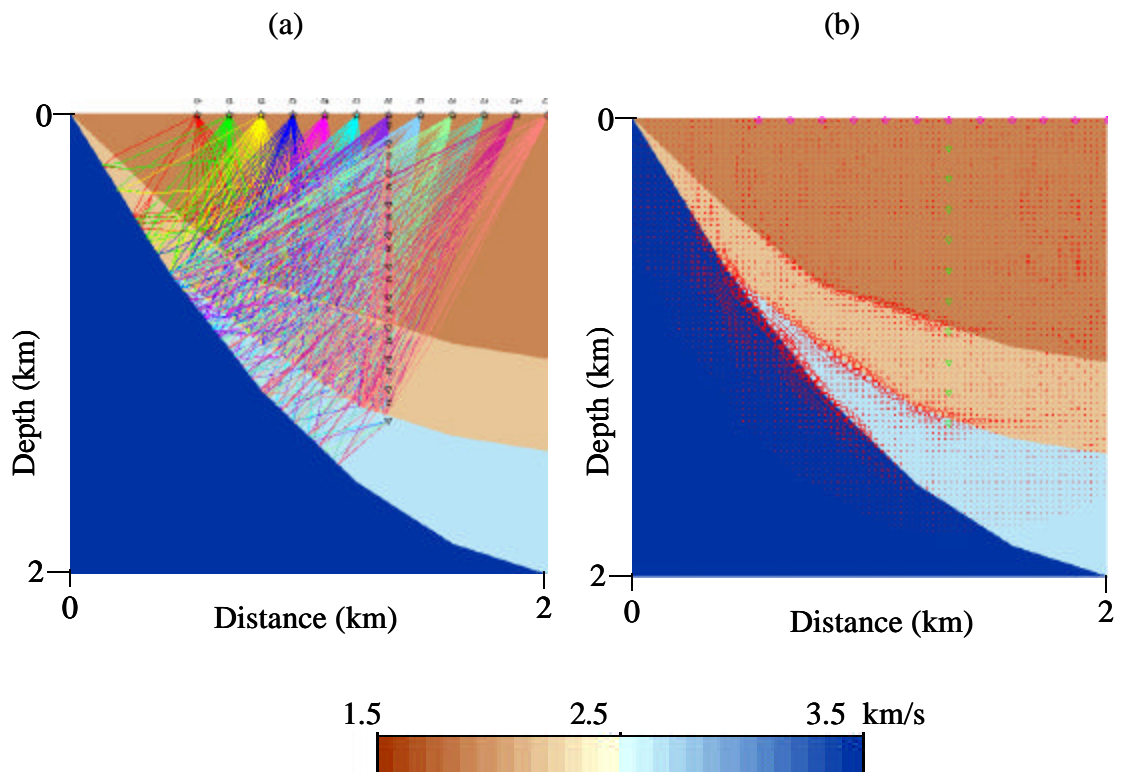


Figure 3.11. Synthetic test of Kirchhoff migration algorithm for a salt model. (a) True model with raypaths from 12 surface sources to the receivers placed in the well, and (b) migration result (position of circles indicate location of reflectors, matching the position of the geologic boundaries in the synthetic salt model).

## 4. Results

In the previous chapters seismic tomography was defined as a method that simultaneously determines interval velocities and reflection interfaces. The goal of the research is to determine a velocity-interface depth model for the Vinton Dome area. This research is a part of an effort of the Allied Geophysical Laboratories to image a 3D VSP dataset. To avoid inherent problems of the non-uniqueness and instability, other geophysical and geologic data have been incorporated into the tomographic process:

- 3D-3C VSP shot gathers,
- time-migrated surface seismic data,
- well logs with stratigraphic markers, and
- initial background velocity model.

The general flow applied for the building of the velocity-interface depth model is given in Figure 4.1. Since tomography has been applied in 2D, we have selected a representative area for our analysis based on the results of the 3D seismic interpretation and the VSP survey geometry. Numerical modeling is performed in the initial model, and its results facilitated event recognition and picking. Once the initial model was established and the traveltimes picked on the real data, seismic tomography has been applied. As the final step, seismic migration is used as a tool to evaluate quality of the velocity-interface depth model. Each of the five basic steps applied for the area of the Vinton Dome was complex and required a series of analyses. This chapter contains descriptions of the analyses performed, results obtained, and a discussion of the results.

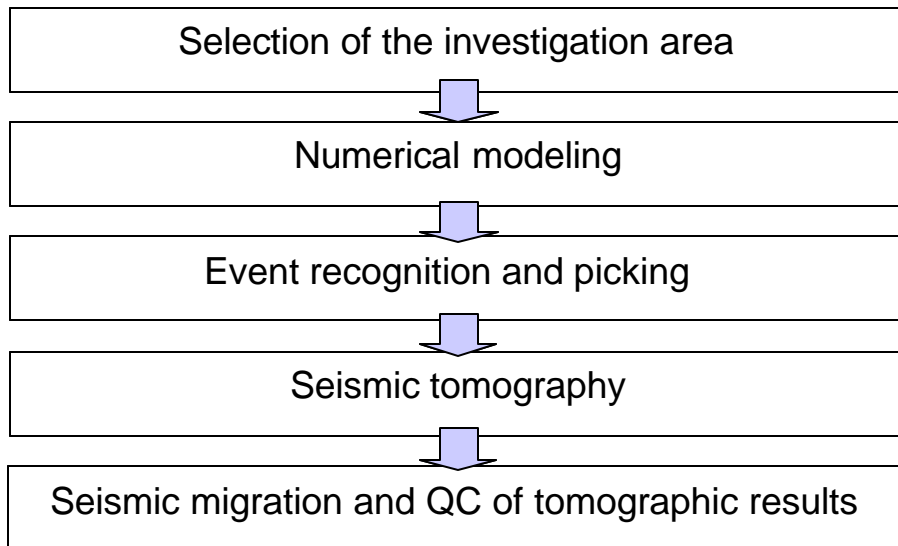


Figure 4.1. General flow for velocity-interface depth model building applied to Vinton Dome VSP data.



## **4.1. Analyses preceding tomographic application**

The two initial steps shown in Figure 4.1, selection of the investigation area and numerical modeling, precede the tomographic application. Each of the steps has an important impact on the performance of seismic tomography and they will be explained in detail in this chapter.

### 4.1.1. Selection of the investigation area

Tomography has been performed in 2D. The basic assumption of 2D geophysical methods is that structure does not change in the direction perpendicular to the profile. The structure of the area has been defined using 3D seismic interpretation of the time-migrated surface seismic volume. The exact position of the profile for the velocity model building has been defined correlating structural information with the survey geometry information.

#### 4.1.1.1. 3D seismic interpretation

Understanding the geologic structure is necessary to select the representative profiles for the application of the 2D tomography. Structural interpretation has been performed on the time-migrated 3D seismic volume, provided by OPEX. Seven stratigraphic horizons, corresponding to the major geologic units previously described in the Chapter 1, have been interpreted: Upper Miocene, Upper-Middle Miocene, Middle Miocene, Top

Anahuac, A Sand, D Sand and Hackberry. In addition, geometry, nature and spatial distribution of the faults are determined. Interpretation has been performed in cooperation with Warren Duncan, Katarina Jovanovic and Marija Djordjevic.

The salt dome is located in the middle of the surveyed area and the salt area is depicted by the white color in Figures 4.2- 4.5. The salt body is narrower at the level of upper horizons, such as the Upper Miocene (Figure 4.2), and it widens with depth. Horizons are the shallowest near the dome, and deepen toward the periphery of the survey area. Dips of the horizons are in general steeper on the southern flank of the dome than on the northern flank. The whole area is characterized by normal faulting, generally oriented in the radial directions with respect to the salt body. Faulting does not disturb horizons in the northwest and the southwest quadrants of the survey. Definition of the fault planes is lost with depth, most probably because of the decrease of the seismic resolution with depth.

#### 4.1.1.2. Correlation of the seismic interpretation with the survey geometry

In order to apply 2D seismic tomography to the Vinton Dome, it was necessary to select areas with the sufficient survey coverage and a relatively simple geology, based on the results of the seismic interpretation. The VSP survey was conducted only in the north part of the area. The thick rectangle (Figures 4.2- 4.5) denotes the area covered by the VSP survey (Figures 4.2- 4.5). The selected profile for the application of the tomography is shown in Figure 4.6. This profile is oriented in the dip direction of the geologic strata, containing twenty shots. An additional criterion for the selection of this profile was the location of two wells with geophysical logs along the profile.

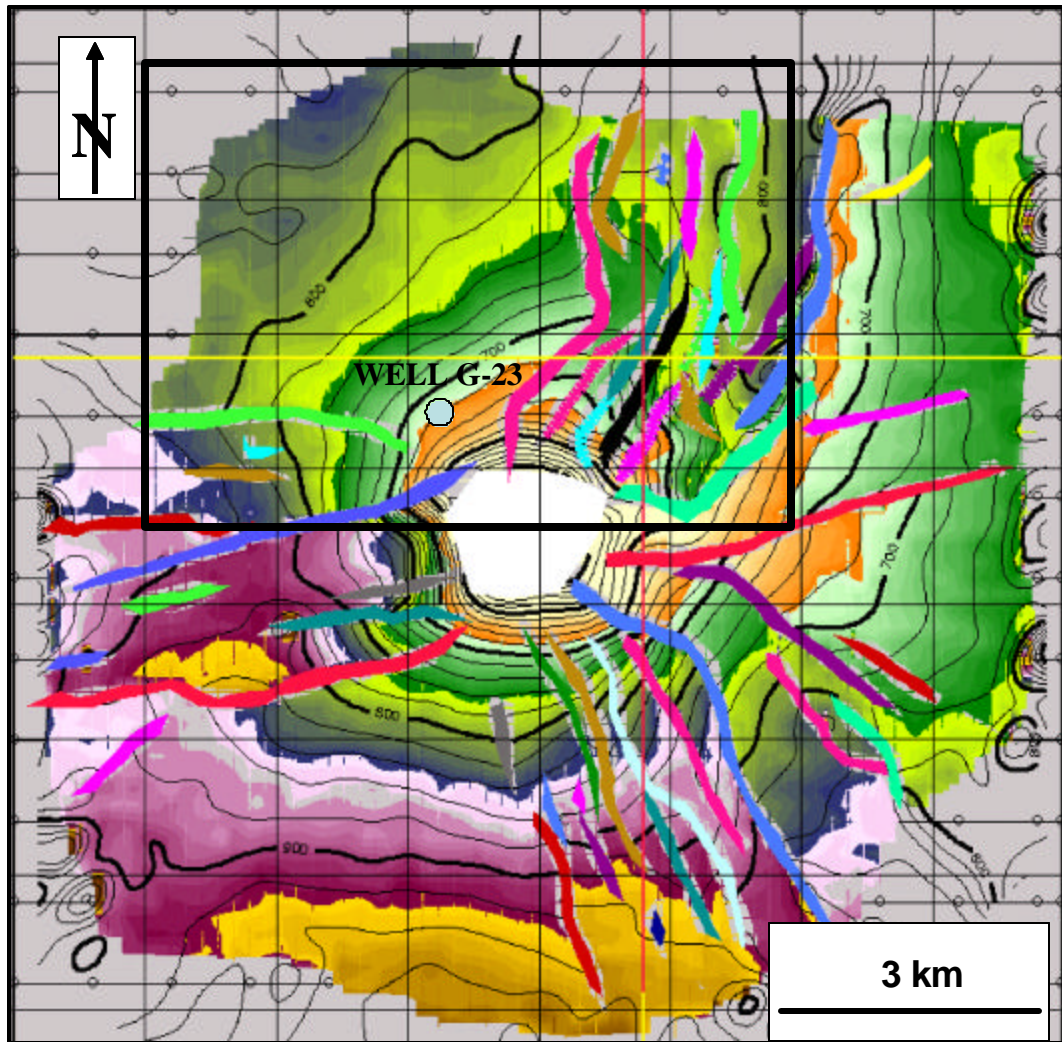


Figure 4.2. Structural map of the top Upper Miocene. Contour lines indicate the two-way travel time to the top of horizon. Radial colored lines are faults. The rectangle outlines the VSP survey area (data courtesy of OPEX).

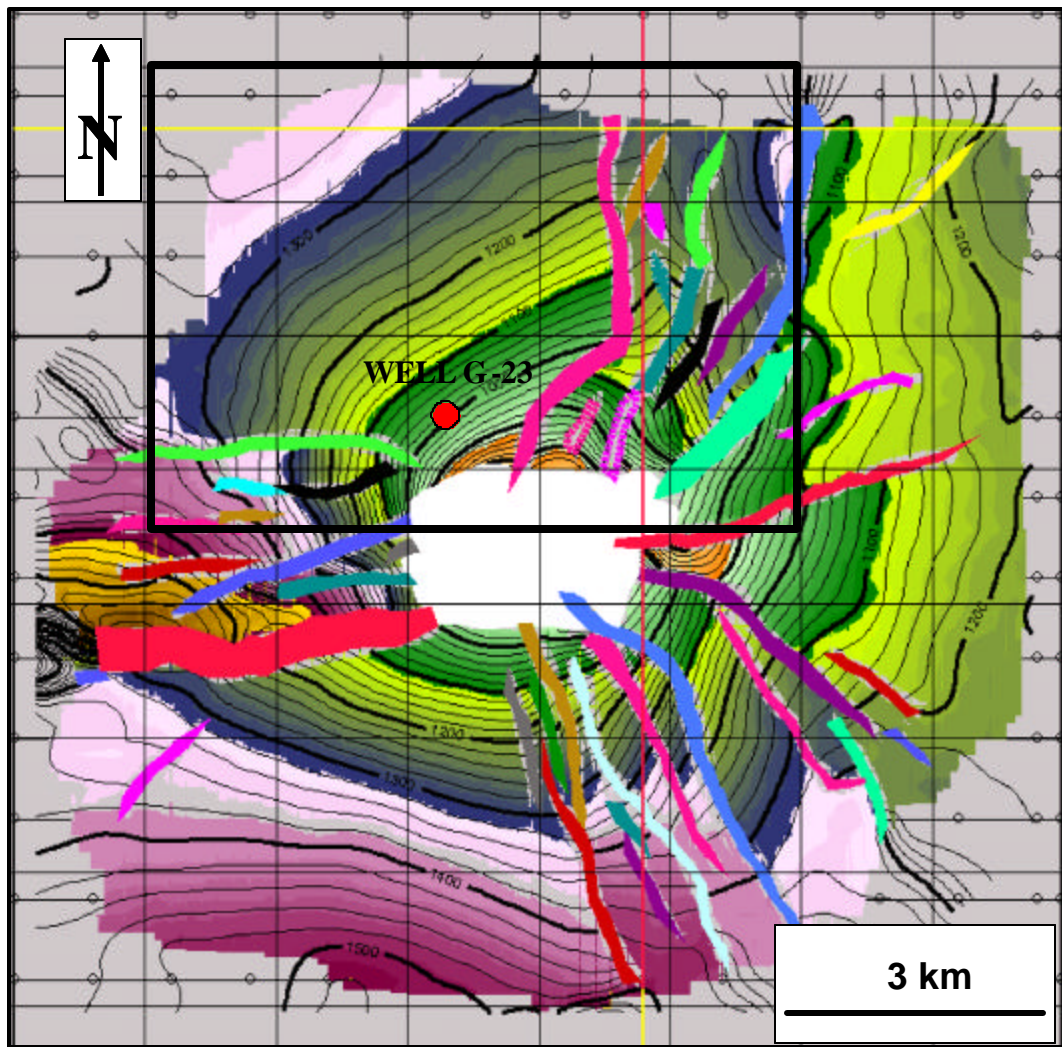


Figure 4.3. Structural map of the top Middle Miocene. Contour lines indicate the two-way travel time to the top of horizon. Radial colored lines are faults. The rectangle outlines the VSP survey area (data courtesy of OPEX).

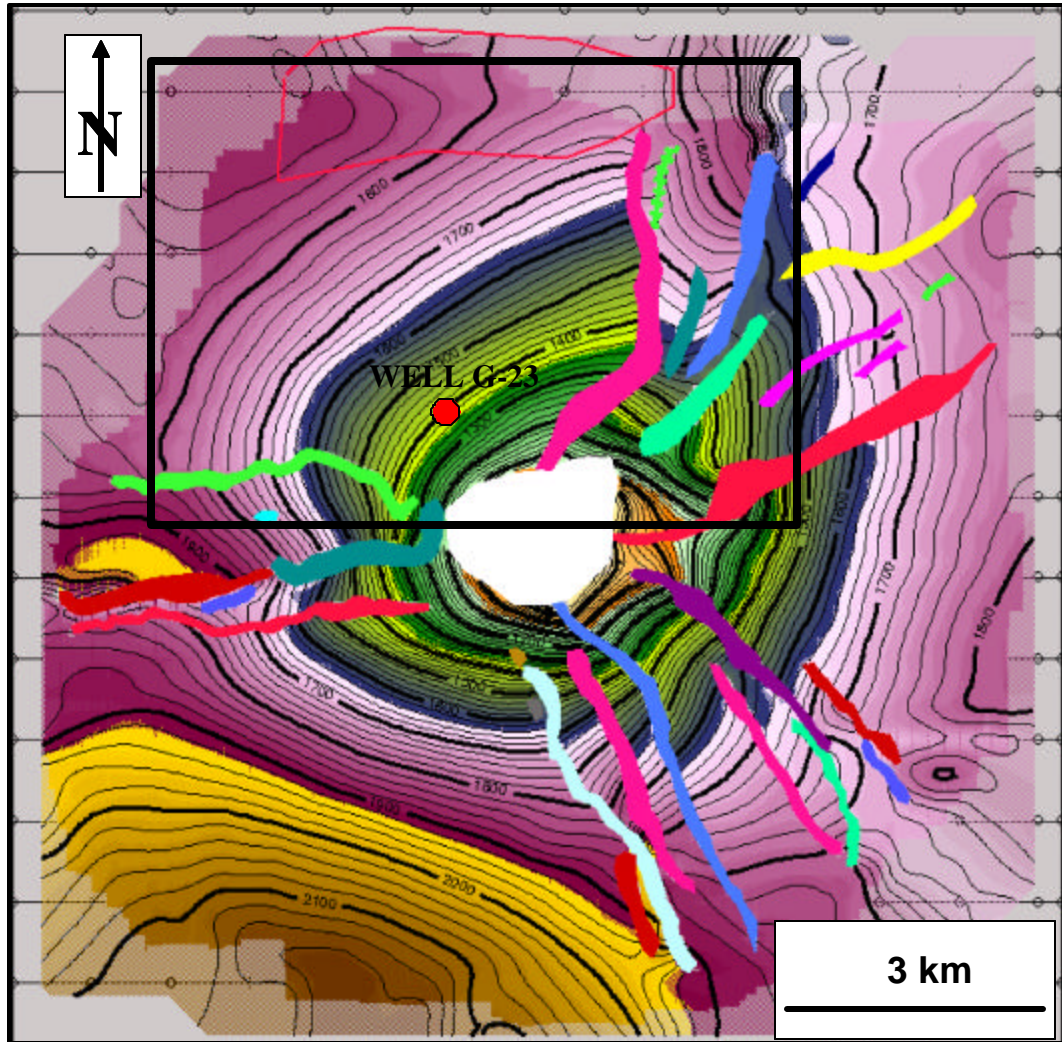


Figure 4.4. Structural map of the top Top Anahuac. Contour lines indicate the two-way travel time to the top of horizon. Radial colored lines are faults. The rectangle outlines the VSP survey area. The number of the faults is reduced compared with those seen in Figures 4.1-4.3, due to the decrease of the seismic resolution with depth (data courtesy of OPEX).

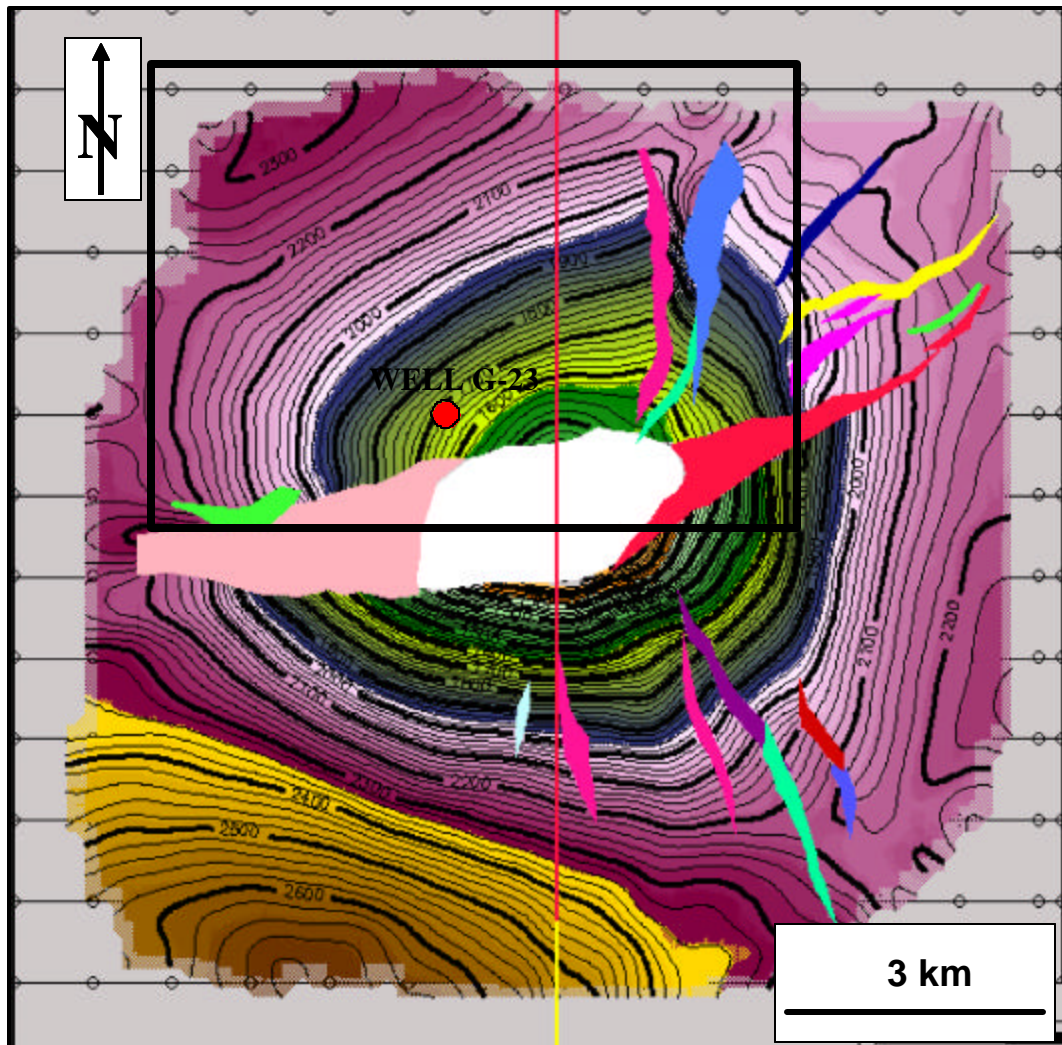


Figure 4.5. Structural map of the top D Sand. Contour lines indicate the two-way travel time to the top of horizon. Radial colored lines are faults. The rectangle outlines the VSP survey area. The number of faults is reduced compared with upper horizons, probably because of the decrease of the seismic resolution with depth. The colored areas indicate fault zones, where mapping of the individual faults was difficult (data courtesy of OPEX).

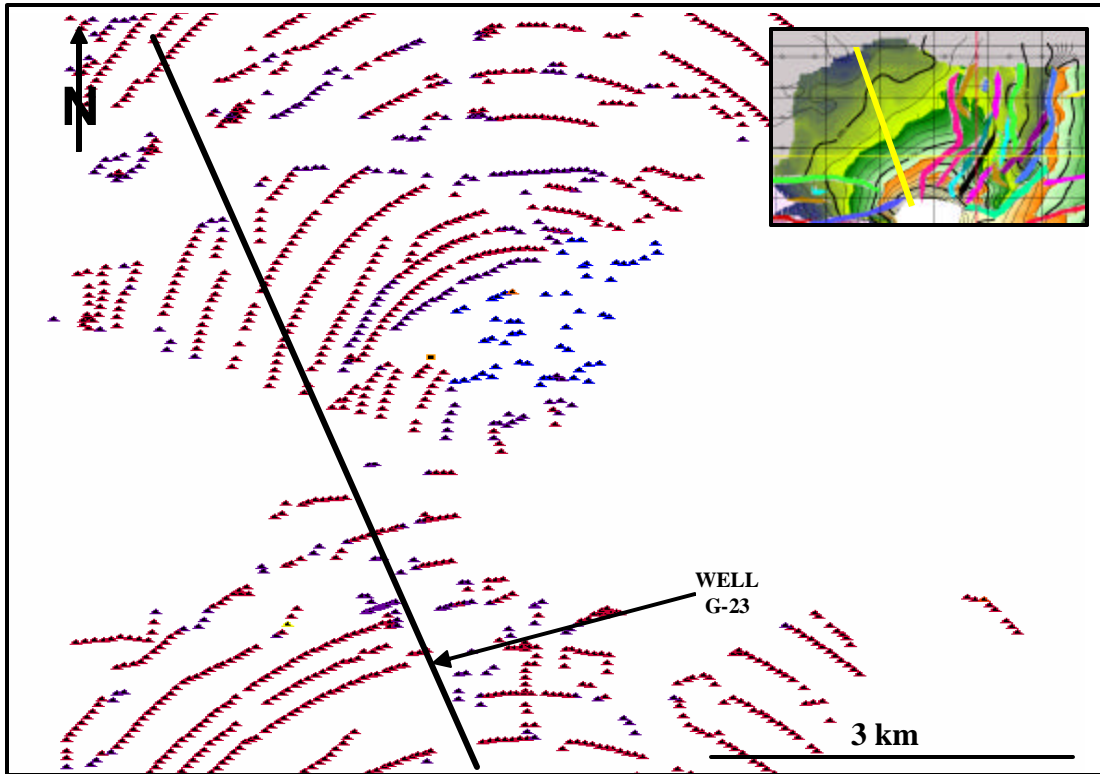


Figure 4.6. Position of the profile selected for the seismic tomography relative to the position of the shots (the circular lines of triangles) and the seismic horizons (inserted image). The selected profile contains 20 shots.

#### 4.1.2. Numerical modeling

##### 4.1.2.1. Construction of the initial velocity model

Dr. Hua-wei Zhou and Warren Duncan have constructed a 3D sediment velocity model, using information from twenty-six sonic logs. Velocity values for sedimentary layers, separated by seven previously described horizons, are defined in this model, with each layer having a vertical gradient of velocities. A profile of P-wave velocities has been extracted from the 3D volume (Figure 4.7). The average values of the velocities from this model has been used for the construction of the initial tomographic velocity model.

Traveltimes for seven horizons in the sedimentary portion of the section and the top of the salt have been picked (Figure 4.8) and converted to depth in order to obtain the initial model for the selected profile. The initial model (Figure 4.9) has eight sedimentary layers with constant velocities, separated by the horizons corresponding to the ones shown on the interpreted section. The salt body is located on the southeast (left) part of the profile.



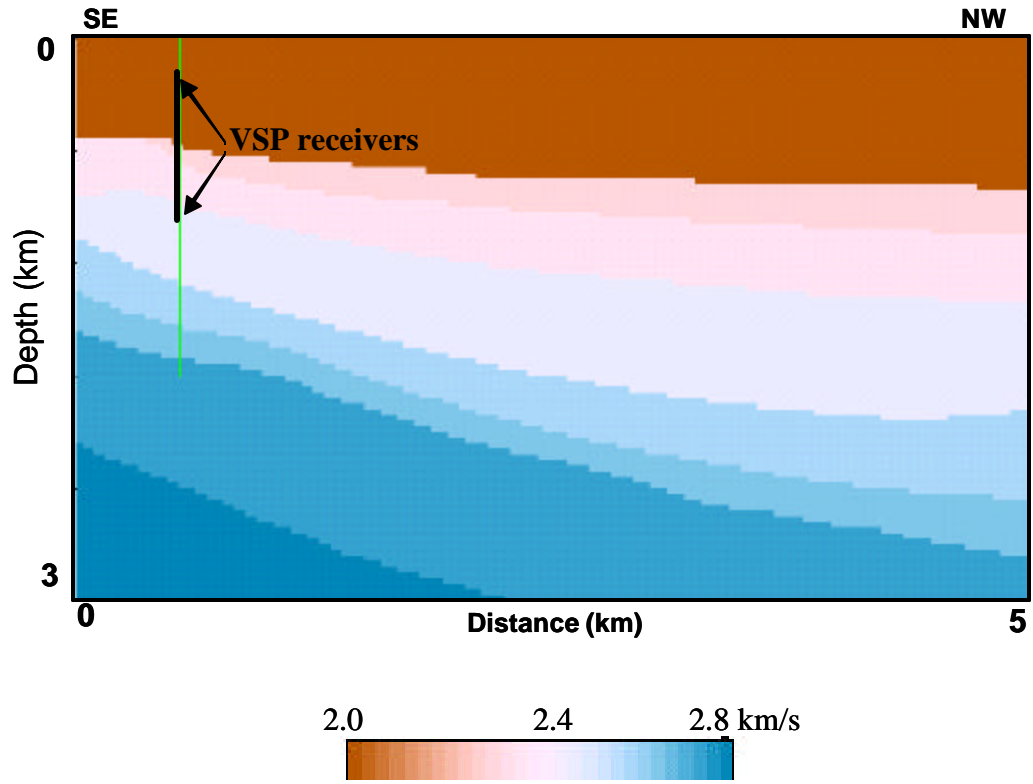


Figure 4.7. P-wave sediment model (courtesy of Zhou and Duncan). The model is constructed using velocity information from sonic logs.

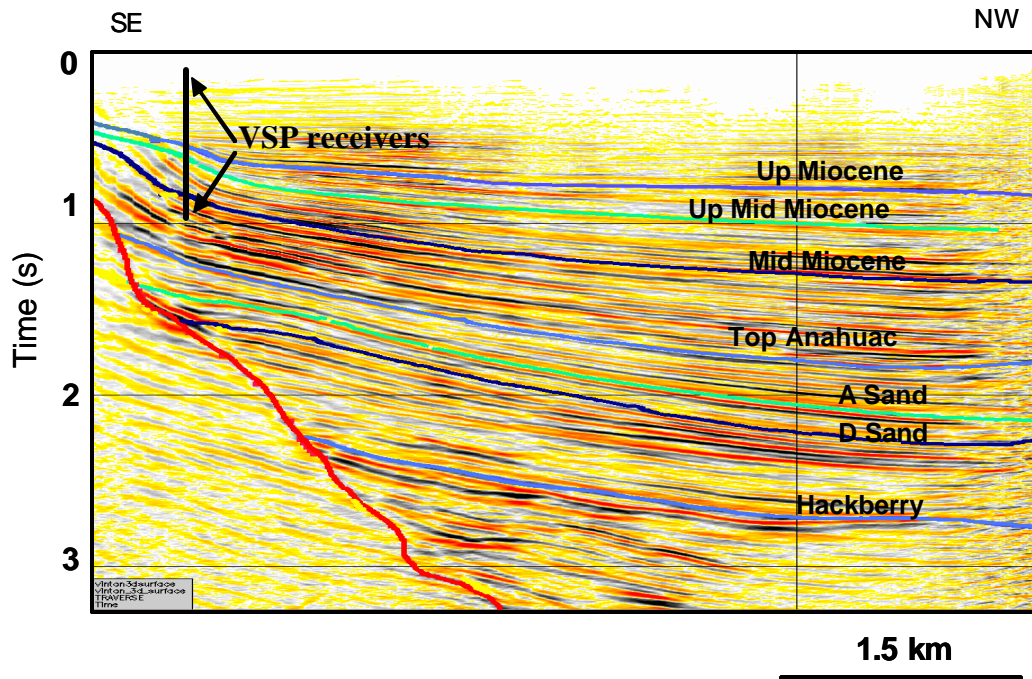


Figure 4.8. Vertical slice through the interpreted seismic volume corresponding to the selected profile.

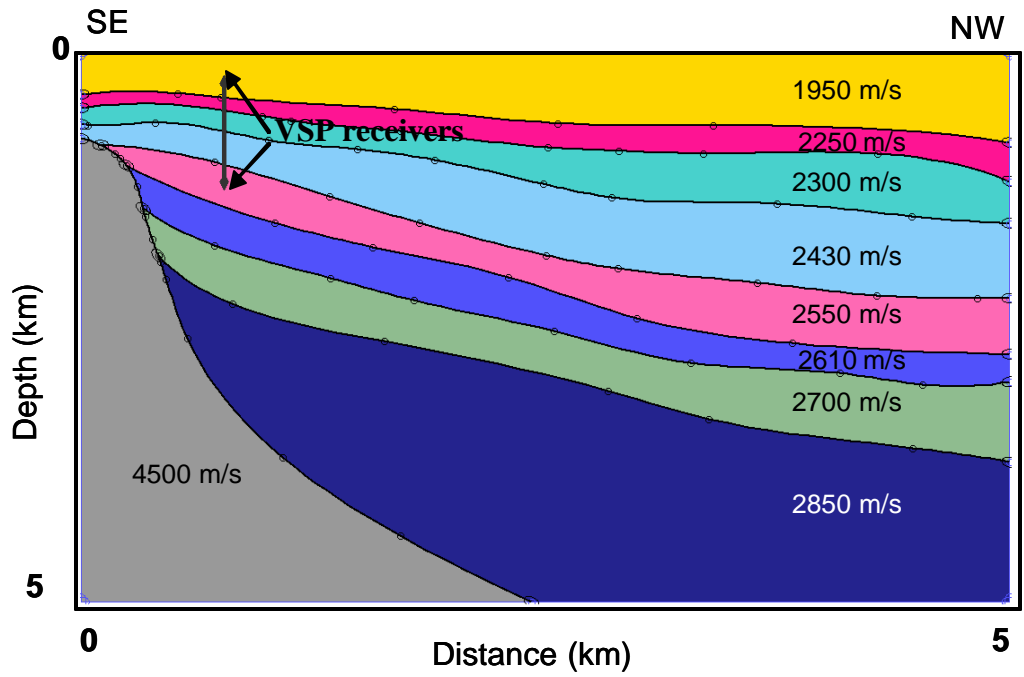


Figure 4.9. Seismic model constructed in GXii. The model consists of eight constant velocity sedimentary layers and the salt body.

#### 4.1.2.2. Ray-trace modeling

The primary goal of the numerical modeling performed in the initial model (Figure 4.9) is to facilitate the understanding and the recognition of events on the VSP records. I have used ray-trace program GXii. Characteristic synthetic data containing upgoing wavefield are shown in Figures 4.10- 4.12.

A near-offset section for a shot located 700m away from the well is shown in Figure 4.10. Upgoing reflections from five upper horizons and the top of the salt are recorded. Horizon reflections are linear, and the salt reflection is curved. For near-offset records, reflections from the top A Sand and the top of the salt coincide, suggesting that it is difficult to distinguish between these two events on the real data. Salt reflection and overlapping of horizon reflections are more pronounced for the shots in the proximity of the well.

A section for a shot with the offset of 1750m is shown in Figure 4.11. Reflections from all interfaces, except the Hackberry, are linear. The curvature of the top of the salt reflection is less evident than on the near-offset section (Figure 4.10). Events from the two upper horizons coincide, suggesting that identification on the real records might be difficult. Reflections from the salt and the top D Sand are crossing each other.

The character of the record for the offset of 3750m (Figure 4.12) is more complex. Reflection from a deeper horizon (Middle Miocene) is recorded earlier than one from the shallower horizon (Upper Miocene). In addition, overlapping of the reflections from the top D Sand and the top of the salt is pronounced. Reflection from the top Hackberry is recorded later than the reflection from the top of the salt.

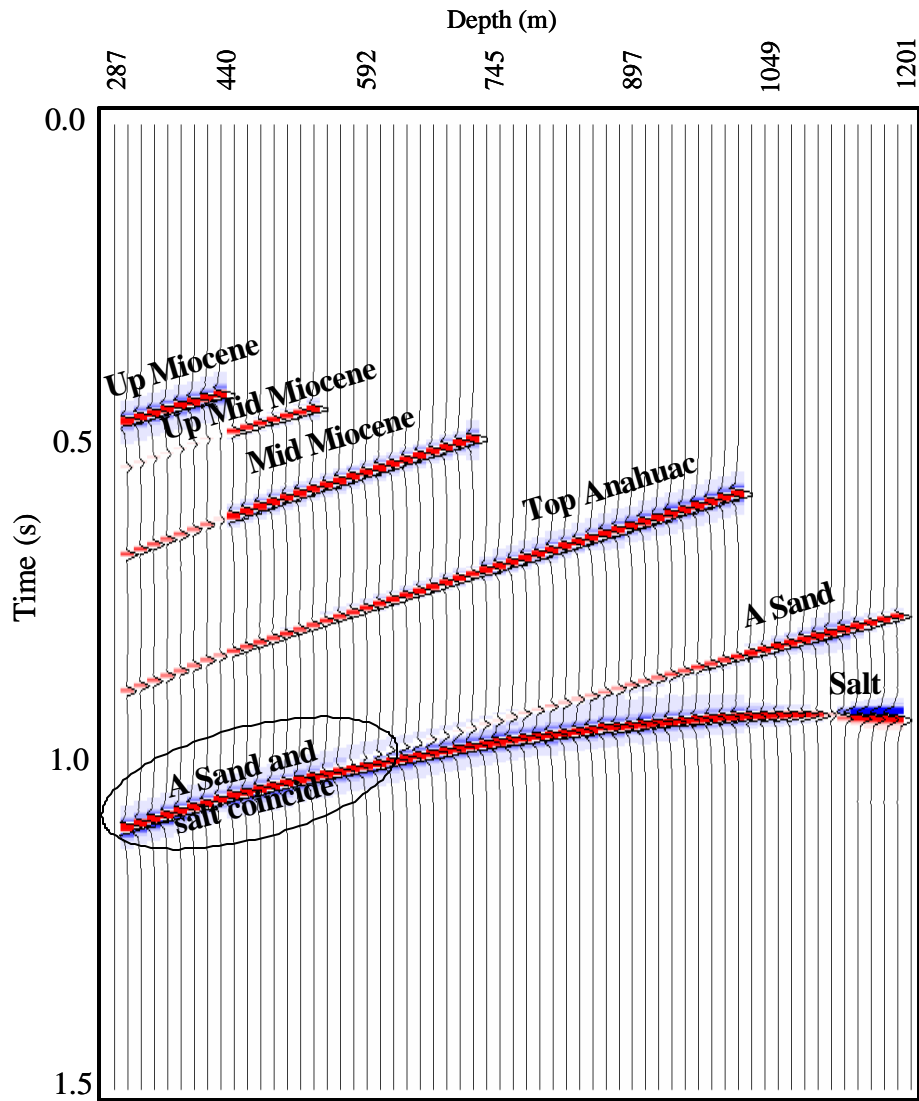


Figure 4.10. Synthetic seismogram calculated for shot 3302 located at  $x=1460\text{m}$  in the seismic model shown in Figure 4.9. All events represent upgoing P-wave reflections recorded on vertical geophone. The black ellipse indicates a region of coincident seismic events.

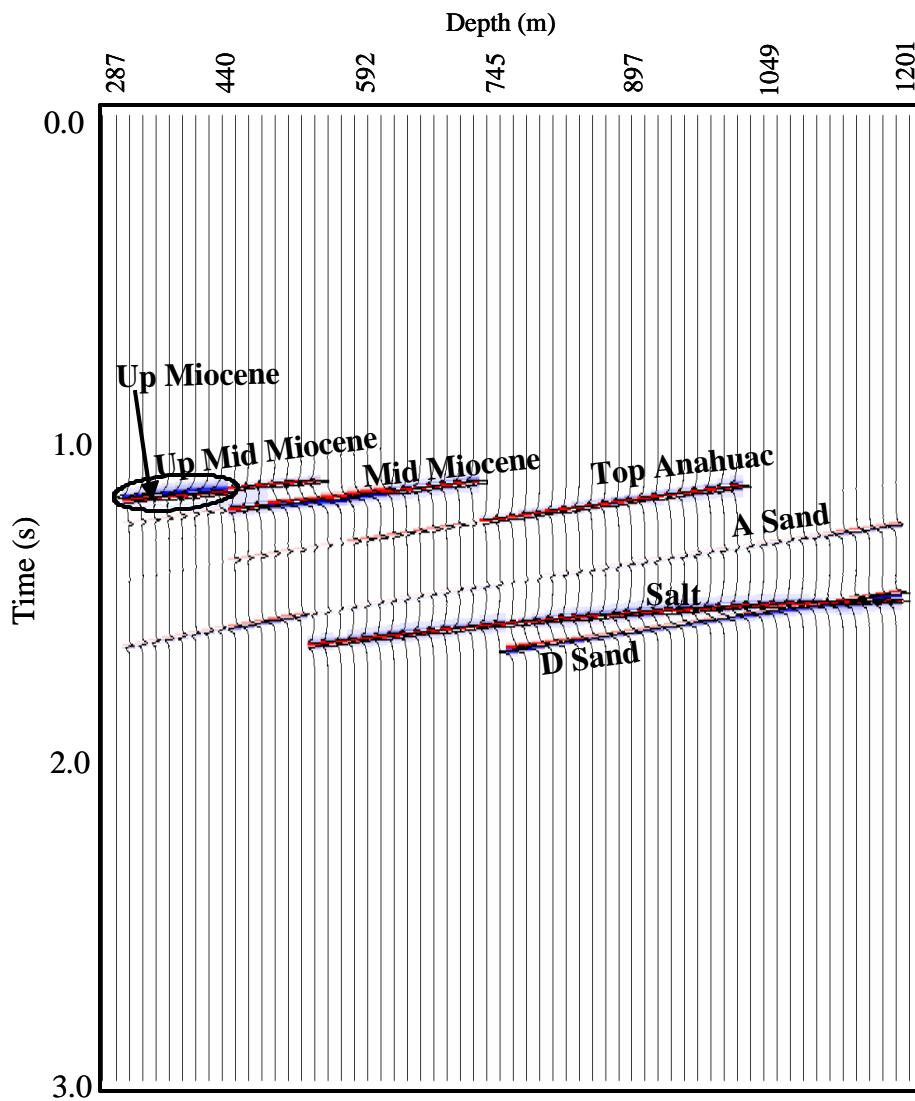


Figure 4.11. Synthetic seismogram calculated for shot 3438 located at  $x=3000\text{m}$  in the seismic model shown in Figure 4.9. All events represent upgoing P-wave reflections recorded on vertical geophone. The black ellipse indicates a region of coincident seismic events.

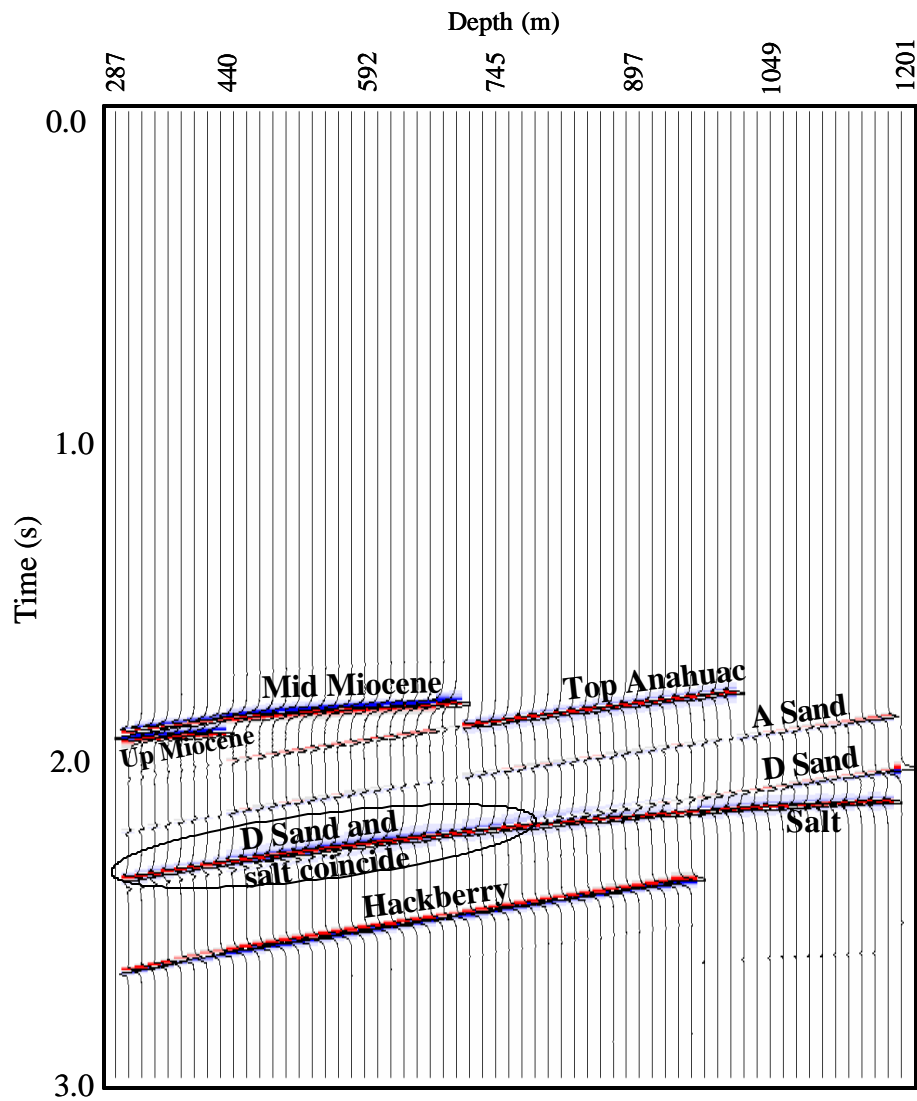


Figure 4.12. Synthetic seismogram calculated for shot 3492 located at  $x=4500\text{m}$  in the seismic model shown in Figure 4.9. All events represent upgoing P-wave reflections recorded on vertical geophone. The black ellipse indicates a region of coincident seismic events.

Although reflections from sedimentary interfaces have a linear character, their mutual relationships indicate that the recognition and separation of the events is difficult for the records with large offsets.

A comparison of the character of the first arrivals between near-, middle- and far-offset records is given in Figure 4.13. First arrivals have a linear character on the near-offset shot record (Figure 4.13a). The traveltimes for the higher channel numbers (longer offset) is longer than the one for the smaller channel numbers (shorter offsets). First arrivals for middle-offsets (Figure 4.13b) and far-offsets (Figure 4.13c) are curved, with the direct waves recorded only on a limited number of channels. The first energy arriving on the geophone for a number of channels, especially on far offsets is reflected energy rather than the transmitted energy.



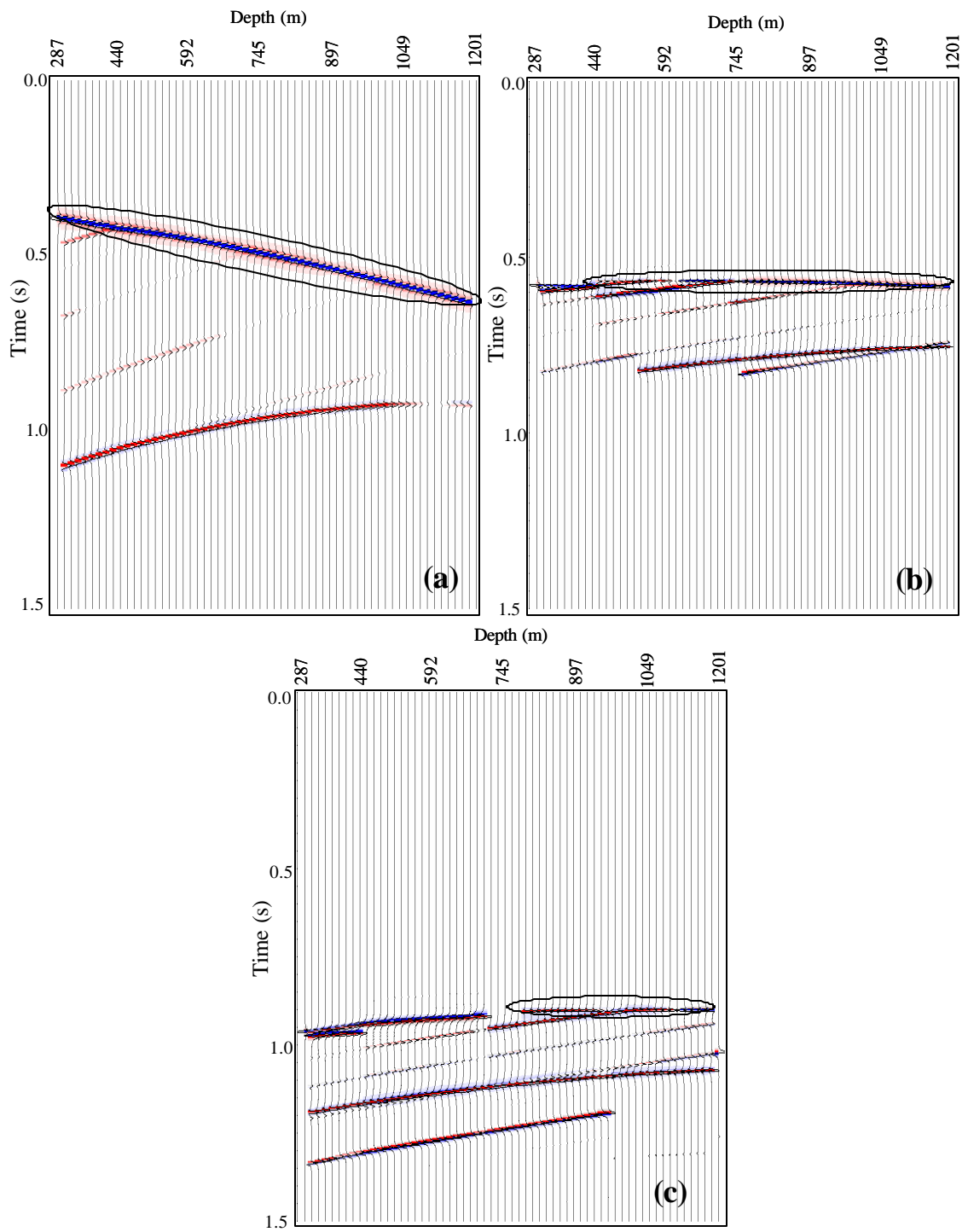


Figure 4.13. Comparison of the character of the first arrivals for the initial model. (a) Shot 3302, (b) shot 3438, and (c) shot 3492. The black ellipse indicates the area of seismic section with direct wave events.

## 4.2. Event picking

### 4.2.1. Selection of the offset range

Synthetic seismograms for all shot records on the profile were compared with the real data. Although the constructed model represents an initial guess of the subsurface geology, synthetic data enabled understanding of the real VSP record and facilitated recognition of the events. Synthetic seismograms showed that reflections from sediment interfaces have linear character. At near offsets, reflections from the shallower interfaces are recorded earlier than ones from the deeper interfaces. For longer offsets, the timing of the events is disturbed, and in certain cases reflections from the deeper horizons are simultaneous or earlier than ones from the shallower horizons. The reflection from the salt is curved, and partially overlapped with the reflections from some of the sedimentary interfaces. First arrivals have linear character only for shorter offsets. For longer offsets, first arrivals are curved. In addition, for longer offsets, the first energy recorded on the geophone is a combination of direct arrivals (transmitted energy), refractions and reflections, making the interpretation of first arrivals difficult. In conclusion, the numerical modeling indicated that recognition and picking of the events is difficult for the offsets longer than 1500m.

Comparison between near-offset and far-offset VSP shot gathers for the Vinton Dome is given in Figure 4.14. Conclusions similar to the one from the numerical modeling can be given. The near-offset shot gather (Figure 4.14a) has a linear first arrival, corresponding to the direct waves from a surface shot to the well receivers. The upgoing

reflections, with a linear character, can be clearly distinguished and the depth of the reflection-direct arrival intersection can be defined. The far-offset shot gather (Figure 4.14b), on the other hand, shows the curved character of the first arrival, with the main portion probably being caused by reflections and not by direct arrivals or refractions. Individual upgoing reflections cannot be clearly distinguished in the upper portion of the record and the precise information on the depth of reflectors cannot be determined.

Taking the results of numerical modeling and the real data comparison into consideration, only shot records with offsets up to 1500m were selected for event picking. For the selected profile, eight shots (out of total 20) have satisfied this criterion.

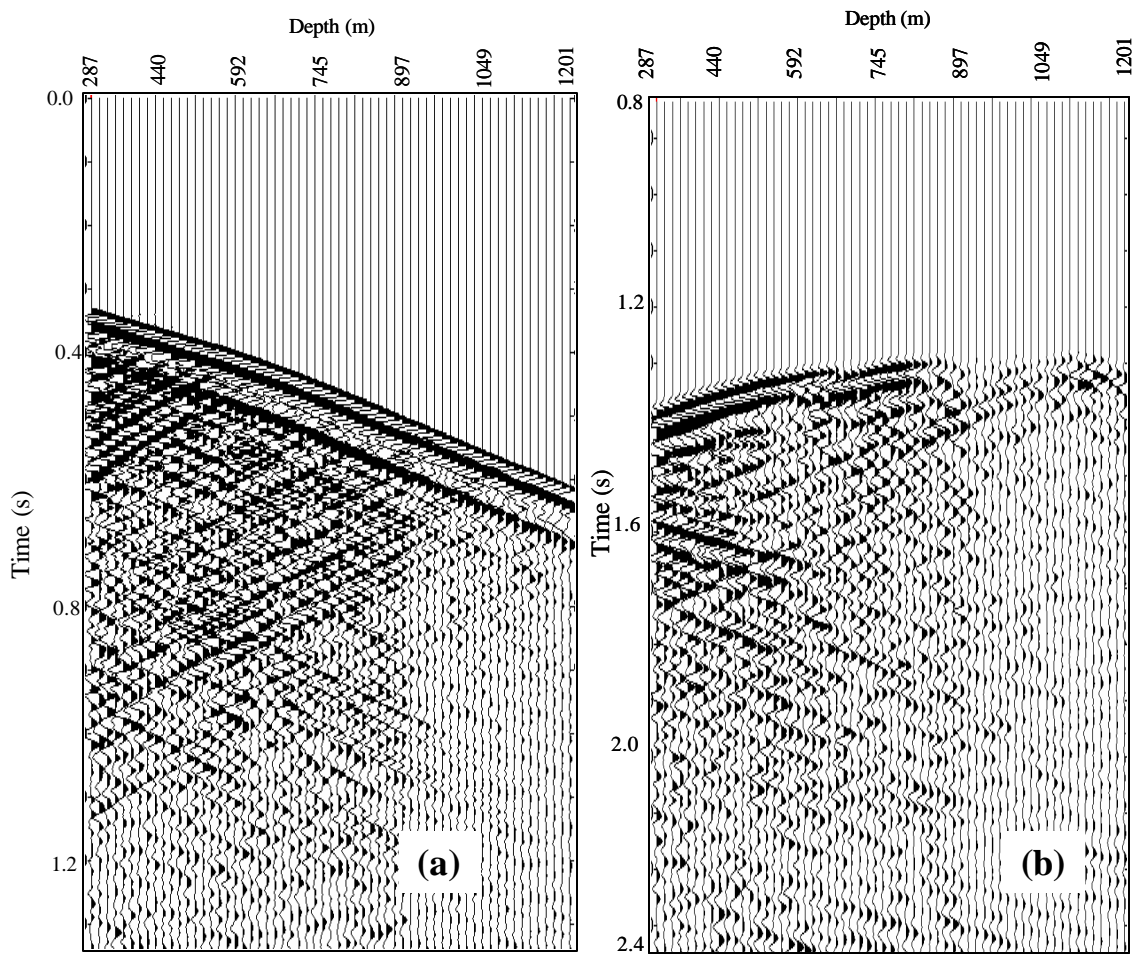


Figure 4.14. Comparison of a near-offset and a far-offset shot record for the VSP Vinton Dome data. (a) Shot-record 3297 with the source-well separation of 520m, and (b) shot-record 3165 with source-well separation of 2500m.

#### 4.2.2. Criteria for event picking

The criteria defined for events picking for the Vinton Dome VSP data are:

*(1) Shot-receiver offset*

As shown previously, the recognition of the events is more difficult with increasing shot-receiver offset. Since the goal of the research is to develop tomographic results with a high confidence level, only data with offsets less than 1500m are considered. Although some events could be recognized on some of the data with longer offsets, the identification and the consistent picking on all shot records could not be performed, and they were not considered for this research.

*(2) Character of events on shot record*

Once eight shots have been selected based on the offset range, the event character is examined. Only events with a high signal-to-noise ratio have been used for picking.

*(3) Depth control and event consistency between gathers*

Great attention has been given to the correlation of events from one gather to another. The intersection of the upgoing reflection and the downgoing first arrival determines the depth of a reflector, and this depth remains the same for a particular reflector on each shot record. This enables picking reflections in a consistent manner, going from one gather to the other.

*(4) Correlation of events with well markers*

Once a certain group of the events is separated using the criteria given above, the correlation of events depth with the well data is performed. Since only eight shot gathers are selected based on the shot-receiver offset, the stability of the tomographic inversion

imposed the usage of a limited number of the layers for the model parameterization. Therefore, correlation of the events depth with the well information about the position of stratigraphic horizons (that are previously interpreted) is performed, and only events corresponding to the described stratigraphic horizons were considered.

#### 4.2.3. Illustration of event recognition and picking

Following the criteria given above, eight shot records have been used for event picking. Shot records, in general, have acceptable quality, enabling the recognition of the events with certainty. One of the shot gathers is shown in Figure 4.15. First arrival has a linear character and its zero crossing is picked. A relatively large number of upgoing reflections with good signal-to-noise ratio can be recognized on the gather, but only a few are selected. Correlation with the depth of horizons at the well indicates:

- the first reflection event corresponds to the horizon Upper Miocene,
- the second reflection event corresponds to the horizon Upper-Middle Miocene,
- the third reflection event corresponds to the horizon Middle Miocene, and
- the fourth and the fifth reflection events correspond to the horizons located between the Middle Miocene and the Top Anahuac.

A record for a shot located close to the salt dome (Figure 4.16) has relatively poorer quality than other common shot gathers, and only the uppermost reflection could be picked. On all other records, such as those shown in Figures 4.17 and 4.18, all five events could be recognized. However, since the fourth and the fifth reflections do not

correspond to the interpreted stratigraphic horizons, only the last reflection is used for the tomographic inversion.

Once four events are recognized and identified, manual picking of both first arrivals and reflections is performed, using a commercial software package SeisUp. The zero crossing time was picked for the first arrivals and the reflection peak for the reflection events. The picked traveltimes were stored in ASCII files.

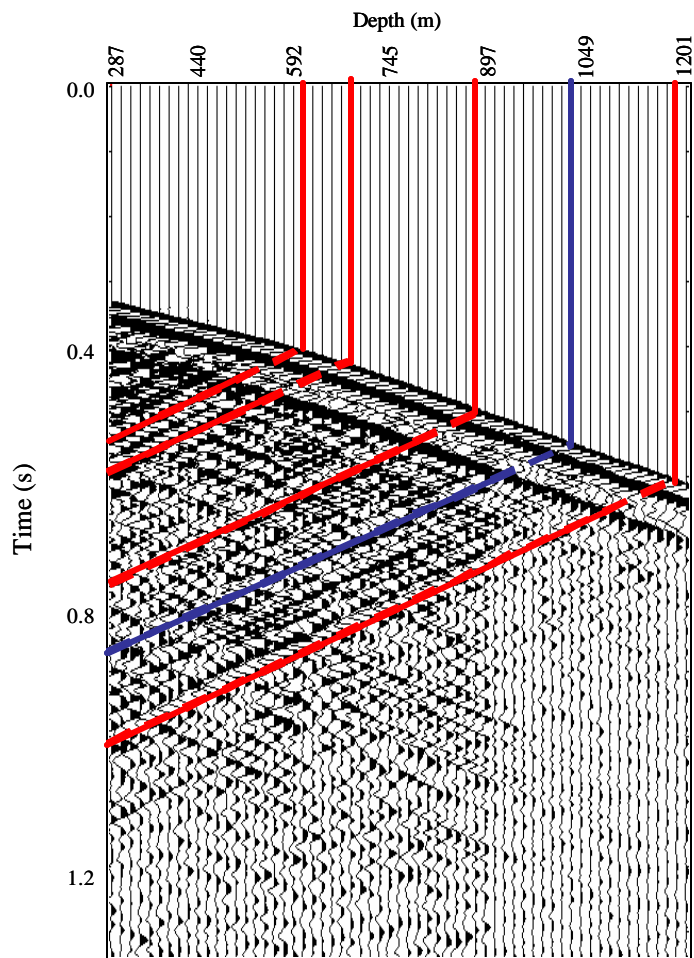


Figure 4.15. Illustration of the picked events for shot 3297 at offset 520m. Vertical lines indicate depth of the reflectors corresponding to the picked event. Red lines show events that are used in the inversion. The blue line event is not used for the final tomographic inversion. Dashed lines indicate areas where picking was not performed due to poor signal-to-noise ratio.



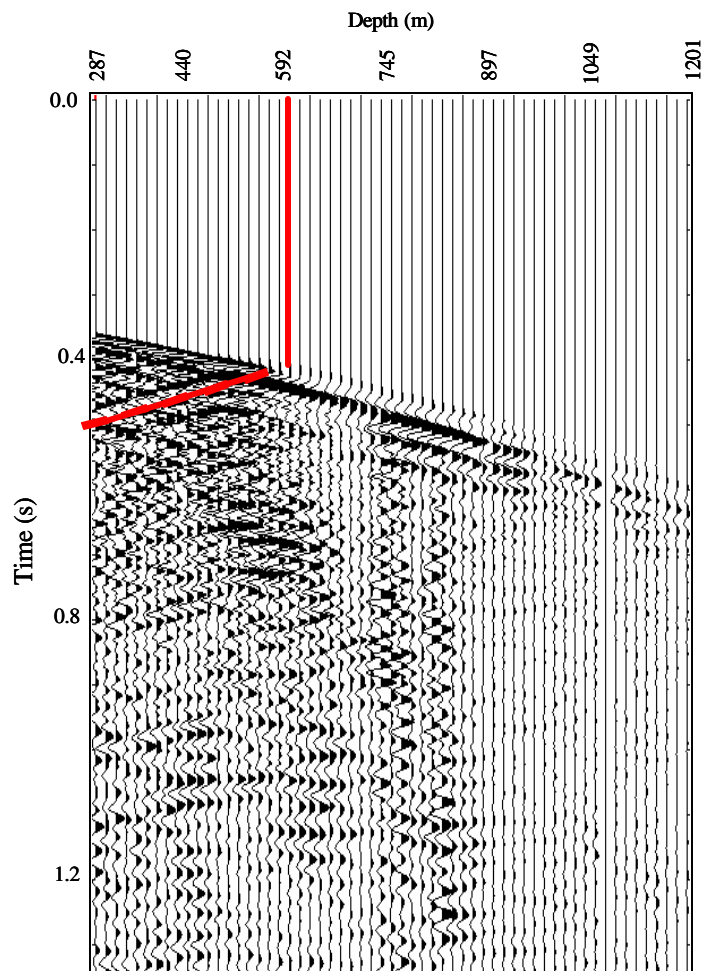


Figure 4.16. Illustration of the picked events for shot 2858 at offset 780m. The vertical line indicates depth of the reflector corresponding to the picked event. The red line shows the event used for inversion.

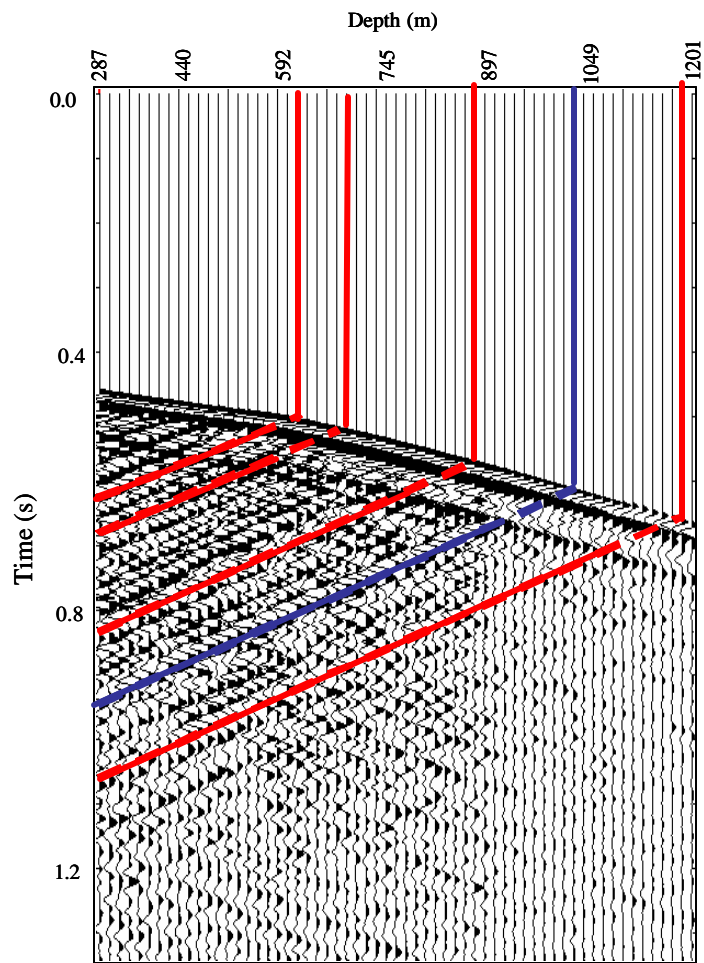


Figure 4.17. Illustration of the picked events for shot 3314 at offset 1200m. Vertical lines indicate the depth of the reflectors corresponding to the picked events. Red lines show events that are used for the inversion; the blue line event was not used for the final tomographic inversion. Dashed lines indicate areas where picking was not performed due to poor signal-to-noise ratio.

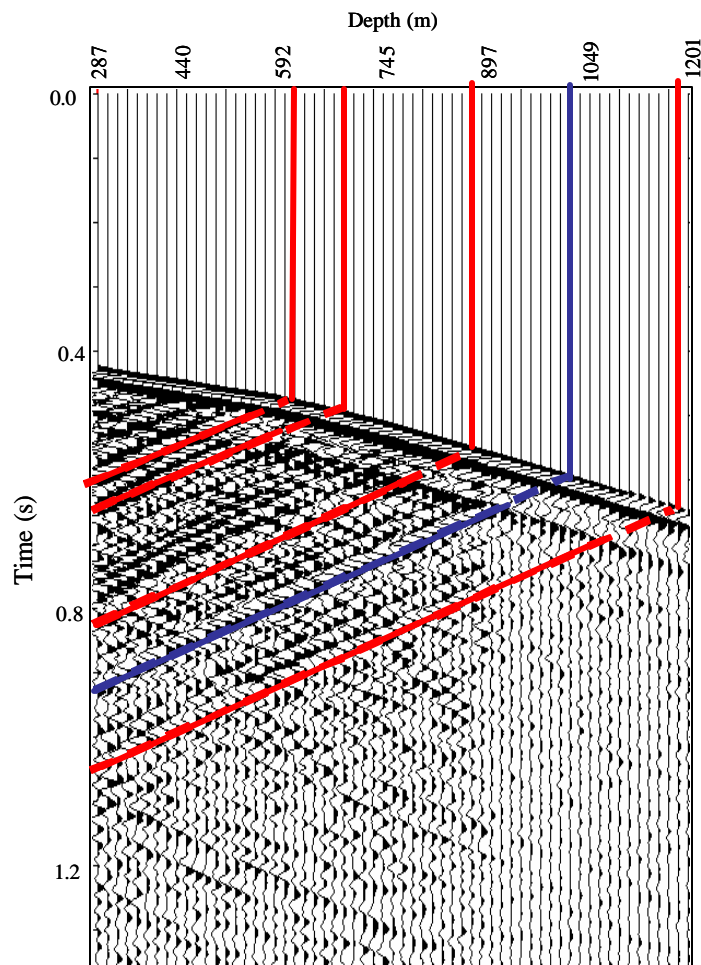


Figure 4.18. Illustration of the picked events for shot 3302 at offset 900 m. Vertical lines indicate the depth of the reflectors corresponding to the picked event. Red lines show events that are used for inversion; the blue line event was not used for the final tomographic inversion. Dashed lines indicate areas where picking was not performed due to poor signal-to-noise ratio.

### 4.3. Seismic tomography

Synthetic testing on two groups of models indicated that each of the tomographic algorithms used has some advantages and pitfalls. The cell-based methods are successful in determining the interface geometry when the velocity of the geologic strata is known. On the other hand, these methods fail to simultaneously determine both the interface geometry and the velocity values for the complex subsurface models. Additional limitations for their application are the poor ray coverage and lack of ray crossing of the VSP data. However, these methods successfully reduce range of velocities, and these values can be used for the subsequent application of the DLT methods.

The deformable layer tomography simultaneously determines both velocity values and interface positions, when the initial guess of the velocity values is similar to the true one, implying the necessity for applying cell-based tomography prior to the deformable layer tomography to improve the initial model and the knowledge of the velocity values. In addition, first arrivals have a smaller depth coverage than reflections, and attention needs to be given to the ray coverage analyses.

The results of synthetic testing are important for defining the general tomographic flow (Figure 4.19). Input data are the initial velocity model, the first arrivals and the reflection traveltimes picks. The first-arrival cell-based tomography has been performed as the initial step with the goal to reduce the range of velocities and provide the geometry for upper layers. The first-arrival DLT has been applied to the models with differing levels of complexity, with the goal to further reduce the velocity range and constrain the velocity model, which will be used as the input for the subsequent implementation of the

reflection tomography. The reflection cell-based and the deformable layer tomography are applied in the later part of the tomographic analyses with the goal to define the final subsurface velocity-interface depth model. The criteria for the quality control and selection of the representative model were statistical, such as the average travelttime error, and geological, such as the agreement of the defined velocities with the sonic log values and the correlation of the reflector's position with the well markers.

Each of the four tomographic methods (Figure 4.19) has been applied in an iterative manner. Results are discussed in detail in this chapter. The tomographic velocity model building is an integrated process, which uses results of each of methods mentioned above to improve the performance of the others.

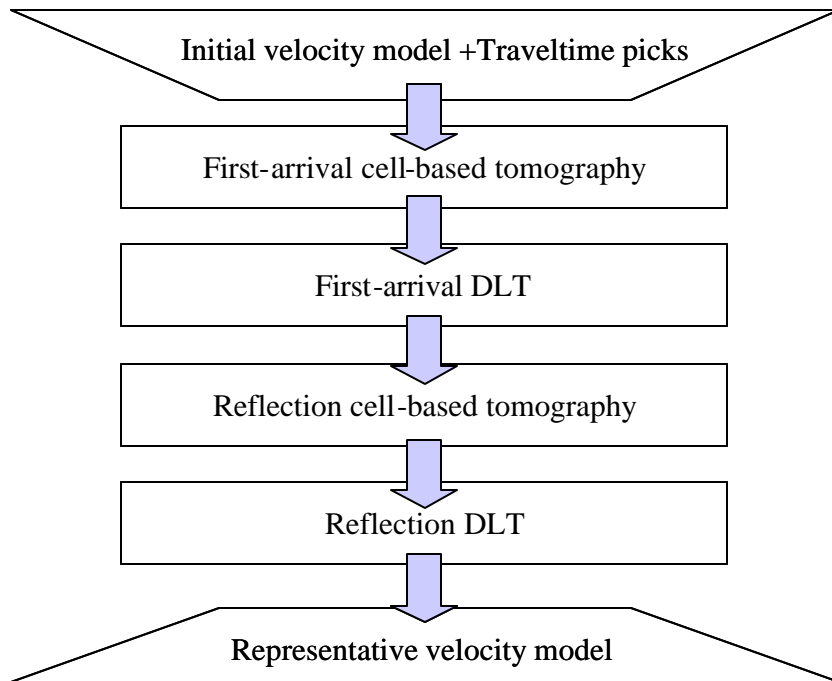


Figure 4.19. General application flow for the seismic traveltime tomography for the Vinton Dome VSP data.

#### 4.3.1. First-arrival cell-based tomography

The cell-based tomography is designed to determine the reflector geometry when the velocity values of the geologic strata are known. Synthetic testing indicates that, due to the large number of unknowns, inversion for both the velocities and the reflector geometry in a complex model is unstable. However, when the subsurface model is simple, it is possible to perform a stable inversion for both velocities and geometry.

The application scheme for the first-arrival cell-based tomography is given in Figure 4.20. In general, tomographic inversion is performed for a defined initial model and QC criteria are applied. When the error and the tie with *a priori* geologic information is acceptable, the results of the first-arrival cell-based tomography are used for the construction of the initial model for the first-arrival DLT. If any QC criteria are not satisfied, the initial model is redefined and the inversion is performed in an iterative manner until the error and the match with the geologic constraints is acceptable.

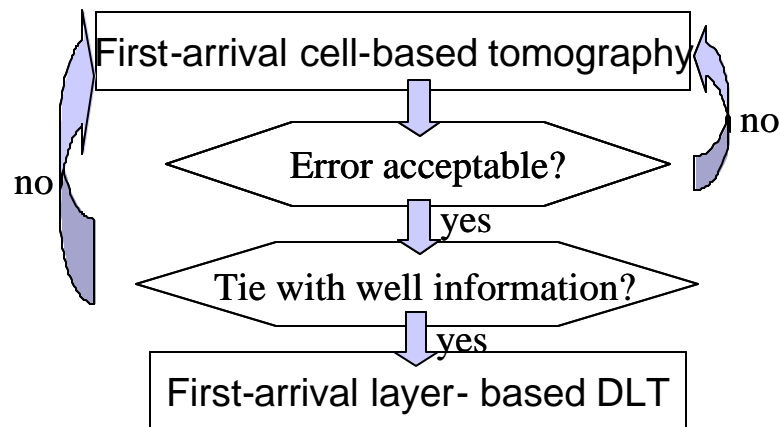


Figure 4.20. Application procedure for the first-arrival cell-based tomography.

Since no *a priori* information was available, a simple initial model is constructed (Figure 4.21). The initial model (Figure 4.21a) is a one-column five-layer model with a constant velocity of 3km/s in each layer. Eight sources are placed on the surface with unequal separation (green triangles), and sixty-one receivers are located in the well (red line in Figure 4.21). The definition of a simple model allows inversion for both the velocity values and the interface position. The result after three iterations is shown in Figure 4.21b. The velocity values for each layer, except the deepest one without ray coverage, are updated and these velocity values are similar to the velocities from sonic logs (Table 4.1). The positions of the interfaces are updated for the upper layers, as a result of a limited depth coverage of the first arrivals. However, selection of a simple model and implementation of the first arrivals only limited the definition of the final model, and the depth tie of well markers and interface positions are not satisfactory.

Table 4.1. Range of the sonic log velocities for sedimentary strata in the Vinton Dome (Courtesy of Zhou and Duncan).

Layer	Velocity at the top (m/s)	Velocity at the bottom (m/s)
Surface	1675	2220
Upper Miocene	2220	2280
Upper-Middle Miocene	2280	2340
Middle Miocene	2340	2510
Anahuac	2510	2630



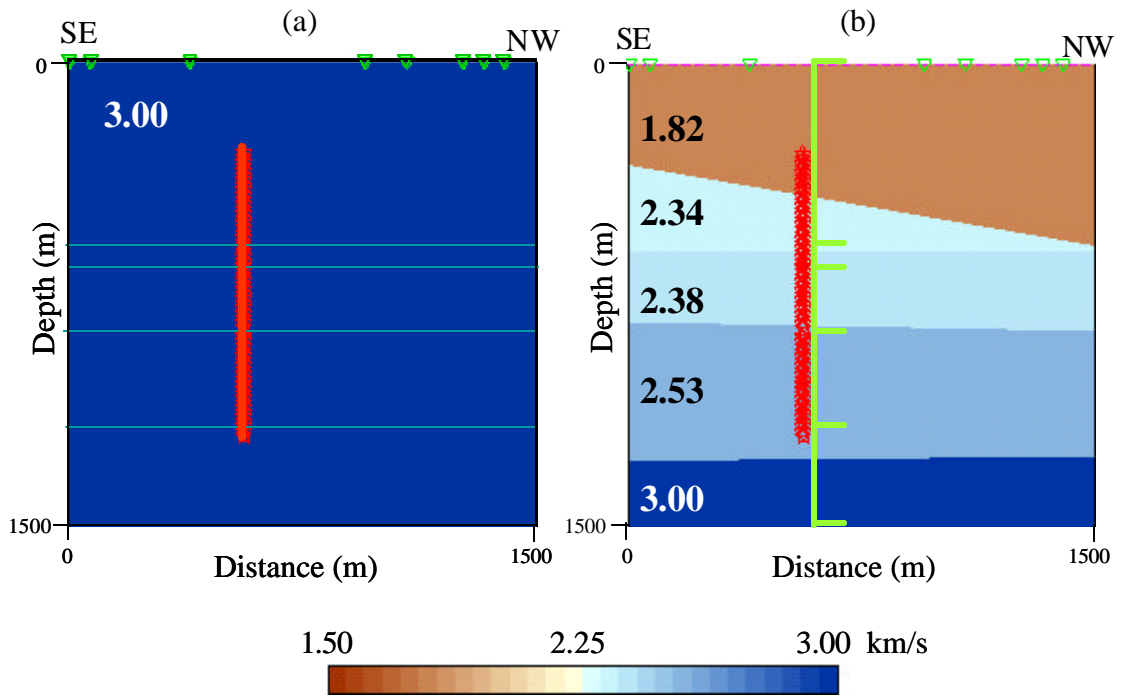


Figure 4.21. The cell-based first-arrival tomography result. I used 5 layers and 1 column to parameterize the model and inverted for both geometry and velocity values. (a) Initial model, and (b) inversion result after three iterations. The green line shows the true position of the horizons, as determined from the well logs.

The statistical criteria for the quality of the final model are satisfied (Table 4.2). Average traveltimes error for all shots is 0.84%, the maximum traveltimes error for an individual shot is 1.58%. The positive correlation between the true and the computed traveltimes is shown in Figure 4.22a and 4.22b.

Table 4.2. Statistics of the tomography applied to Vinton Dome data.

DLT method	Number of layers	Number of columns	Channels	Cumulative average error	Average error for shot number								
					2858	2946	3031	3137	3297	3302	3314	3312	
First-arr.	Cell-based	5	1	All	0.84	1.19	1.58	1.32	0.65	0.55	0.44	0.44	0.55
	Layer-based	5	1	All	0.78	0.96	1.61	1.30	0.61	0.44	0.37	0.42	0.54
	Layer-based	5	2	All	0.71	1.10	1.42	1.15	0.83	0.31	0.35	0.26	0.27
	Layer-based	5	3	All	0.89	1.29	1.24	1.10	0.61	0.36	0.46	0.28	0.26
	Layer-based	5	5	All	0.64	1.14	1.30	1.13	0.61	0.21	0.17	0.17	0.17
Reflection	Cell-based	5	1	All	2.08	6.05	1.29	1.96	2.34	2.99	1.90	1.90	1.34
	Layer-based	5	1	Even	2.24	1.45	5.30	3.22	1.63	2.94	1.67	0.95	0.74
	Layer-based	5	1	Odd	1.72	1.78	5.12	3.53	1.43	2.61	1.59	1.07	0.93
	Layer-based	5	3	Even	2.24	1.45	5.30	3.22	1.63	2.94	1.67	0.95	0.74
	Layer-based	5	3	Odd	1.57	2.28	3.08	3.50	1.23	2.19	1.61	1.12	0.96

The cell-based first-arrival tomography offers important information for the application of other tomography algorithms: a reduced range of velocities, and the trend of the interface geometry in shallower layers. The average traveltimes error is small. However, since the initial model is simple, the tie between the interface position and the well markers is not established. The model defined by the first-arrival cell-based tomography is used to construct an initial model for the first-arrival DLT.

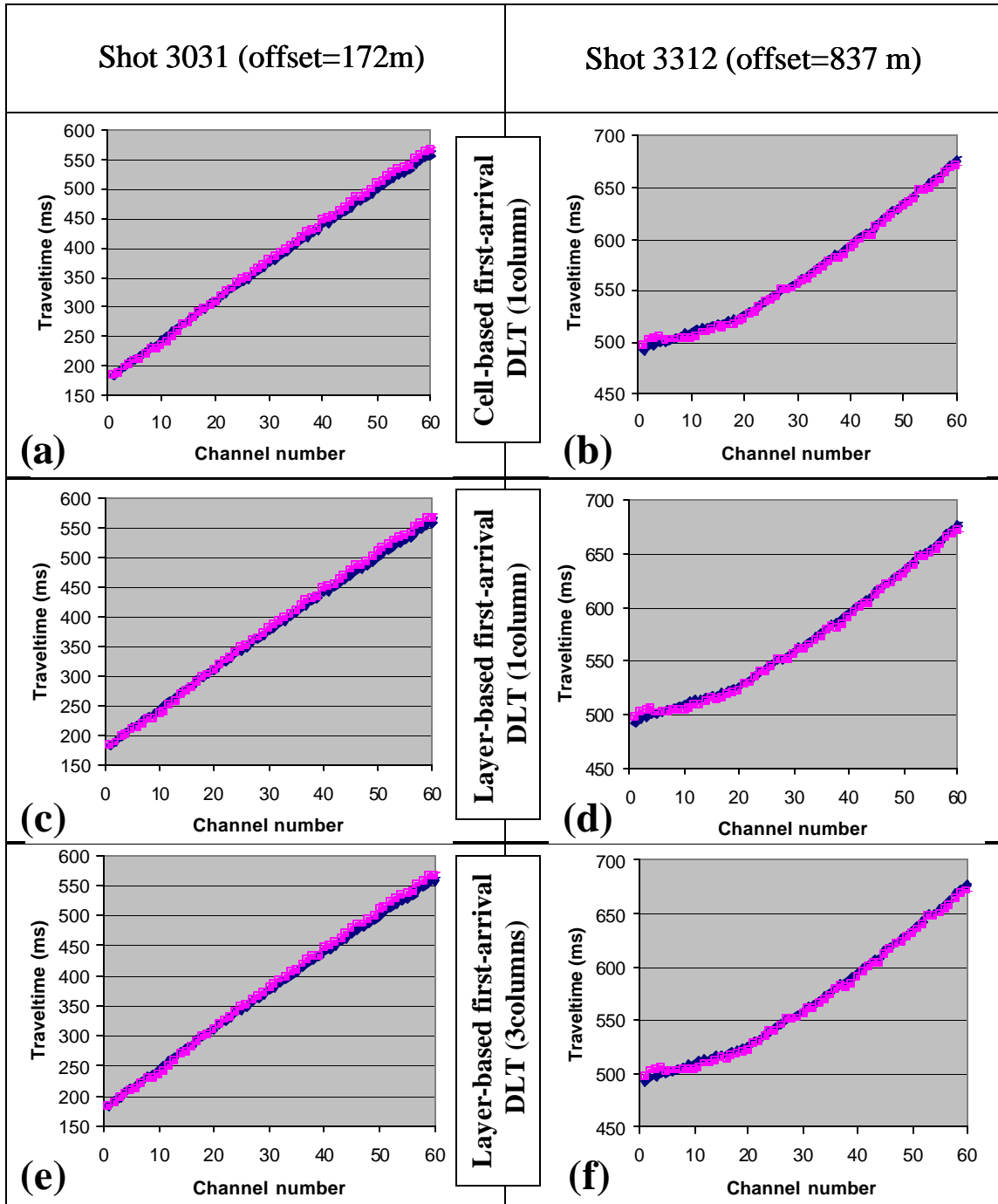


Figure 4.22. Comparison of the observed (blue curve) and the computed (pink curve) traveltimes obtained using first-arrival tomography (shots 3031 and 3312). (a) Cell-based tomography for shot 3031, (b) cell based tomography for shot 3312, (c) 1 column DLT for shot 3031, (d) 1 column DLT for shot 3312, (e) 3 columns DLT for shot 3031, and (f) 3 columns DLT for shot 3312.

#### 4.3.2. First-arrival DLT

The DLT algorithm enables inversion for both the velocity values and the interface positions, for an initial model where the velocity range is similar to the true. Limited lateral and depth coverage of first arrivals need to be accounted for during the parameterization of the initial model. The velocity value obtained by the first-arrival cell-based method is used as an initial value for the first-arrival DLT. The first-arrival DLT is performed in a number of steps (Figure 4.23).

A single column model is initially defined (Figure 4.23). Once the acceptable statistical error and the depth tie is obtained for a single column model, inversion for the two-column model is performed. The modifications of the model are subsequently performed into the three- and the five-column models. The results are evaluated and the representative model is selected for the reflection cell-based DLT.

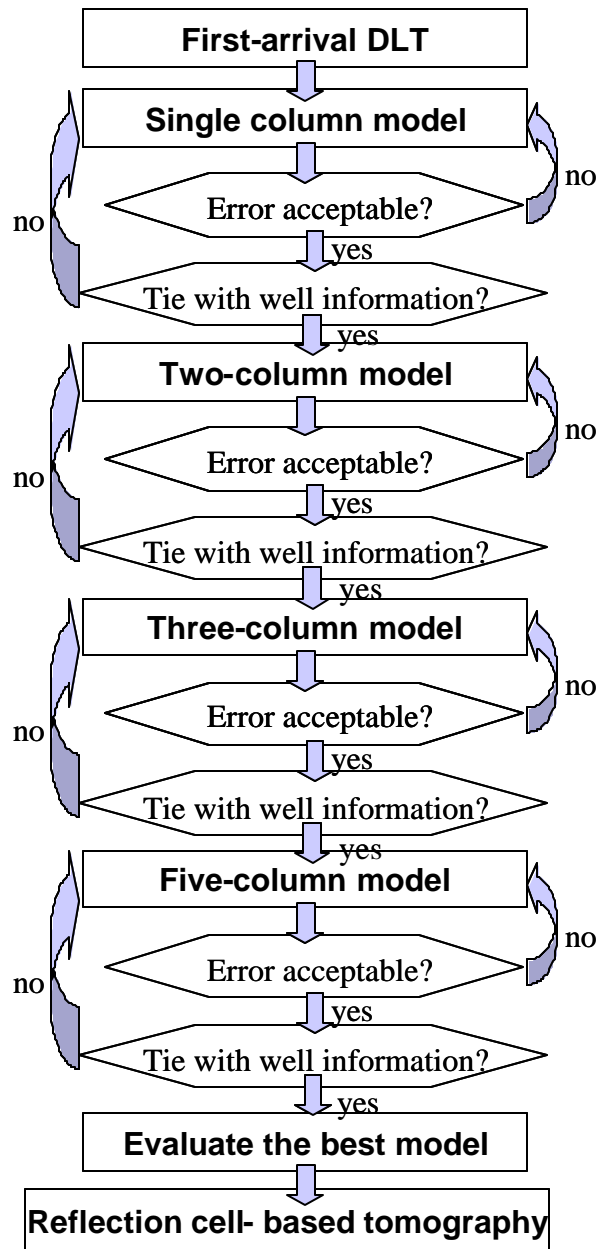


Figure 4.23. Application flow for the first-arrival deformable layer tomography, showing how the model parameterization is successively refined.

#### 4.3.2.1. Single column first-arrival DLT

The initial model for the single column application of the first-arrival DLT is flat (Figure 4.24a), with the velocity values obtained from the cell-based first-arrival tomography. Five iterations of the inversion are performed until a model shown in Figure 4.24b is obtained. The final model consists of five layers dipping to the right side of profile, away from the salt dome (salt dome's relative position is on the left, southeast, side of the profile). Velocity values are slightly reduced from the initial model, especially in the second layer. Compared with the sonic logs measurements (Table 4.1), the model represents the upper bound of velocity values. The correlation of the interface positions with well markers (Figure 4.24b) is improved compared to the cell-based first-arrival tomography, especially for the third interface. The average cumulative error (Table 4.2) is 0.78%, with the error values for each shot being reduced from the cell-based tomography model. The positive correlation of the observed and the computed traveltimes is obtained for all shots (Figure 4.22c and 4.22d).

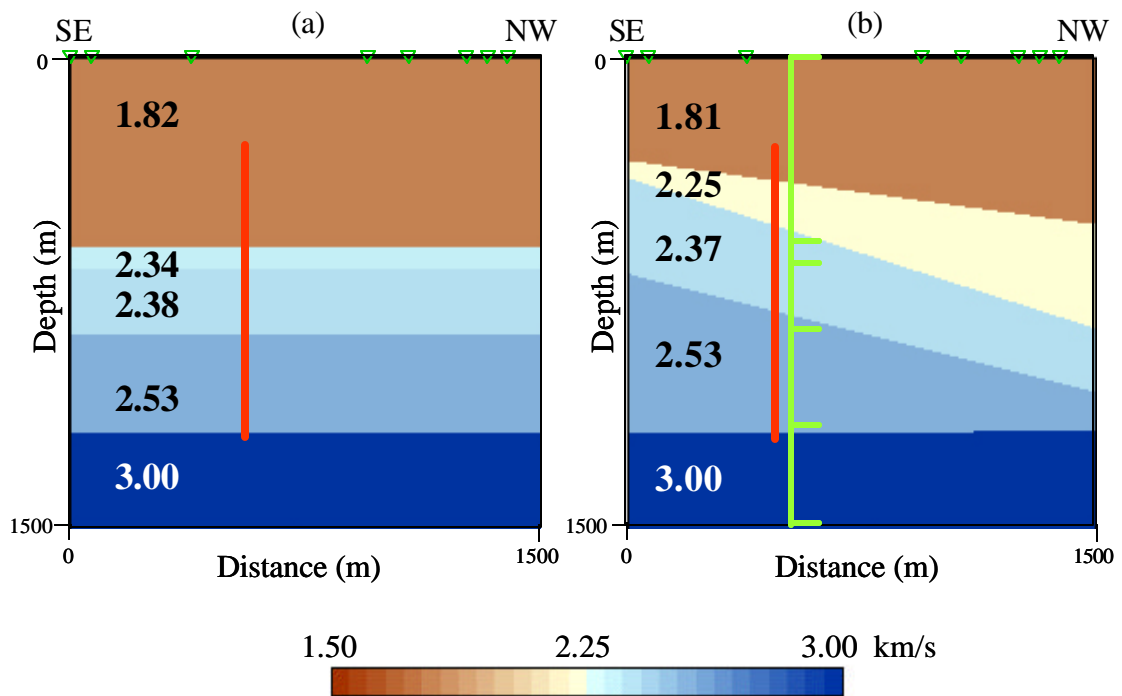


Figure 4.24. The first-arrival single-column five-layer DLT inversion. (a) Initial model, and (b) inversion result after five iterations. The green line shows the true position of horizons, as determined from well logs.

#### 4.3.2.2. Multi column first-arrival DLT

The model obtained from the single column parameterization is used as an input for this stage. The model is separated into two equal columns (Figure 4.25a), and iterative tomographic inversion is performed. The result of the fifth iteration is given in Figure 4.25b. Velocities are changed compared with the single-column model, with a decrease of the velocity values in the shallow layers and a slight increase in the deeper layers, and values correspond to the upper bound of the well log values (Table 4.1). Dips of the layers are slightly modified compared to the single-column model, with steeper dips of the layers closer to the dome (left side of the model in Figure 4.25b) and more gentle dips of the layers away from dome. The average error is decreased to the 0.71% (Table 4.2). The depth tie is satisfactory for the deeper interfaces, and poor for the shallower interfaces.

Once satisfactory error is reached for the two-column model, the level of the parameterization is increased into three- (Figure 4.26) and five-column models (4.27). For both of these parameterizations, the initial model is defined in the previous step of tomographic application (Figure 4.25) and the tomographic inversion is applied in five iterations. The final results for three-column (Figure 4.26) and five-column (Figure 4.27) first-arrival DLT are similar. Minor differences exist in the velocity values, while the definition of the interfaces is the same. The average error of the five-column model is smaller than the one for the three-column model (Table 4.2). In general, both results are of comparable quality, and the relatively good depth tie of the interface position with the well markers is reached for the deeper layers.



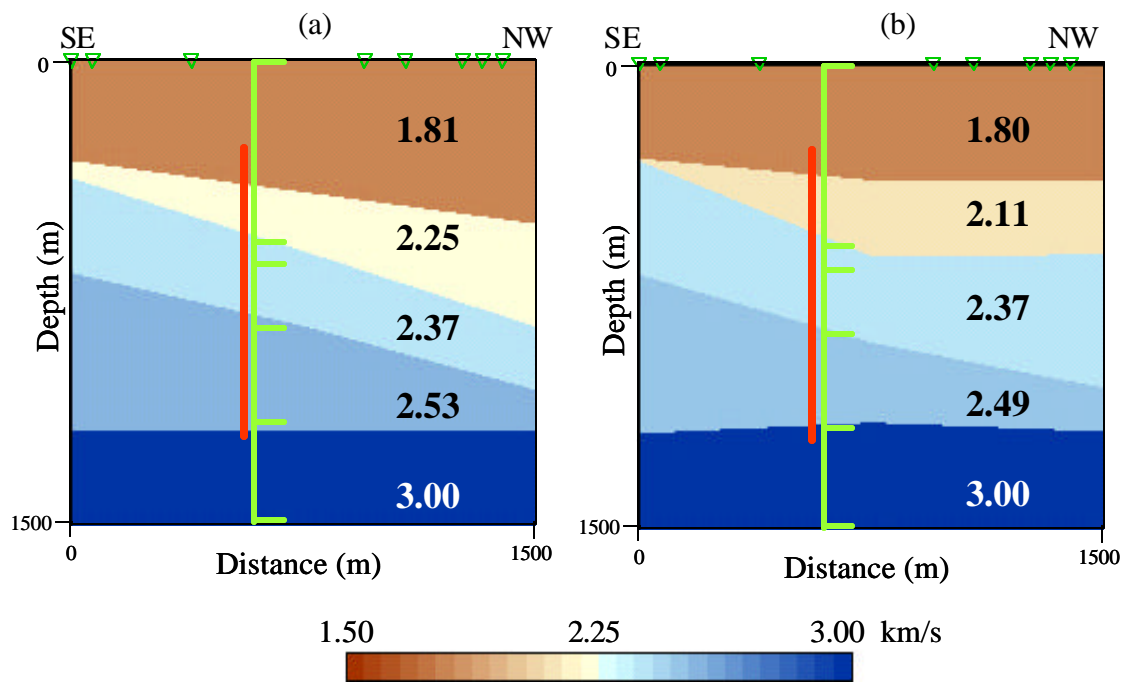


Figure 4.25. The first-arrival two-column five-layer DLT inversion. (a) Initial model, and (b) the inversion result after five iterations. The green line shows the true position of horizons, as determined from well logs.

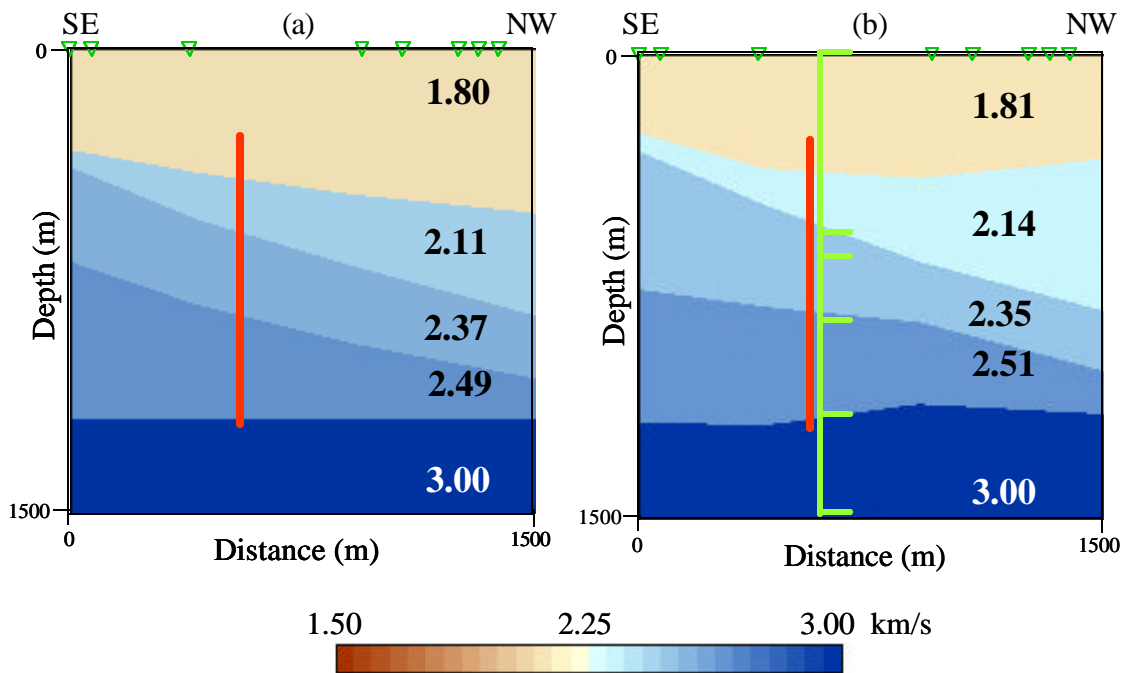


Figure 4.26. The first-arrival three-column five-layer DLT inversion. (a) Initial model, and (b) the inversion result after five iterations. The green line shows the true position of horizons, as determined from well logs.

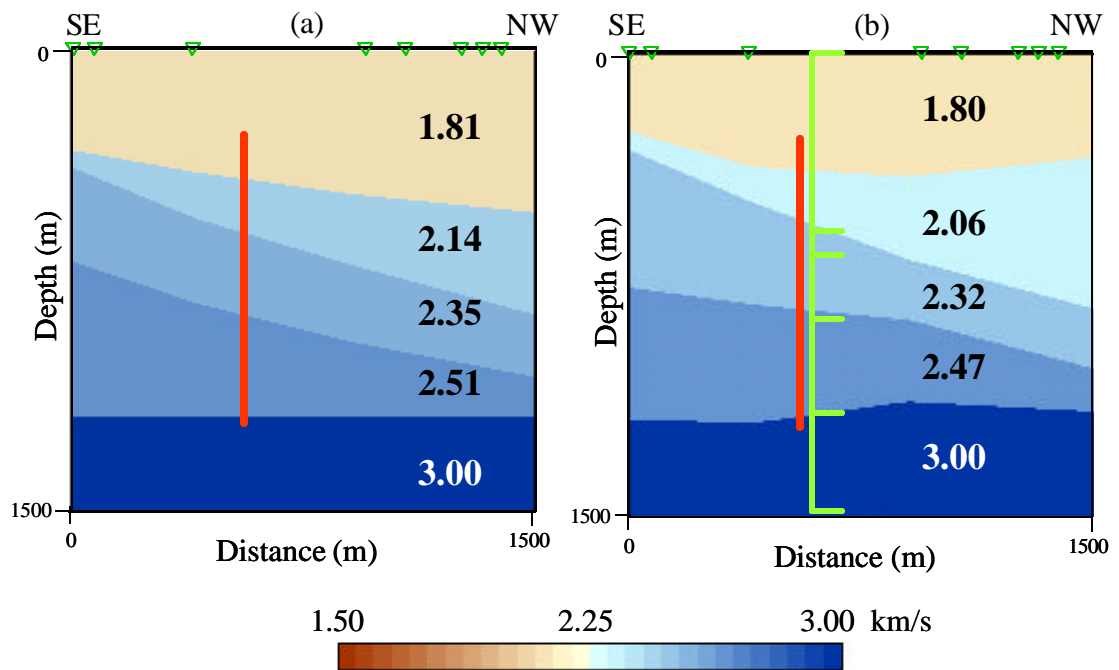


Figure 4.27. The first-arrival five-column five-layer DLT inversion. (a) Initial model, and (b) the inversion result after five iterations. The green line shows the true position of horizons, as determined from well logs.

First-arrival tomography for the models described above provided mutually consistent values of velocities and similar trends for the subsurface geometry. They can be used as initial models for the application of reflection tomography. Since first arrivals have a limited depth coverage, it is expected that the implementation of the reflection tomography will improve the definition of the subsurface model.

### 4.3.3. Reflection cell-based tomography

Synthetic examples indicated that first arrivals and reflections usually cover differing areas of the seismic section and the reconstruction of the subsurface model is restrained by the ray coverage. First arrivals constrain the velocity values (Al-Rufaii, 2002), while reflections provide information on the reflector geometry. Models provided by the first arrival tomography, as previously shown, have consistent velocity values and the interface geometries. The model defined by the three-column first-arrival DLT is used as input for the cell-based reflection tomography (Figure 4.28). A number of tomographic inversions using the cell-based algorithm have been performed until a satisfactory error and the tie with well information is reached. The results of the cell-based reflection tomography have been used as an input for the reflection DLT.

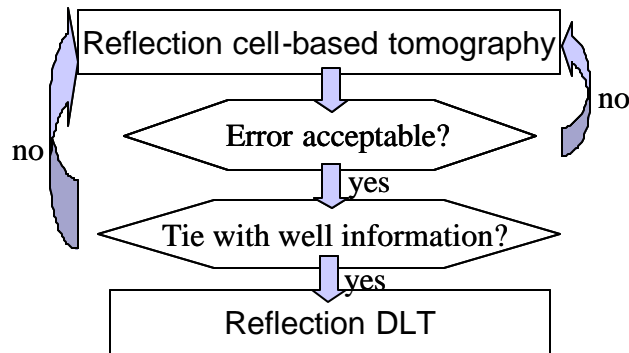


Figure 4.28. General application scheme for reflection cell-based tomography.

The initial model for the application of the cell-based reflection tomography is flat, with the velocity values averaged from the first-arrival tomographic models (Figure 4.29a). A simple one-column parameterization is used to invert for the reflection velocity-interface depth model. Although the average error is satisfactory (Table 4.2), the final values of the velocities (Figure 4.29b) differ from the ones defined using first arrivals, as well as the ones from the well logs (Table 4.1), indicating that further inversion is needed. In addition, the position of the second and the third interfaces were not updated, implying the need for the application of reflection DLT.

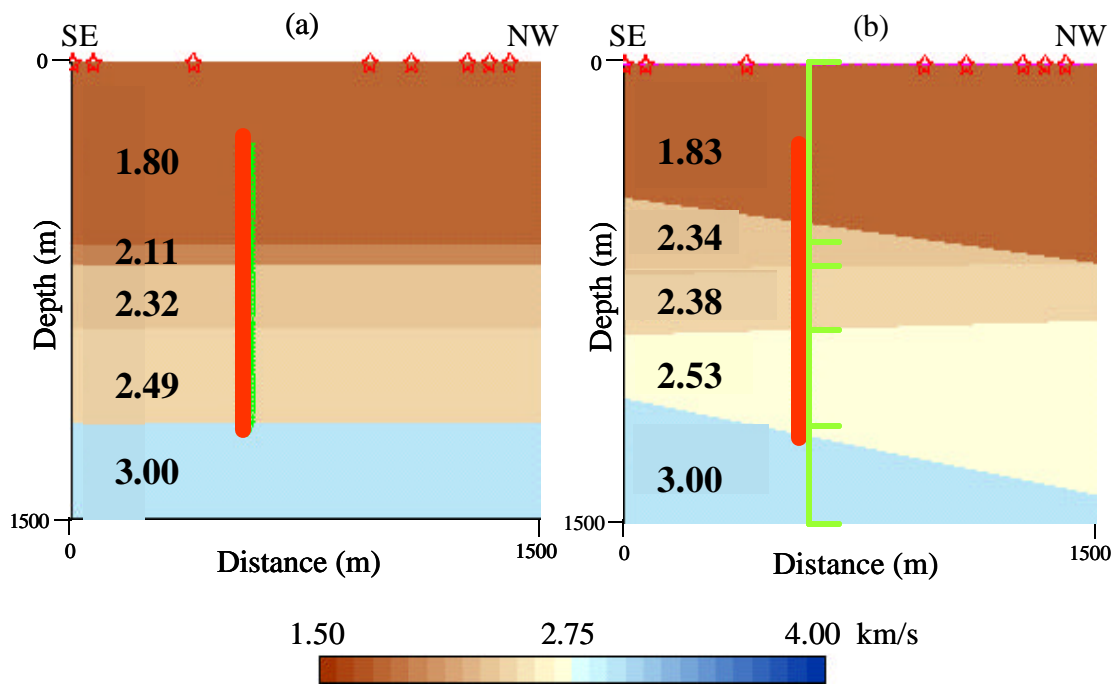


Figure 4.29. Cell-based one-column five-layer reflection tomography inversion. (a) Initial model, and (b) inversion result after five iterations. The green line shows the true position of horizons, as determined from well logs.

#### 4.3.4. Reflection deformable layer tomography

As indicated by the synthetic testing, the reflection DLT defines both the geometry of the reflection interfaces and the values of velocity, in the case when the initial velocity values are in a range close to the real values. The previous tomographic algorithms provided different velocity models, that have mutually similar velocity values and interface dipping trends. The goal of the reflection deformable layer tomography is to reduce the velocity range and define the geometry of the subsurface reflectors. In order to fulfill this goal in a consistent manner, a specific application scheme is defined for the reflection deformable layer tomography (Figure 4.30). Similar to the previously described algorithms, a single column model is defined first. Two-column and three-column models are extensions of the one-column model.

In order to examine the consistency of the results, the data space is divided into two subvolumes. Reflection traveltimes are separated into two groups: traveltimes that correspond to the channels with even numbers and traveltimes corresponding to the channels with odd number. Tomographic inversion is independently performed for each of the subvolumes, for each model parameterization (Figure 4.30). Only if the result of the tomographic inversion is the same for the two subvolumes, the higher order of the model parameterization is pursued. The implementation of the two independent datasets allowed for a consistency check of the tomographic results, imposing the additional criteria for quality control.



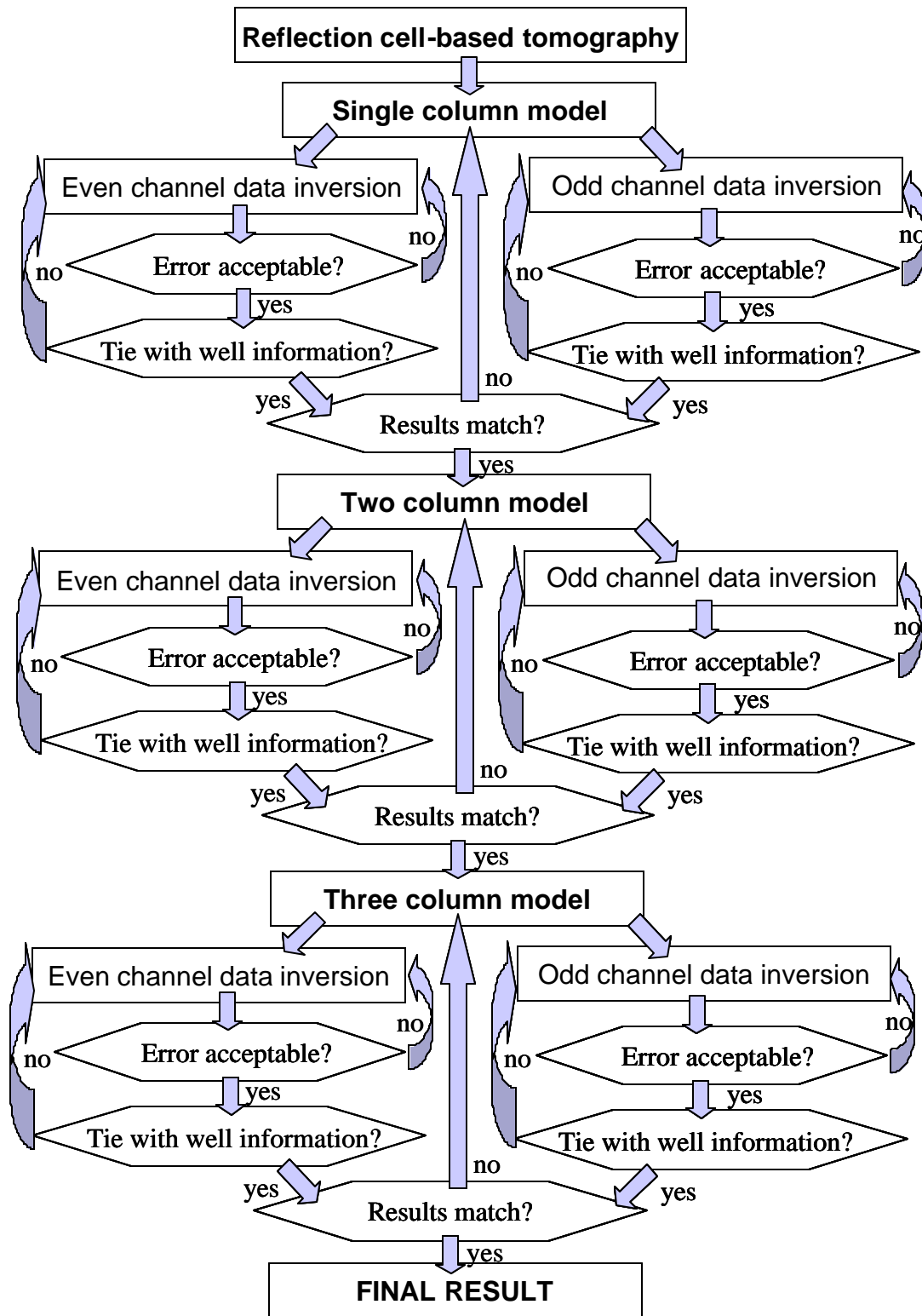


Figure 4.30. General application scheme for the reflection DLT.

#### 4.3.4.1. Single-column reflection DLT

The model defined as the final result of the reflection cell-based tomography is used as the initial model for the reflection DLT (Figure 4.31a). Six tomographic iterations are performed for each of the two data subvolumes. The obtained results are the same for the both datasets, with the same values for the inverted velocities and the position of interfaces that differs for maximum of 5m on the grid points. The final model consists of five dipping layers (Figure 4.31b), with the interfaces dip angle being reduced toward deeper parts of the model. The velocity value of the uppermost layer is 1.77km/s, while the three following layers have the velocity values that differ by only 10m/s from one layer to another. There are two possible explanations for the reflectivity presence in the areas with uniform velocities: reflectivity is primary caused by changes in density; or the area is characterized by a fine layering and the collective reflectivity is a sum of the reflectivity of individual layers. In a statistical sense, the cumulative travelttime error is slightly smaller for the dataset containing odd channels than the one containing even channels (Table 4.2). However, both of these datasets yield essentially the same subsurface model and the statistical difference between datasets is insignificant.

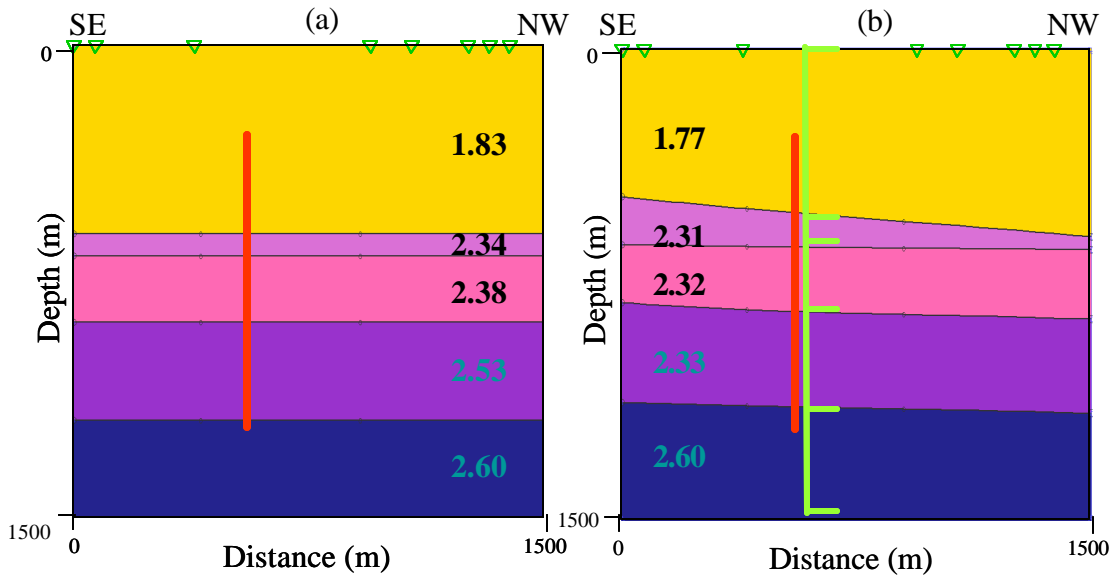


Figure 4.31. Reflection one-column five-layer DLT inversion for both geometry and velocity. Only odd number channels were used for the inversion. (a) Initial model, and (b) inversion result after six iterations. Position of the interfaces correlates well with the true horizon position (shown with green).

#### 4.3.4.2. Multi column reflection DLT

The final model obtained in the single column application of the reflection DLT has been used as the input for the multi-column application. Reflection DLT has been successfully applied for two- and three-column models. A five-column model has been adopted as well, but due to the insufficient ray coverage, the reflector geometry inversion was not stable.

Two- and three-column model parameterization provided essentially the same tomographic results and therefore discussion of the results for the three-column model parameterization will be given. The single-column model is used as the initial model and six iterations are applied (Figure 4.32). Similar to the example described previously, both datasets (odd and even channels) yielded the same results (Figure 4.32b).

Velocity values in three middle layers are constant, indicating that the reflectivity is probably caused by changes in density. The positions of the interfaces correlate well with the positions of the well markers. Reflective interfaces are dipping away from the salt dome, with the dipping angle being smaller than the one previously determined using other algorithms.

I have compared velocities from the sonic log measurements and the 1D velocity trend determined from tomography (Figure 4.33). Tomographic velocities represent a long wavelength trend of the sonic velocities. Average sonic wave velocity does not change significantly in the upper portion of the sedimentary section, which is consistent with the tomographic results, suggesting that the reflectivity is primary caused by changes in density.

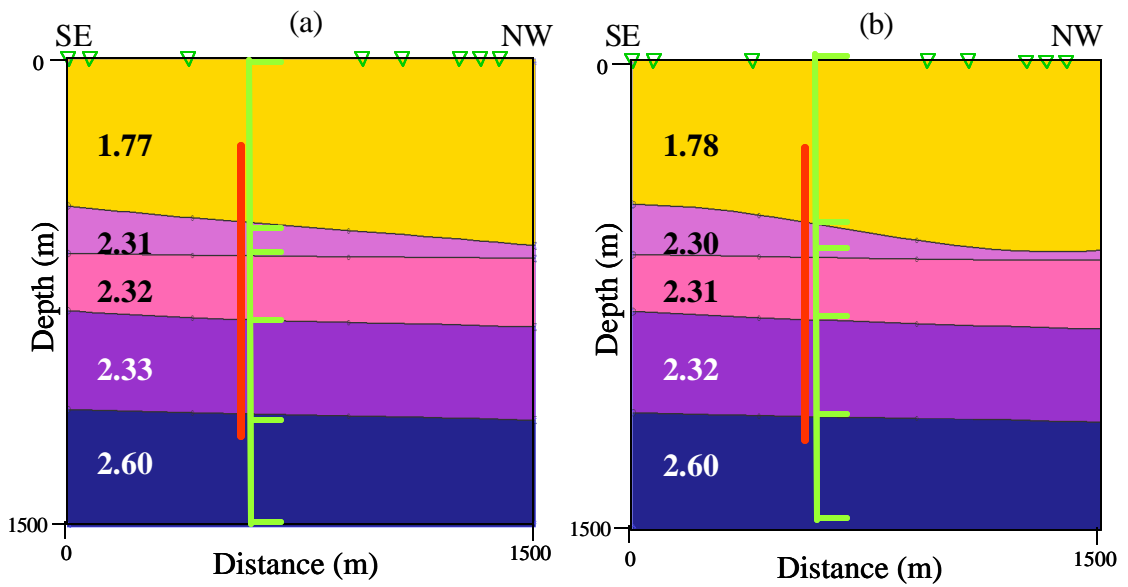


Figure 4.32. Reflection three-column five-layer DLT inversion. Only even numbered channels were used for inversion. (a) Initial model, and (b) inversion result after six iterations. Position of the interfaces correlates well with the true horizon position (shown with green).

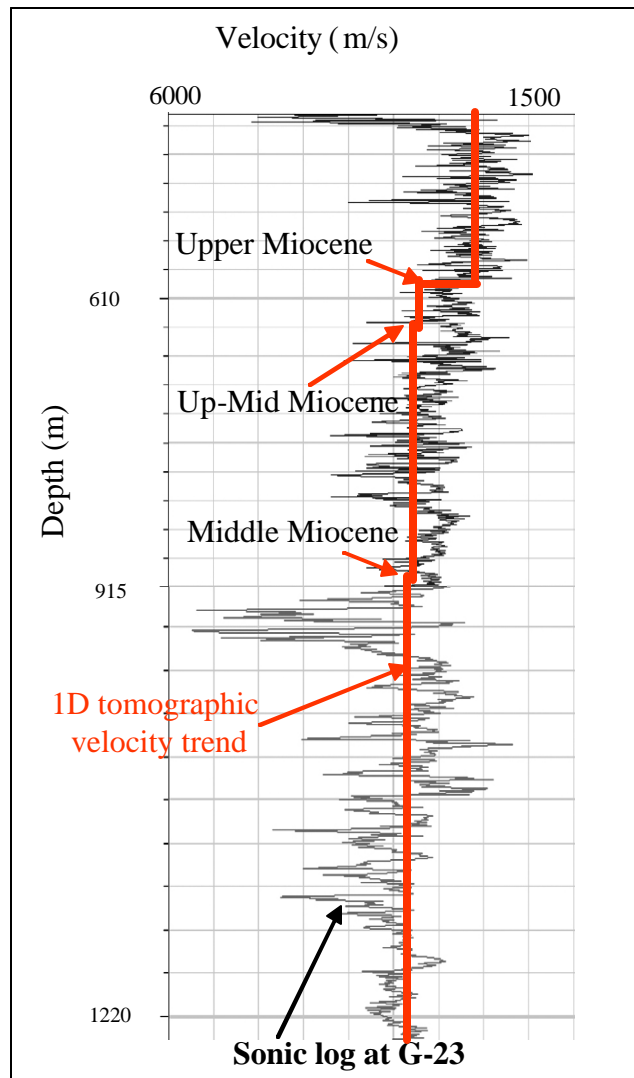


Figure 4.33. Comparison of the sonic log velocities and the 1D velocity from the final tomographic model. The black curve represents measured sonic velocities, the red line the 1D velocity trend determined from tomography at the well position. The horizontal scale is linear in slowness.

The three-column model statistically yields the same cumulative average error as the one-column model, with slightly smaller error for the data subvolume in which only the odd channels have been used (Table 4.2).

Comparison of the observed and the computed traveltimes for all reflection tomography algorithms is given in Figure 4.34. It can be seen that a positive correlation between the true and the computed traveltimes is obtained for all shots, using the tomography methods described above.

In general, all tomographic models have similar traveltime error, despite the fact that models have different geometry and velocity values. This is a typical example of non-uniqueness in seismic inversion. For this reason, it is vitally important to constrain tomographic velocity models using all available geological information.

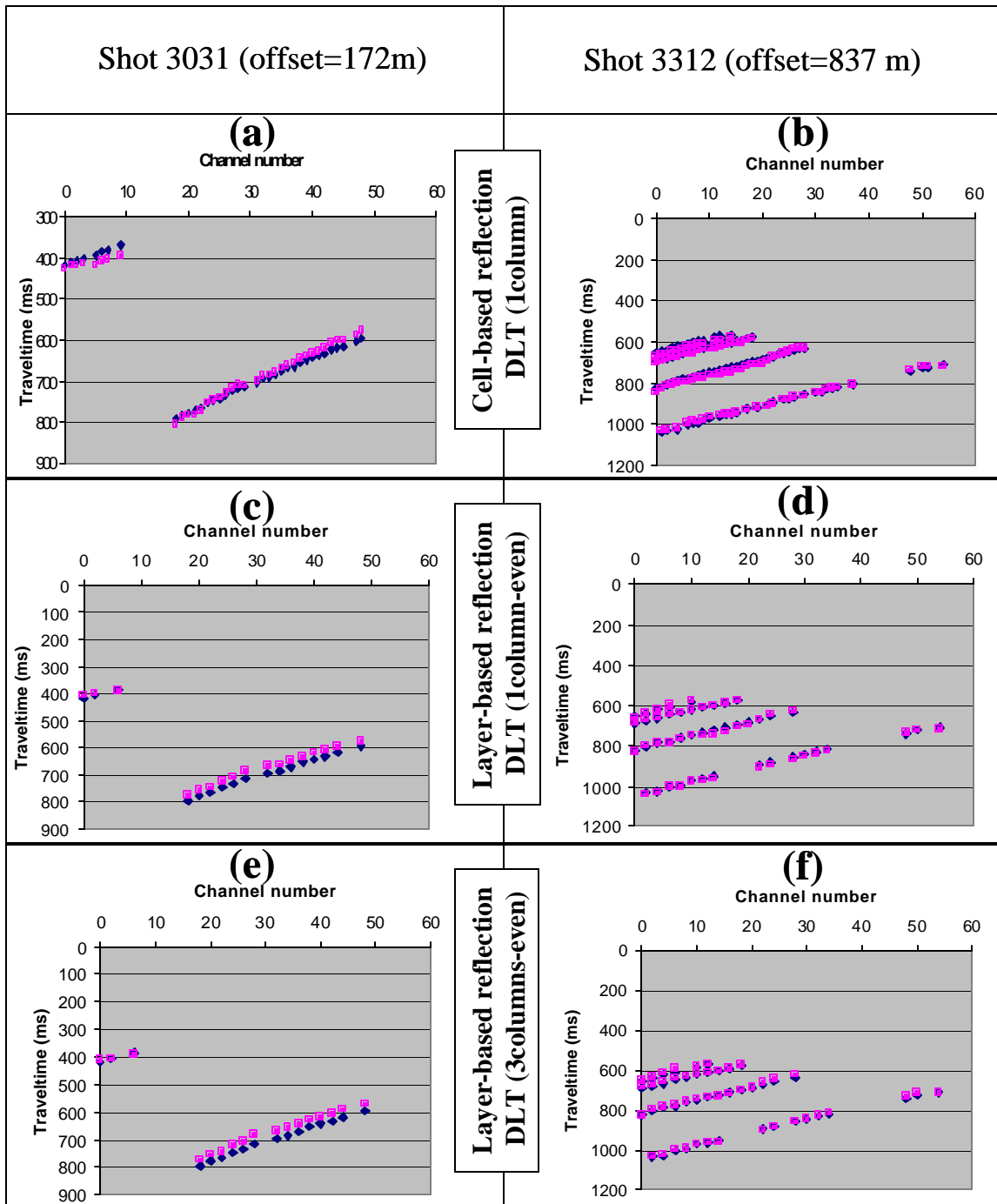


Figure 4.34. Comparison of the observed (blue diamonds) and the computed (pink squares) traveltimes obtained using reflection tomography (shots 3031 and 3312). (a) Cell-based tomography for shot 3031, (b) cell based tomography for shot 3312, (c) 1 column DLT for shot 3031, (d) 1 column DLT for shot 3312, (e) 3 columns DLT for shot 3031, and (f) 3 columns DLT for shot 3312.



#### **4.4. Kirchhoff migration**

Although migration of the Vinton Dome VSP data is not the primary goal of this thesis, Kirchhoff migration, developed by Dr. Hua-wei Zhou, was applied to the unprocessed shot records on the selected profile. The velocity-interface depth model defined in the final step of tomographic procedure, reflection layer-based DLT, is used to perform the prestack depth Kirchhoff migration. The image obtained using this algorithm is shown in Figure 4.35. The image quality is relatively poor due to the narrow aperture of the VSP data. A relatively large number of seismic events can be recognized on the migrated seismic section, and their interpretation is difficult. By correlation of the events with the position of well markers, it is possible to imply that the position of some of the reflectors corresponds to the realistic ones. Some of the steep dipping events are possibly caused by the reflections from the top of the salt. However, it is difficult to judge the exact position of the salt reflection. It is possible that there are multiple images of the salt body, as a consequence of the influence of a 3D body on the 2D image.

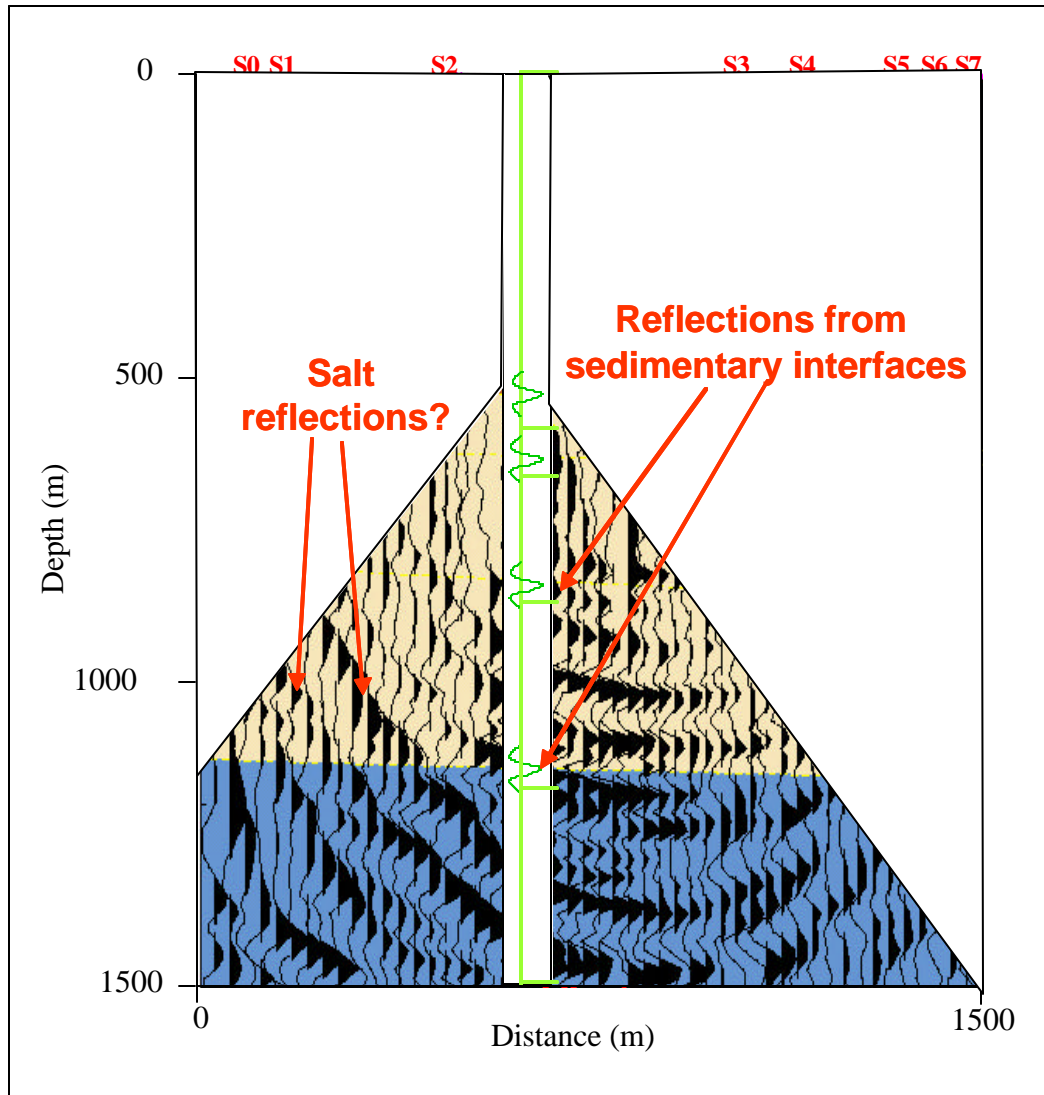


Figure 4.35. Results of the Kirchhoff migration applied to eight shot records using the final tomographic model. Peaks on the overlie indicate the true position of seismic reflectors.

## 5. CONCLUSIONS

Seismic traveltimes tomography using both first arrivals and reflections proved to be a valuable method for the determination of the velocity-interface depth model. I have used two approaches toward seismic tomography in this research: cell-based and deformable-layer tomography. Deformable layer tomography is developed as an extension of the cell-based approach. DLT allows each layer to have a constant or vertically varying velocity, and enables more realistic simulation of the subsurface geology, incorporation of additional geologic information and faster and more stable tomographic inversion.

I have designed several synthetic tests to address the stability and the performance of the two tomographic algorithms, and to understand the best practices for their application on the VSP datasets. Synthetic testing indicates that the cell-based methods can successfully reconstruct the geometry of the subsurface reflectors when the velocity is known, but fail to simultaneously determine both the velocity values and the interface positions. However, the cell-based tomographic approach can be used to reduce the initial velocity range. The deformable layer tomography enables stable inversion for both velocities and interface positions, but only when the initial velocities are close to their true values. Although synthetic testing showed that both methods perform well in certain situations, it also implied that neither the cell-based nor the deformable layer tomography could independently determine both the velocity values and the reflector geometry in stable manner. The synthetic testing enabled the design of a flow a the real data application, which recommends application of the deformable layer tomography after

cell-based methods have been used to reduce the initial guess of the velocity range and provide more insights into the reflector geometry, using both first arrivals and reflections.

VSP seismic tomography for the Vinton Dome area proved to be both highly interpretive and iterative, demanding incorporation of a number of geologic and geophysical constraints. Main problems faced during this research were: non-uniqueness and instability of the tomographic solution, event recognition and picking, velocity-depth ambiguity, poor ray coverage and lack of crossing rays, complexity of events, and inconsistency of events from one VSP gather to another.

A number of analyses were performed prior to the tomographic inversion in order to ensure an accurate initial velocity model and reduce some of the above listed problems. Seismic interpretation, performed on the time-migrated surface seismic data, provided understanding of the subsurface structure and allowed me to incorporate more *a priori* geologic information into the seismic inversion, thereby reducing the problems of non-uniqueness and instability. Correlation of the seismic interpretation and the VSP survey geometry allowed me to select a profile along a structurally simple 2D dip line, reducing the problems that might be associated with the application of a 2D tomographic algorithm to a 3D faulted salt dome. Numerical modeling facilitated the recognition of the seismic events on VSP gathers, and showed that the identification of the sediment reflections and salt flank reflection becomes more difficult as offsets are increased.

As expected, recognition and picking of reflection events were the major difficulties during tomographic application. In the case of Vinton Dome, picking was highly interpretive and was performed using a number of criteria. Only shot records with offsets smaller than 1500m have been used for picking. In addition, attention has been given to

the consistency of the events between gathers and the character of the events, such that only events with sufficient signal-to-noise ratio and which are consistent from one gather to the next have been selected for picking. I have performed manual picking of the four reflective events, corresponding to the Upper Miocene, Upper-Middle Miocene, Middle Miocene horizons, as well as a horizon located above the Top Anahuac. Selection of a rather rigorous criteria for event recognition and picking limited me to define the velocity model only in the upper portion of the sedimentary section for the Vinton Dome area. Picking is performed in the prestack domain, reducing the problem of velocity-depth ambiguity (Lines, 1993). I used traveltimes of both first arrival and reflection events, thereby reducing ambiguity by simultaneously determining the velocity and the interface position (Mao and Stuart, 1997).

Two of the major problems of seismic tomography, non-uniqueness and instability, as well as the problem of poor ray coverage, were addressed in the seismic inversion. I applied seismic tomography in a successive and iterative manner. The cell-based first arrival tomography was performed first, providing an initial update on the values of seismic velocities and geometry of the uppermost layer interface. This updated model was then further refined using first arrival DLT. In order to enable a stable inversion, I progressively increased the complexity of the subsurface model, using tomographic velocity-interface information from coarser model parameterizations as the initial model for the subsequent finer parameterizations. After first-arrival tomography, reflection tomography was applied. Cell-based reflection tomography provided additional information on the values of the velocities and the reflector positions. Finally, reflection DLT was used to obtain a stable, geologically reasonable model, that fits all picked

events and constraints. In order to evaluate uniqueness and stability of my solution, I divided the dataset into two subsets, of alternate odd and even channels, and inverted them separately. I accepted the final velocity-interface depth model only when two subsets provided mutually consistent results and when the position of the reflection interfaces and the velocity values corresponded to the *a priori* information from well logs. The final velocity model, defined by the application of the iterative flow described above, indicates that the subsurface layers are dipping away from the location of the salt dome, which is consistent with our understanding of halokineses. The velocity in the layer above the Upper Miocene horizon was found to be 1.77km/s. Velocities between the Upper Miocene and the lowest horizons did not differ significantly. This correlates with the very small increase of velocities in the sonic logs. Reflectivity of the sedimentary interfaces in this portion of the subsurface is most probably caused by varying density, with velocities playing a minor role in impedance variations.

Although significant progress has been made in understanding the performance of the available tomographic algorithms, including the development of the application flows for integration of the different data, and for the definition of velocity models for the Vinton Dome area, I believe that significant research needs to be undertaken in the future. It is necessary to further refine our DLT algorithms, enabling seismic inversion for an anisotropic environment. Most of the results in this thesis were obtained using data recorded on vertical geophones. It is therefore necessary to refine techniques for the separation of events on all three components, develop converted wave DLT and obtain a S-wave velocity model. Since tomographic velocity model building in this research has been applied only to near-offset data, it is necessary to further develop techniques for

event recognition on longer offset data, and incorporation of long-offset information into inversion. In the future I plan to perform joint seismic tomographic inversion using both prestack surface seismic data and VSP data. Joint seismic tomography should enable us to extend this rather localized velocity model and provide more velocity information due to increased ray coverage, as well as to increase confidence in the definition of the velocity model. The future plan is to extend all the methods into three-dimensions and build an integrated 3D velocity model for the Vinton Dome area.

## REFERENCES

- Al-Rufaii, K., 2002, Seismic tomography in areas associated with complex near-surface structures: Ph. D. dissertation, University of Houston.
- Aki, K. and Lee, W.H.K., 1976, Determination of three-dimensional velocity anomalies under a seismic array using first P arrival times from local earthquakes: 1. A homogenous initial model: *Journal of Geophysical Research*, **81**, 4381-4399.
- Aki, K. and Richards, P.G., 1980, *Quantative seismology, Theory and methods*: W.H.Freeman and Co.
- Anderson, D.L. and Dziewonski. A.M., 1984, Seismic tomography: *Scientific American*, **251**, 60-68.
- Balch, A.H., Lee, M.W., Miller, J.J., Ryder, R.T., 1982, The use of vertical seismic profiles in seismic investigations: *Geophysics*, **47**, 906-918.
- Bishop, T.N., Bube, K. P., Cutler, R. T., Langan, R. T., Love, P. L., Resnick, J. R., Shuey, R. T., Spindler, D. A. and Wyld, H. W., 1985, Tomographic determination of velocity and depth in laterally varying media: *Geophysics*, **50**, 903- 923.
- Burke, R.A., 1957, Summary of oil occurrence in the Anahuac and Frio formations of Texas and Louisiana: *Gulf Coast Association of Geological Societies Transactions*, **7**, 239.
- Carcione, J.M., Herman, G.C., ten Kroode, A.P.E., 2002, Seismic modeling: *Geophysics*, **67**, 1304-1325.



- Chen, S.T., Zimmerman, T.J., Tugnait, J.K., 1990, Subsurface imaging using reversed vertical seismic profiling and crosshole tomographic methods: *Geophysics*, **55**, 1478-1487.
- Chiu, S.K.L. and Stewart, R.R., 1987, Tomographic determination of three-dimensional seismic velocity structure using well logs, vertical seismic profiles, and surface seismic data: *Geophysics*, **52**, 1085-1098.
- Clayton, R.W., 1996, LARSE I progress report, LARSE home page (<http://www.scecdc.scec.org/larse.progress.html>).
- Constance, P.A., Roche, S., Bloor, R., Bicquart, P., Bryans, B., Gelinsky, S., Holland M., Ralph, J. G., 1999, Simultaneous acquisition of 3-D surface seismic data and 3-C, 3-D VSP data: 69th Ann. Internat. Mtg: Soc. of Expl. Geophys. Expanded Abstracts, 104-107.
- Hardage, H.A., 1995, Vertical seismic profiling- PartA: Principles: Geophysical Press.
- Kosloff, D., Sherwood, J., Koren, Z., MacHet, E. and Falkovitz, Y., 1996, Velocity and interface depth determination by tomography of depth migrated gathers: *Geophysics*, **61**, 1511- 1523.
- La Begat, S. and Farra, V., 1997, P-wave traveltme and polarization tomography of VSP data: *Geophysical Journal International*, **131**, 100-114.
- Lines, L., 1993, Ambiguity in analysis of velocity and depth: *Geophysics*, **58**, 596- 597.
- Liu, Z., 1997, An analytical approach to migration velocity analysis: *Geophysics*, **62**, 1238- 1249.
- Lizarralde, D. and Swift, S., 1999, Smooth inversion of VSP traveltme data: *Geophysics*, **64**, 659-661.

- Lutter W.J., Fuis, G. S., Thurber, C. H., Murphy, J., 1999, Tomographic images of the upper crust from the Los Angeles basin to the Mohave Desert, California: Results from Los Angeles Region Seismic Experiment: *Journal of Geophysical Research*, **104**, B11, 25543-25565.
- Marr, J.D., 1971, Seismic stratigraphic exploration- part 1: *Geophysics*, **36**, 311-329.
- Mao, W. and Stuart, G.W., 1997, Transmission-reflection tomography: Application to reverse VSP data: *Geophysics*, **62**, 884-894.
- Matsuoka, T. and Ezaka, T., 1992, Ray tracing using reciprocity: *Geophysics*, **57**, 326-333.
- McMechan, G.A. and Hu, L.Z., 1986, On the effect of recording aperture in migration of vertical seismic profile data: *Geophysics*, **51**, 2007-2010.
- Moser, T.J., 1991, Shortest path calculation of seismic rays: *Geophysics*, **56**, 56- 67.
- Paige, C.C. and Saunders, M.A., 1982, LSQR: An algorithm for sparse linear equations and sparse least squares: *ACM Trans. Math. Software*, **8**, 43-71, 195-209.
- Stewart, R.R., 1991, *Exploration Seismic Tomography: Fundamentals: SEG Course Notes Series, Vol. 3.*
- Stewart, R.R., Huddleston, P.D., Kan, T.K., 1984, Seismic versus sonic velocities: A vertical seismic profiling study: *Geophysics*, **49**, 1153-1168.
- Stork, C., 1992, Reflection tomography in the postmigrated domain: *Geophysics*, **57**, 680- 692.
- Thompson, S.A. and Eichelberger, O.H., 1928, Vinton salt dome, Calcasieu Parish, Louisiana: *Amer. Assoc. of Petrol. Geol. Bull.*, **12**, 385-394.

- Van Avendonk, H.J.A., Harding, A.J., Orcutt, J.A., Holbrook, W.S., 2001, Hybrid shortest path and ray bending method for traveltimes and raypath calculations: *Geophysics*, **66**, 648-653.
- Warren, A.D., 1957, The Anahuac and Frio sediments in Louisiana, *Gulf Coast Association of Geological Societies Transactions*, **7**, 221-237.
- Whitmore, N.D. and Lines, L.R., 1986, Vertical seismic profiling depth migration of a salt dome flank: *Geophysics*, **51**, 1087-1109.
- Williamson, P.R., 1990, Tomographic inversion in reflection seismology: *Geophysical Journal International*, **100**, 255-274.
- Wilson, F. and Noel, J.A., 1983, A gravity analysis of west-central Calcasieu Parish, Louisiana: *Gulf Coast Association of Geological Societies Transactions*, **33**, 243-250.
- Yilmaz, O., 1987, *Seismic data processing: SEG Series on Investigations in Geophysics*.
- Zhang, Z., Lin, G., Chen, J., Harris, J.M., Han, L., 2003, Inversion for elliptically anisotropic velocity using VSP reflection traveltimes: *Geophysical Prospecting*, **51**, 159-166.
- Zhou, H., J. A. Mendoza, C. A. Link, J. Jech, and J. A. McDonald, 1993, Crosswell imaging in a shallow unconsolidated reservoir: *The Leading Edge*, **12**, 32-36.
- Zhou, H., 1997a, Reflection multi-scale tomography for velocities and interfaces: in preparation.
- Zhou, H., 1997b, Determination of velocities and interfaces by multi-scale tomography: 67th Ann. Internat. Mtg: Society of Exploration Geophysicists, Expanded Abstracts, 1877-1880.

Zhou, H., 2002, Multi-scale tomography for crustal P and S wave velocities in southern California: Pure and Applied Geophysics, in press.

Zhou, H., 2003, Multi-scale travelttime tomography: Geophysics, in press.

## Appendix A

### Construction of kernels

In reflection tomography inversion for small perturbations in either slowness or depth of an interface as a function of the travel-time residuals is performed. It is possible to consider a reflection ray at a boundary (Figure A.1) before and after the boundary has been perturbed (moved for a small distance  $\delta z$ ). For the reflected ray, the increased path length due to such small perturbation is given as  $2\delta z \cdot \cos\Theta_1$ . Therefore, the perturbed traveltimes and the partial derivative with respect to that depth perturbation are given respectively as:

$$dt = s_1 \cdot 2 \cdot dz \cos \Theta_1, \text{ and} \quad (\text{A1})$$

$$\frac{dt}{dz} = s_1 \cdot 2 \cdot \cos \Theta_1, \quad (\text{A2})$$

where  $s_1$  is represented with relation  $1/v_1$ .

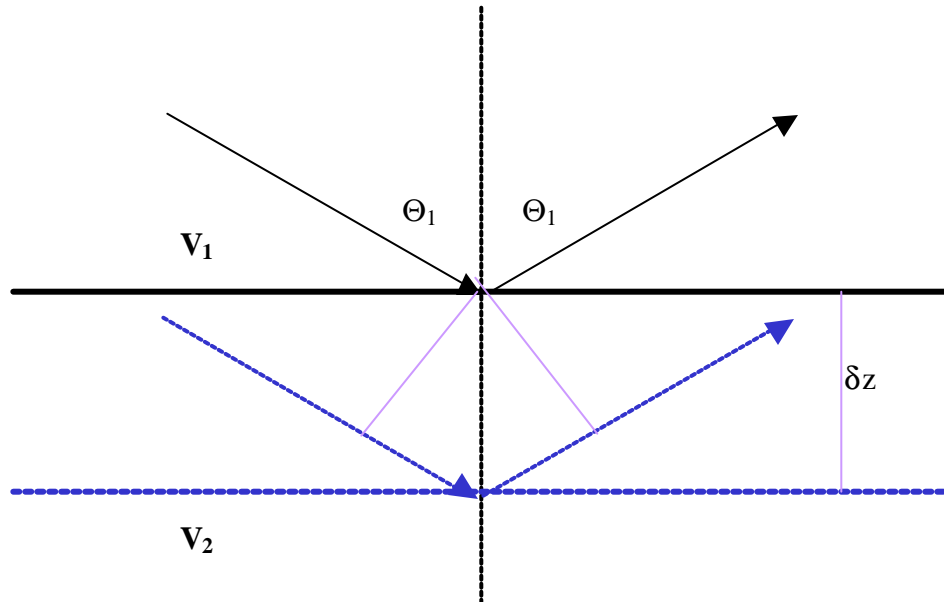


Figure A.1. The raypath of the reflected ray before and after a small depth perturbation (Al-Rufaii, 2002).

For a refracted ray (Figure A.2), the partial derivative is given as:

$$\frac{dt}{dz} = s_1 \cos \Theta_1 - s_2 \cos \Theta_2. \quad (\text{A3})$$

Equations (A2) and (A3) are also valid for dipping interface.

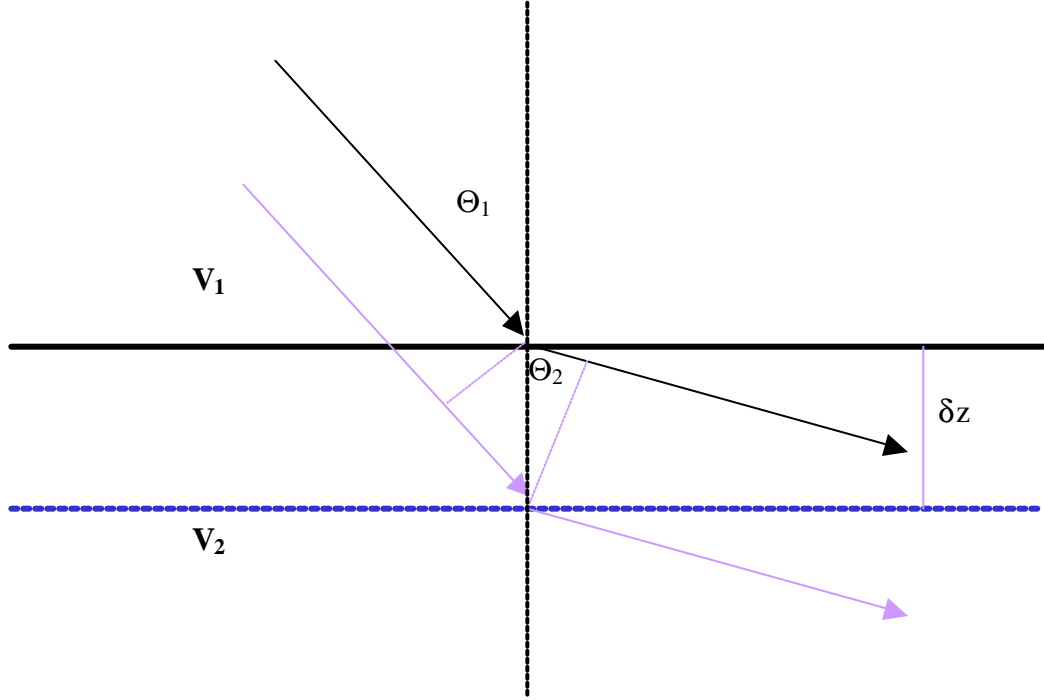


Figure A.2. The raypath of the refracted ray before and a after small depth perturbation (Al-Rufaii, 2002).

The two Frechet kernels  $k_{s_{ij}}$  and  $k_{z_{il}}$  can be evaluated using a 3D model shown in Figure A.3. All three corner points of the triangular interface segment ABC are traversed with the model vertical lines. A raypath SRG is reflected from the interface at a point R, and the raypath SRT is transmitted through the interface at point R. The idea is to derive the travel-time perturbation due to the vertical perturbations at each of the three corner points. Point Q is the intersection between BC and the extension of AR. Line AQ has a dip angle  $\delta$  with respect to the horizontal.

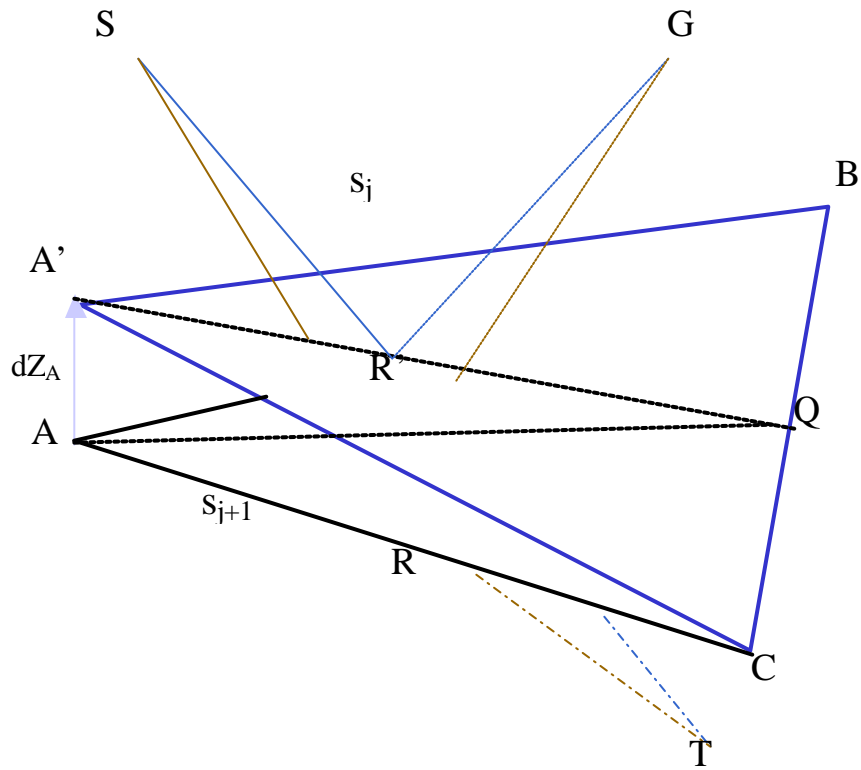


Figure A.3. Illustration of a 3D triangular interface segment ABC perturbed to A'BC (Al-Rufaii, 2002)

The cosine of the dip angle is given as:

$$\cos \mathbf{d} = \frac{|X_A - X_Q|}{|AQ|}, \quad (\text{A4})$$

where  $X_A$  and  $X_Q$  are the horizontal coordinates of points A and Q and  $|AQ|$  is the distance between these two points. The incidence, reflection and refraction angles are defined as  $\alpha$  and  $\beta$ , respectively.

Perturbing one corner point, for example A, by a vertical distance  $\Delta Z_A$  to A', then the reflection point R is perturbed to position R'. Though A' is perturbed vertically from A,

the perturbation from R to R' may have vertical and horizontal components. The distance between R and R' is expressed as:

$$|RR'| = \frac{|X_R - X_Q|}{|X_A - X_Q|} \Delta Z_A \cos \mathbf{d} = \frac{|X_R - X_Q|}{|AQ|} \Delta Z_A, \quad (\text{A5})$$

where  $X_R$  is the horizontal coordinate of the reflection point R.

By Fermat's principle, it is possible to assume that both the incidence angle  $\alpha$  and the refraction angle  $\beta$  are unchanged with respect to the small perturbations from R to R'. The length of the incidence leg SR of the raypath is given as:

$$\Delta l_1 = -|RR'| \cos \mathbf{a} = -\Delta Z_A \cos \mathbf{a} \frac{|X_R - X_Q|}{|AQ|}, \quad (\text{A6})$$

which equals to  $\Delta l_2$ , the length change of the reflection leg RG.

Therefore, the ratio between the traveltimes and the interface perturbations of the reflection ray is expressed as:

$$\mathbf{k}_{il} = \frac{\Delta t_i}{\Delta Z_A} = (-\Delta l_1 s_j - \Delta l_2 2s_j) / \Delta Z_A = -2s_j \cos \mathbf{a} \frac{|X_R - X_Q|}{|AQ|}, \quad (\text{A7})$$

where  $s_j$  is the slowness of the cell above the interface segment ABC.

Similarly, the length change of the refraction leg RT is:

$$\Delta l_3 = |RR'| \cos \mathbf{b} = \Delta Z_A \cos \mathbf{b} \frac{|X_R - X_Q|}{|AQ|}. \quad (\text{A8})$$

Hence, the ratio between the traveltimes and the interface perturbations for the transmitted ray through point R is:



$$\mathbf{k}_{il} = \frac{\Delta t_i}{\Delta Z_A} = (-\Delta l_1 s_j - \Delta l_3 s_{j+1}) / \Delta Z_A = (s_{j+1} \cos \mathbf{b} - s_j \cos \mathbf{a}) \frac{|X_R - X_Q|}{|AQ|}. \quad (\text{A9})$$

According to whether a given raypath is reflected or transmitted at an interface segment, the corresponding kernels at all corner points of the interface are calculated using equations (A8) and (A9) as evaluated in the reference model. The formula derived above is applicable to both single-scale tomography and multi-scale tomography, with the differences in grid scales.

## Appendix B

### Multiscale tomography

The formulation of the multiscale tomography is given next. According to the ray theory, the travelttime of the ray can be expressed as a linear integral of the slowness along the ray path. Therefore, the travel-time of a given ray is a function of the slowness variable  $s$  and the depth variable  $z$  of the interface traversed by the ray, Using the well known travel-time integral and taking the length variable  $l_i$  of the ray as a function of the depth variable, we have (Zhou, 1997a):

$$t_i = \int_{l_i(z)} s dl_i(z). \quad (B1)$$

When partial differentiation with respect to  $s$  and  $z$  is applied to equation (B1), we have:

$$dt_i = \int_{l_i(z)} ds dl_i(z) + \int_{l_i(z)} s \frac{d}{dz} [dl_i(z)] dz. \quad (B2)$$

For a defined model partition, the integrals on the right hand side of the equation above can be approximated by a linear combination of Frechet kernels  $k_{-s} = dl(z)$  and

$k_{-z} = s \frac{d}{dz} [dl_i(z)]$  so that

$$dt_i = \sum_j^J k_{-s_{ij}} ds_j + \sum_j^J k_{-z_{il}} dz_l, \quad (B3)$$

where  $J$  is total number of slowness cells and  $L$  is total number of interface nodes that have to be upgraded by inversion. The kernel  $k_{-s_{ij}}$  constrains the  $i$ -th ray and  $j$ -th slowness cell, while the kernel  $k_{-z_{il}}$  places constraints on  $i$ -th ray and  $l$ -th interface node.

Inversion of equation (B3) in order to determine  $\{ds_j\}$  and  $\{dz_l\}$  is used to perform tomographic procedure.

The multi-scale tomography uses multi-cell inversion and it enables simultaneous determination of velocities and interfaces using reflection traveltimes in more effective way than single-scale reflection tomography (Zhou, 2003). Model unknowns are decomposed into components of different wavelength for inversion and the solution is obtained by a combination of different wavelengths in a process that can be regarded as superposition.

The forward equation for multi-scale tomography can be defined as:

$$dt_i = \sum_m^M w_s^{(m)} \sum_j^J k_{-s_{ij}}^{(m)} ds_j^{(m)} + \sum_n^N w_z^{(n)} \sum_l^L k_{-z_{il}}^{(n)} dz_l^{(n)}, \quad (\text{B4})$$

where  $ds_j^{(m)}$  is the slowness perturbation of the  $j$ -th cell of the  $m$ -th cell size and  $dz_l^{(n)}$  is the depth perturbation at the  $l$ -th grid point of the  $n$ -th grid spacing, and  $w_s^{(m)}$  and  $w_z^{(n)}$  are weighting coefficients satisfying the following conditions:

$$\sum_m^M w_s^{(m)} = 1 \quad \text{and} \quad (\text{B5})$$

$$\sum_n^N w_z^{(n)} = 1. \quad (\text{B6})$$

It can be seen that single-scale tomography can be regarded as a special case of multi-scale tomography, when only one grid scale is used. The final results of inversion can be defined with equations

$$ds_j = \sum_m^M w_s^{(m)} ds_j^{(m)} \text{ and} \tag{B7}$$

$$dz_l = \sum_m^M w_z^{(n)} dz_l^{(n)} . \tag{B8}$$

Multi-scale tomography differs from single-scale tomography in the partitioning of the model into cells.